공학박사 학위논문

A study on the preparation of stimuli-responsive hydrogels and their applications

자극 응답성 하이드로젤의 제조와 응용에 관한 연구

2020년 2월

서울대학교 대학원
재료공학부
이 경 민

A study on the preparation of stimuli-responsive hydrogels and their applications

자극 응답성 하이드로젤의 제조와 응용에 관한 연구

지도교수 장 지 영

이 논문을 공학박사 학위논문으로 제출함
2020 년 2 월

서울대학교 대학원
재료공학부
이 경 민

이경민의 박사학위논문을 인준함
2020 년 2 월

위 원 장	박 종 래	(인)
부 위 원 장	장 지 영	(인)
위 원	조 원 호	(인)
위 원	안 철 희	(인)
위 원	김 형 우	(인)

Ph.D. Thesis

A study on the preparation of stimuli-responsive hydrogels and their applications

Kyoung Min Lee

2020

Department of Materials Science and Engineering

Seoul National University

Abstract

A study on the preparation of stimuli-responsive hydrogels and their applications

Kyoung Min Lee
Department of Materials Science and Engineering
Seoul National University

A hydrogel is a three-dimensional network polymer that is comprised of hydrophilic polymer chains physically or chemically cross-linked. This materials has the ability to retain a large amount of water within its network. In particular, stimuli-responsive hydrogels that can respond to external stimuli have gained significant interest because of their applicability in the development of new responsive systems taking advantage of elasticity, volumetric change, storage capability, and chemical diversity. In this study, a variety of stimuli-responsive hydrogels capable of exhibiting different functions were designed, synthesized and characterized.

Firstly, stimuli-responsive hydrogels films were prepared. In general, when processed as films, hydrogel materials show enhanced properties, including faster responses and higher loading capacities, and enhanced interfacial

interactions. In this study, A functional polyacrylamide hydrogel film containing a rhodamine-based probe was prepared. The probe plays two fundamental roles: in the fabrication of the film via redox-initiated radical polymerization and in providing a fluorescence response to Al^{3+}. The amine-containing probe initiated the polymerization reaction at room temperature; the resulting film synthesized through the one-step reaction was transparent and stretchable, elongating by more than five times under tensile tension. The fluorogenic probe in the film showed a sensitive, selective response to Al^{3+} with a detection limit of 1.5 mM. Furthermore, after detection, the addition of ethylenediaminetetraacetic acid (EDTA) to the film turned off the fluorescence from the probe; this facilitated reversible fluorescence sensing when the film was repeatedly exposed to Al^{3+}. The facile preparation method can be expanded to incorporate other multi-functional amine probes that can impart hydrogel films with autonomous, responsive systems.

Secondly, the multifunctional effect of molybdenum disulfide (MoS_2) has been studied, which enables a bottom-up design of nanocomposite hydrogels. The MoS_2 nanoplatelet forms radical species through a redox reaction with persulfate under aqueous conditions while initiating the polymerization of acrylic monomers and providing non-covalent cross-linking points without requiring external stimuli or extra cross-linkers, leading to the formation of hydrogels that

are in situ embedded with the inorganic flakes. Furthermore, the addition of MoS_2 could induce more rigid and elastic networks compared to those in control hydrogels using a typical cross-linker at the same level; for example, 0.08 wt% MoS_2 resulted in a composite hydrogel of which the elastic modulus was 2.5 times greater than that from a hydrogel using *N*,*N*′-methylenebis(acrylamide) as the showing phase transition during polymerization. The composite hydrogels are self-healable, taking advantage of reversible physical cross-links. Thus, two cut hydrogel strips could be readily re-joined by heating at 70 °C, and the resulting whole strip showed mechanical strength similar to that of the pristine sample before it was cut. This synthetic approach would give way to the modular design of MoS_2-containing composite hydrogels.

Lastly, The study focused on the preparation of hydrogels by reweighing the effect of cross-linking density on physical properties, which provided green fabrication of bilayered hydrogels that consist of homogeneous structural motifs but show programmed responses via sequential radical polymerization. In particular, when two hydrogel layers containing different cross-linking densities were joined together, an integrated linear bilayer shows heterogeneous deformation triggered by water. The linear hydrogel bilayer bending into a circle was checked. In addition, An electric circuit switch using a patterned hydrogel was demonstrated. Anisotropic shape change of the polyelectrolyte switch closed

an open circuit and lights a light-emitting diode in red. This proposed fabrication and engineering could be expanded to other superabsorbent systems and create smart responses in cross-linked systems for biomedical or environmental applications.

Keywords: hydrogel, stimuli-responsive materials, redox polymerization, rhodamine 6G, hydrogel film, aluminum sensor, bilayer hydrogel, superabsorbenet polymer, molybdenum disulfate, self-healing

Student Number: 2014-21457

Contents

List of Figures

Chapter I.

Chapter II.

Figure II-3. (a) Dynamic frequency sweep data for solution 2 in the presence of the promoter 1 and KPS and (b) the control experiment conducted the same conditions expect in the absence in 1.

Figure II-4. Dynamic frequency sweep data for an aqueous of 2 in presence of rhodamine 6G and KPS.

Figure II-5. (a) Representative tensile stress–strain curves for the hydrogels and (b) Change in Young's modulus and toughness of the hydrogels.

Figure II-6. (a) A representative photograph of actual tensile testing, (b) the porous network structure of the dried hydrogel, (c) Images of the stretchable film.

Figure II-7. (a) Fluorescence emission spectra of the film obtained upon the addition of Al^{3+} and (b) change in emission intensity of the film with different concentrations of Al^{3+}. Images of the hydrogel films before and after exposure to 3.00 mM of Al^{3+} are obtained under 365 nm irradiation.

Figure II-8 (a) Change in the intensity of fluorescence monitored form film over the course of exposure time and (b) fluorescence emission spectrum form remaining Al^{3+} solution.

Figure II-9 (a) Selective enhancement in emission intensity of the film and (b) reversible on–off fluorescence switching of the hydrogel film.

Chapter III.

Figure III-1. Schematic description for the preparation of a composite hydrogel containing 2H MoS_2 flakes. The MoS_2 Photograph of acylindrical hydrogel is shown in the inset.

Figure III-2. Gelation test for the formation of MoS_2-containing composite hydrogels via redox initiation, while the exfoliated MoS_2.

Figure III-3. (a) Change in Young's modulus of the composite hydrogels, (b) representative tensile stress–strain curves for the hydrogels.sive Young's modulus, (c) compressive stress at 60% strain of the hydrogels.

Figure III-4. (a) Change in Young's modulus of the composite hydrogels and (b) representative tensile stress–strain curves for the hydrogels.

Figure III-5. (a) Compressive stress–strain curves measured at different time intervals during the gelation, (b) changes in the Young's modulus as time elapsed, (c) Dynamic time sweep data for an aqueous solution, (d) change in temperature during the gelation.

Figure III-6. Investigation of radical formation by MoS2 and KPS using bromophenol blue (BPB) Photographs in the inset visualize the radical formation.

Figure III-7. Evolution of the 1T phase of MoS_2 after gelation when observed by XPS. The spectra for (a) Mo 3d core level peaks and (b) S 2p core level peaks.

Figure III-8. (a) Scanning electron microscopy (SEM) after lyophilization and (b) transmission electron microscopic (TEM) image of MoS_2 after polymerization

Figure III-9. (a) Compressive stress–strain curve from the composite hydrogel prepared under dark conditions (black), (b) the curves of the hydrogels obtained from DMA (light gray) or after copolymerization of DMA and acrylamide (gray), (c) compressive stress–strain curve of the hydrogel using $MoSe_2$.The inset shows

the photograph of the resulting cylindrical hydrogel. Photographs of (d) DMA (e) 1:1 acrylamide–DMA (w/w).

Figure III-10. (a) Self-healing of the hydrogel materials, (b) Photograph of the healed hydrogel taken under 365-nm irradiation, (c) Representative tensile stress–staincurves of a pristine hydrogel strip (red) and the healed one(black), (d) Photographs of the healed strip when stretched by hand and relaxed.

Chapter IV.

Figure IV-1. Schematic description for the preparation of a poly(acrylic acid)-based hydrogel film.

Figure IV-2. (a) Change in degree of swelling of hydrogel films and (b) representative volumetric change in film 2.

Figure IV-3. (a) SEM images of as-prepared sample and (b) after swelling in waterfor 48 h.

Figure IV-4. (a) Photograph of measuring temperature of the polymerizing solution of 2 and (b) Change in the temperature of the solution during radical polymerization.

Figure IV-5. (a) Representative tensile stress−strain curves from the hydrogel and (b) change in toughness (blue), elongation at fracture (black).

Figure IV-6. Young's modulus (a), elongation at fracture (b), and toughness (c) of hydrogel films 1, 3, and 6, measured at 80 °C (red). The results from 25 °C (black) and (d) Change in Young's modulus of 3 after exposure to different temperatures.

List of Tables

Chapter I.

Introduction

I-1. Introduction to hydrogels

I-1-1. Definition of a hydrogel

Traditionally, there are many ways to define a hydrogel. The most common definition is that a hydrogel is a three-dimensional polymeric network that has the ability to retain a large amount of water within its network [1,2]. Another definition is a polymeric network structure that exhibits the ability to swell and maintain a significant fraction of water [3,4]. Hydrophilic groups on a polymer backbone allow hydrogels to absorb water, whereas the cross-links between polymer chains prevent them from dissolving in water. Many hydrophilic materials, both naturally occurring and synthetic, meet the definition of hydrogels [5-8].

Recently, researchers have defined hydrogels as a three-dimensional network of polymer chains consisting of two- or multi-component system, and water that fills the pores of the network between the chains [9]. Depending on the properties of the components used and the cross-link density, the hydrogel network can adsorb various amounts of water in equilibrium. Capillary, osmotic and hydration forces that are related to water absorption, are counterbalanced by

expansion resisting forces generated by the crosslinked polymer chain. The hydrogel network absorbs water until these two forces achieve an equilibrium state. The physical properties of the hydrogel such as mass transport, diffusion ability, and mechanical strength, are determined by the amount of water in the equilibrium swollen state. Hydrogels exhibit excellent biocompatibility because of their high water content [10].

I-1-2. Classification of hydrogels

Hydrogels can be prepared using different kinds of material and synthetic methods. Therefore, they can be categorized based on their different characteristics as shown in Fig. I-1. The most popular classification is based on the type of crosslinking method, which includes physical and chemical crosslinking. Physical crosslinking hydrogels are prepared by the reversible interaction between crystallization, van der Waals forces, hydrogen bonding, and ionic interaction [11-14]. In particular, ionic interactions can induce crosslinking at ambient conditions. The main advantage of physical crosslinking is biomedical or environmental safety, due to the absence of chemical crosslinking agents. In addition, physical crosslinking hydrogels exhibit stimuli-responsible

properties in addition to self-healing and injectable properties at room temperature [15].

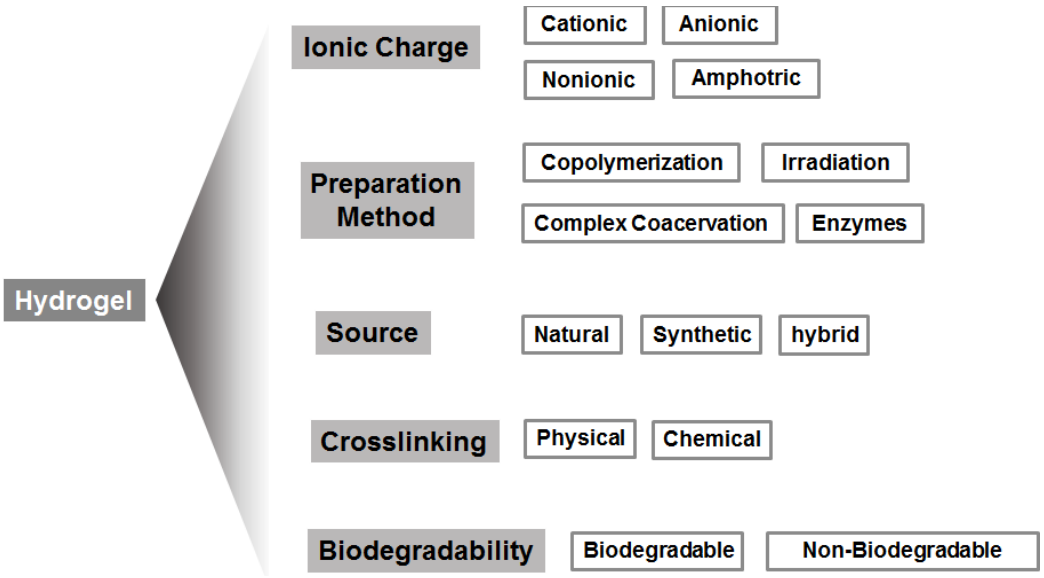

Figure I-1. Categorization of hydrogels according to different criteria.

Chemical crosslinking involves a permanent reaction, which entails the grafting of a monomer onto the main polymer backbone, or the connection of polymer chains via crosslinking agents [16]. In this approach, a very small quantity of multi-functional crosslinking agents is added to a solution of polymers. The polymer must have a suitable functional group to react with the

crosslinking agent. This technique is appropriate for the preparation of hydrogels from naturally-occurring as well as synthetic polymers. When the main component of a hydrogel is not a polymer but a monomer, chemical crosslinking hydrogels are prepared by various polymerization methods such as chain-growth polymerization, gamma and electron beam polymerization, and addition and condensation polymerization. Among these methods, chain-growth polymerization is the most common approach and includes free radical polymerization of a hydrophilic monomer containing a carbon double bond [17].

Compared with physical crosslinking hydrogels, chemical crosslinking hydrogels exhibit enhanced stability under physiological condition, and excellent mechanical properties [18]. In particular, dynamic covalent chemistry is used as a potent approach to design thermodynamically-controlled materials, by utilizing a reversible covalent bond as a linkage. This concept can be applied to hydrogels [19,20]. The incorporation of reversible covalent bonds that are illustrated in Fig I-2 into a hydrogel network, presents a new strategy for the design of hydrogels with dynamic properties.

Another classification standard of hydrogels is the source used for hydrogel preparation. Hydrogels can be categorized as natural, synthetic, or hybrid, depending on the materials used for fabrication. Natural polymers that can be used to prepare hydrogels include collagen, gelatin, and polysaccharide (alginate,

cellulose, agarose) [21-23]. They can be easily obtained from natural sources at low prices and exhibit excellent biocompatibility. Therefore, natural-polymer-based hydrogels are used in the preparation of physiological hydrogels because they are components of the in vivo extracellular matrix.

In contrast, synthetic hydrogels are made from artificial materials such as acrylamide, poly(vinyl alcohol), (Hydroxyethyl)methacrylate, and acrylic acid [24]. These materials are more reproducible than natural source materials. Although polymerization conditions such as temperature and humidity affect their final structure, synthetic hydrogels also show flexibility in terms of altering physical properties and chemical composition.

Hybrid hydrogels are a combination of natural and synthetic materials. They benefit from the advantages of natural and synthetic hydrogels. For example, synthetic vinyl monomers are grafted onto natural polysaccharides to add additional functionality to the polysaccharides polymers, without loss of biodegradability [25].

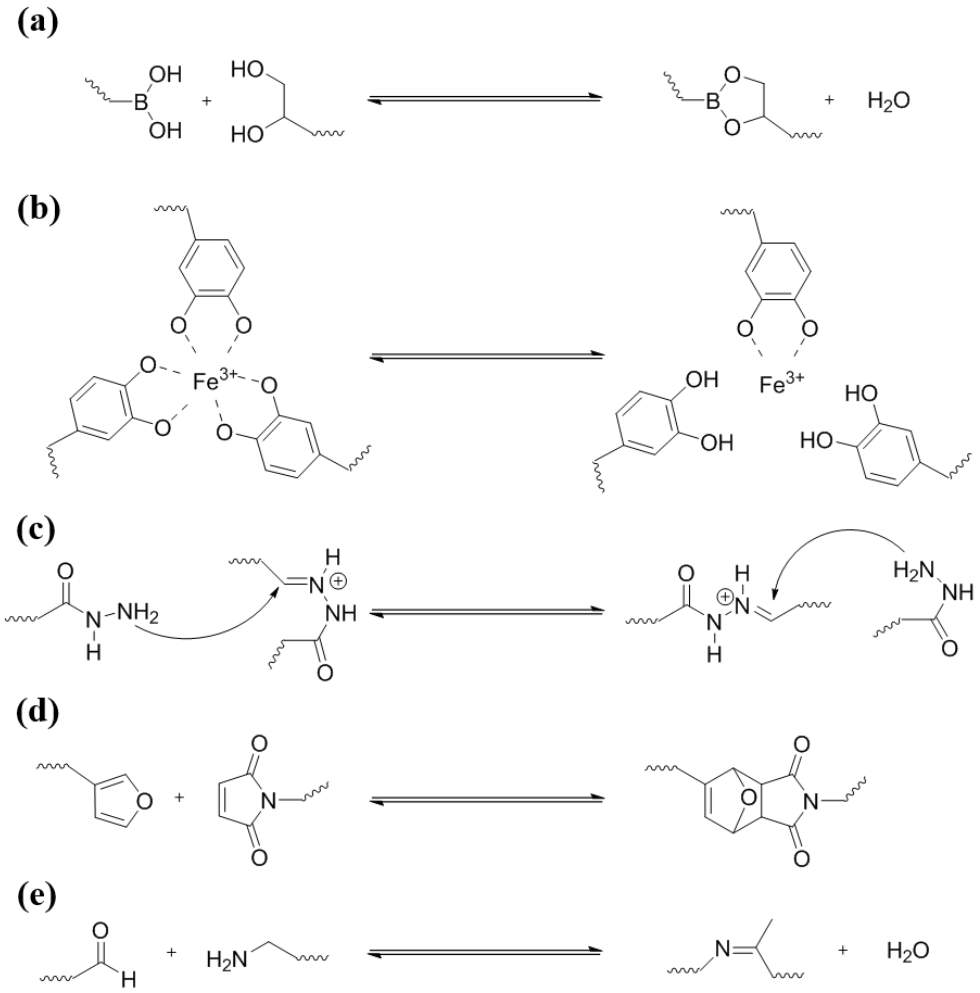

Figure I-2. Representative reversible reactions for the preparation of hydrogelsschematic route of reversible covalent bonds: (a) boronic ic ester formation and hydrolysis, (b) catechol-Fe chemistry, (c) dynamic acyl hydrazone exchange reaction, (d) furan-maleimide furan-maleimide Diels-Alder reactionas an example of cycloaddition reactions, (e) imine formation and hydrolysis/enamine form.

I-2. Properties of hydrogels

Hydrogels are characterized by their swelling/deswelling behavior, excellent mechanical properties, absorption capacity, cytotoxicity, and biocompatibility. Based on these properties, hydrogels are promising materials in a wide variety of fields [26-28]. The type and concentration of the materials used in the preparation of hydrogels play an important role in the determination of the properties of hydrogels [29]. In the following section, the properties of hydrogels are discussed based on several factors.

I-2-1. Swelling/deswelling behavior

The ability to absorb aqueous solutions is the most important property of hydrogels. Most hydrophilic networks in hydrogels have a high capacity for water uptake [30]. They can swell, absorb, and retain aqueous solutions up to hundreds of times of their dry weight. The change in a hydrophilic network via the absorption of an aqueous solution is illustrated diagrammatically in Fig I-3, and this phenomenon is known as swelling.

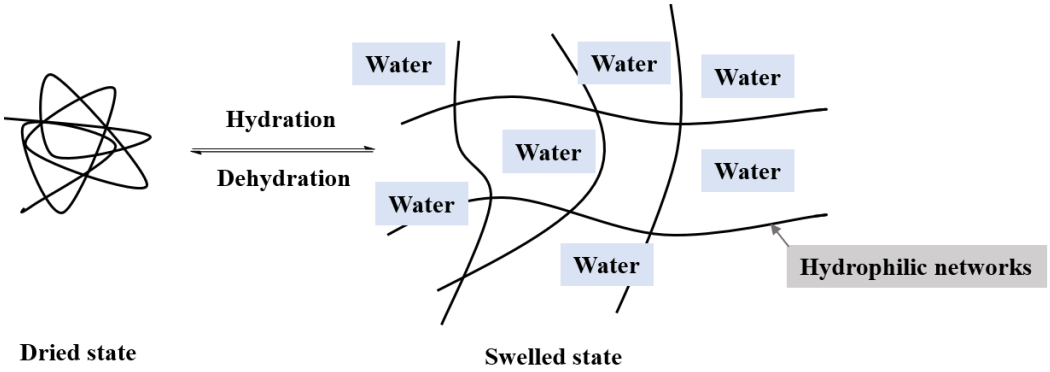

Figure I-3. Depiction of volumetric change in hydrogels during hydration and dehydration

When a dried hydrogel is immersed in distilled water at room temperature, they begin to swell. Swelling can be estimated by weighting the dry sample and the swollen-state sample. Before weighing, the swollen-state sample is displaced from water, and the surface of the sample should be carefully wiped with tissue paper to remove any surface moisture, which can significantly affect the weight of the swollen-state. The swelling ability was quantified using the swelling ratio as represented in eq. **I-1**.

$$\text{swelling ratio} = (w_s - w_d)/w_d \qquad \text{(eq. } \mathbf{I\text{-}1)}$$

where W_d is the weight of the dried hydrogel sample and W_s is the weight of the swollen-state hydrogel at a specific time.

The swelling kinetics of hydrogels can be divided into relaxation-controlled

(non-Fickian) and diffusion-controlled (Fickian) swelling kinetics [31]. The swelling kinetics is controlled by diffusion when the relaxation of the hydrogel polymer chain occurs at a slower rate compared to water diffusion into the hydrogel network.

The cross-linking density is the most significant factor that influences the swelling behavior of hydrogels [32]. The definition of the cross-linking density is the density of the chains or segments that connect two infinite parts of the polymer network. Therefore, the higher the crosslinking density, the more polymer structures are integrated using cross-linking agents. Hydrogels with a high cross-linking density exhibit a compacted structure, and absorb a smaller amount of water compared to those with a lower cross-linking density.

The cross-inking density of hydrogels and the equilibrium volumetric swelling ratio are calculated based on the following procedure. Died hydrogel samples were immersed in distilled water for several days until the samples reached an equilibrium state. The equilibrium volumetric swelling ratio (Q) was calculated using eq. **I-2** based on the swollen-state mass (M_s) and lyophilized hydrogel (M_d) as follows:

$$Q = 1 + \frac{\rho_{poly}}{\rho_{solv}}\left(\frac{M_s}{M_d} - 1\right) \qquad \text{(eq. I-2)}$$

where p_{poly} is the density of the polymer solution and p_{solv} is the density of the solvent. The cross-linking density (p_x) was calculated using a modified form of the Flory-Rehner equation (neglecting chain ends) as shown eq. **I-3** [33] as follows:

$$\rho_x = \frac{-1}{V_{solv}}\left(\frac{In(1-v_\rho)+v_\rho+\chi v_p{}^2}{v_p{}^{\frac{1}{3}}-(\frac{1}{2})v_p}\right) \qquad \text{(eq. } \textbf{I-3)}$$

where V_{solv} is the molar volume of the solvent, χ is the solvent polymer interaction parameter, and v_p is the equilibrium polymer volume fraction (1/Q).

The physical properties of hydrogels are affected by the change of environmental parameters such as pH, electric signal, temperature, and ionic species [34,35]. When changes in water content and the size of hydrogels occur, physical change may occur at the macroscopic level. Hydrogels containing ionic functional groups exhibit different properties depending on the change of the external environmental pH. A typical example of a pH-sensitive hydrogel is poly(acrylic acid). The degree of ionization of the carboxyl group on the polymer backbone significantly affects the swelling ratio of poly (acrylic acid) based hydrogels.

Poly(*N*-isopropyl acrylamide) is a temperature-responsive polymer that can be synthesized from N-isopropyl acrylamide. When a hydrogel is cross-linked, it forms a three-dimensional structure. The hydrogel undergoes a reversible lower

critical solution temperature (LCST) phase transition from a swollen-state to a shrunken dehydrated state. Temperature-responsive phase transition of poly(N-isopropyl acrylamide) occurs at a temperature close to that of the human body, expelling its water contents. As a result, several researchers have attempted to apply poly(*N*-isopropyl acrylamide) to tissue engineering and controlled drug delivery [36-38].

I-2-2. Mechanical properties

The mechanical properties of hydrogels determine the suitable field for application. For example, hydrogels used for different applications should have outstanding mechanical properties [39]. The mechanical properties of hydrogel mostly depend on the crosslinking density [40]. The more cross-linking agents are involved in hydrogel network structure, the shorter the distance between the cross-linked segments. A larger force is required to detect these shorter segments. Thus, hydrogels with a higher cross-linking density exhibit superior mechanical properties in terms of strength, hardness, and stiffness. For example, when a hydrogel is prepared using hyaluronic acid (HA) as a crosslinker, a network with a low cross-linking density is formed, which results in a softer hydrogel. Therefore, various strategies such as crosslinking or conjugation are used to

improve the mechanical properties of HA-based hydrogel [41].

The mechanical strength of the hydrogel is enhanced by increasing the cross-linking density. However, when the hydrogel has an extremely high cross-linking density, it becomes too brittle for practical use. Therefore, it is important to control the amount of cross-linking agents during the preparation of hydrogels [42].

The method used to determine the mechanical properties of hydrogels is similar that used for basic mechanical testing. Hydrogels exhibit a time-dependent mechanical behavior because of their intrinsic viscoelasticity, and time-dependent deformation mechanism due to fluid flow [43,44]. Thus, time is an important factor in the mechanical testing of hydrogels. Characterization can be performed in either the time or frequency domain. There are several common testing techniques, as illustrated in fig I- [45-49].

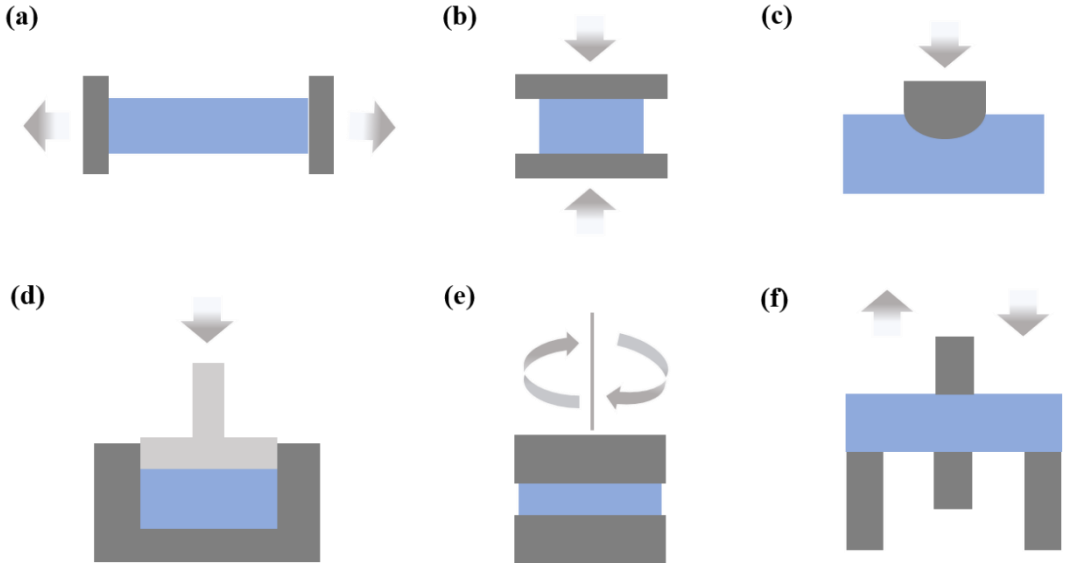

Figure I-4. Schematic diagram of the various techniques used for the determination of the mechanical properties of hydrogels: (a) tensile test, (b) compressive test, (c) indentation, (d) confined compression, (e) shear rheometry, (f) dynamic mechanical analysis (DMA).

I-3. Preparation of hydrogels

I-3-1. Covalent reactions

Radical polymerization is the most potent method to fabricate hydrogels among the covalent approaches. Hydrophilic monomers such as acrylamide (AAm), acrylic acid (AA), methacrylic acid (MAA), vinyl acetate (VA; the monomer for poly(vinyl alcohol), PVA), N,N-dimethylacrylamide (DMA), N-isopropylacrylamide (NIPAM), and 2-hydroxyethyl methacrylate (HEMA) have been widely used and polymerized by radical initiation (Fig. I-5a) [50-52]. Other monomers having water-soluble groups (e.g., carboxylate, sulfonate, quaternary ammonium, and phosphate groups, or zwitterions) are also used in hydrogel-based materials (Fig I-5b) [53-55]. Interestingly, hydrophilic, bio-extractable monomers (e.g., Tulipalin A and β-pinene) can also be polymerized to make hydrogel polymers (Fig I-5c) [56]. For cross-linking reactions, bi- or trifunctional cross-linkers are incorporated during polymerization to establish entangled network structures (Figure I-6d).

The monomeric vinyl species mentioned above are polymerized by water-soluble initiators such as persulfates (e.g., ammonium persulfate, APS; potassium persulfate, KPS) or acetophenone derivatives (e.g., IRGACURE® series), which

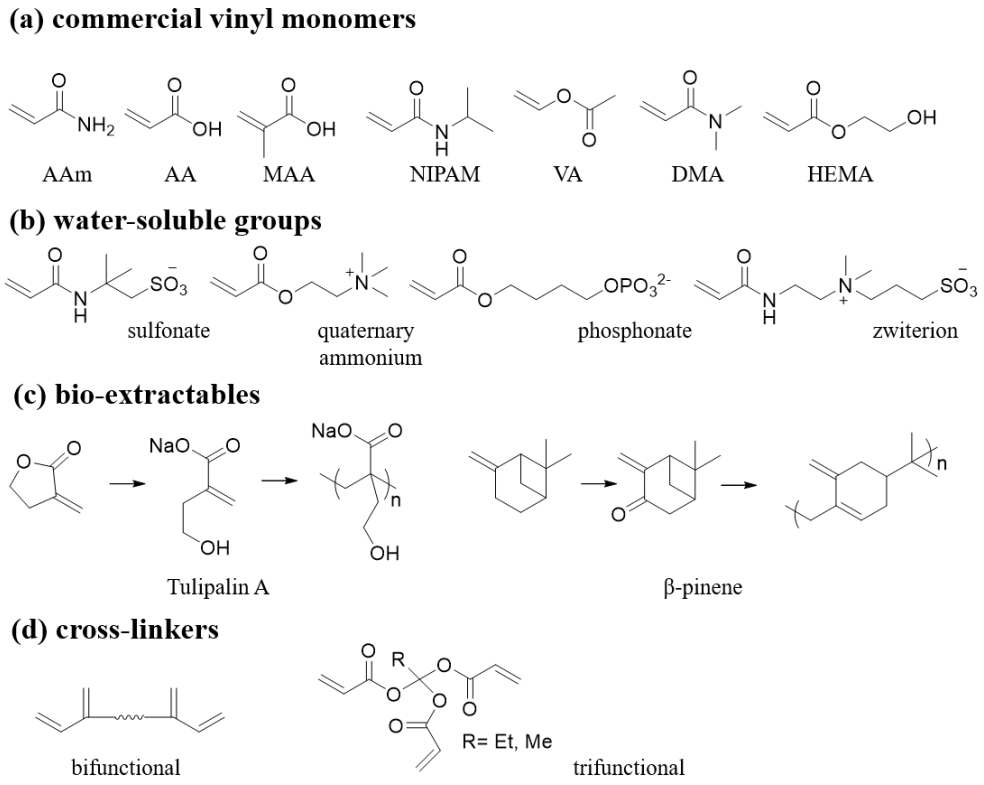

Figure I-5. Chemical structures of (a) commercial vinyl monomers, (b) monomers with water-soluble groups, (c) bioextractable monomers, (d) multifunctional cross-linkers

initiate polymerization after exposure to heat or light [57]. Redox reactions also form initiate polymerization after exposure to heat or light [58]. Redox reactions also form hydrogels without covalent cross-linking. During radical copolymerization of DMA and AA, aluminum oxide nanoparticles induced non-covalent cross-linking via secondary interactions, which gave rise to a three-dimensional colloidal array of nanocomposites that can be used to monitor the strain of materials via color change and can be applied for intraocular pressure tonometry or blood gas analysis (Fig I-6b) [59].

The acid group was also used for the selective detection of paracetamol, an analgesic drug, in an electrochemical sensor. Copolymerization of AA, AAm, and MBAm afforded a hydrogel matrix containing both acidic and basic groups, which prevented the denaturation of enzyme (polyphenol oxidase, PPO) incorporated in the matrix. The oxidation of paracetamol was monitored by cyclic voltammetry (Fig I-6c) [60] without covalent cross-linking. During radical copolymerization of DMA and AA, aluminum oxide nanoparticles induced non-covalent cross-linking via secondary interactions, which gave rise to a three-dimensional colloidal array of nanocomposites that can be used to monitor the strain of materials via color change and can be applied for intraocular pressure tonometry or blood gas analysis (Fig I-6b) [61]. The acid group was also used for the selective detection of paracetamol, an analgesic drug,

in an electrochemical sensor. Copolymerization of AA, AAm, and MBAm afforded a hydrogel matrix containing both acidic and basic groups, which matrix that selectively oxidizes paracetamol and senses it electrochemically prevented the denaturation of enzyme (polyphenol oxidase, PPO) incorporated in the matrix. The oxidation of paracetamol was monitored by cyclic voltammetry (Fig I-6c) [62].

In addition to radical polymerization, other chemical reactions that form diverse chemical linkages have been used for the preparation of hydrogels. Because radical polymerization is suitable for the construction of various polymer backbone structures, other bond-making reactions have been adopted for post-polymerization modification or cross-linking reaction via substitution or addition reactions. Among the reactions, condensation reactions are primarily used such as imine condensation. Imine bonds, specifically Schiff bases, are reversibly formed covalent bonds and can be easily controlled by an acid-catalyzed condensation reaction, eliminating a water molecule in the process [63].

I-3-2. Supramolecular Chemistry

Self-assembly is an efficient approach for the fabrication of a macroscopic, well-ordered, polymeric structure, with useful physical or chemical properties.

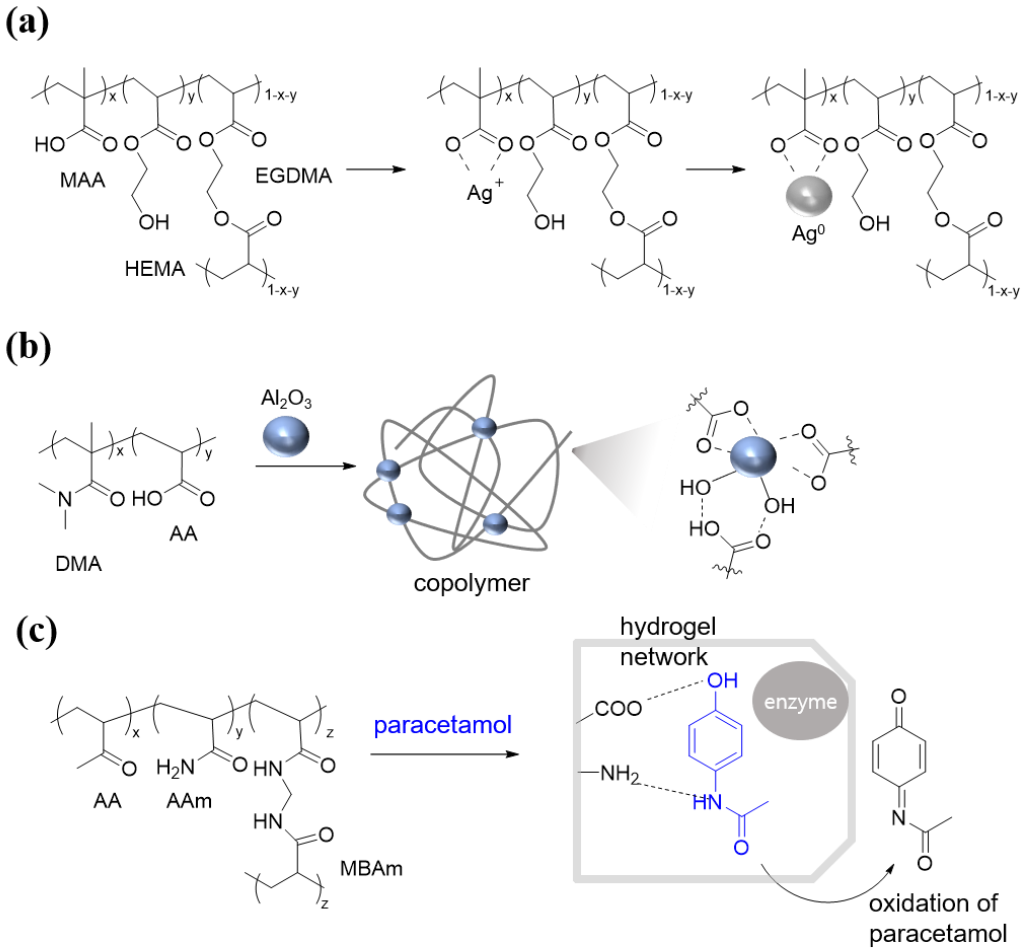

Figure I-6. (a) Chemical structure of hydrogel sensor, (b) non-covalent cross-linking of poly(N,N-dimethylacrylamide-co-acrylic acid) by aluminum oxide nanoparticles, (c) enzyme-incorporated hydrogel matrix that selectively oxidizes paracetamol and senses it electrochemically.

Small molecules or polymers are autonomously assembled under controlled conditions that are mostly dependent on concentration or temperature, thus forming assembled structures that contain microscopic, crystalline domains. The resulting hierarchical structures are subject to hydrogen bonding, π - π stacking, electrostatic interactions, or van der Waals interactions [64,65]. As an example, Das' group synthesized a small-molecule hydrogelator containing fluorescent pyrene, phenylalanine, and phenylboronic acid receptor moieties (Fig I-7a). The gelator exhibited thermo-reversible gelation properties in water, and was able to detect glucose based on changes in fluorescence [66]. Ma et al. prepared supramolecular hydrogels and investigated a reversible sol-gel transition induced by external stimuli [67]. A small-molecule gelator was synthesized from a benzimidazole derivative after functionalization with hydrazide, and further formed a hydrogel network through metal coordination with terbium(III) ions in water (Fig I-7b). The resulting hydrogel exhibited not only highly sensitive luminescence, but also thermo-reversibility in response to heat and pH. A multi-component hydrogel also was demonstrated by Yang et al. [68]. The system consists of a cationic organogelator and an anionic, low-molecular-weight dye. The resulting hierarchical structure can identify adenosine-phosphates. The addition of mono- or diphosphates such as AMP or ADP preserved the structure, although ion exchange occurred. However, in the case of the triphosphate ATP,

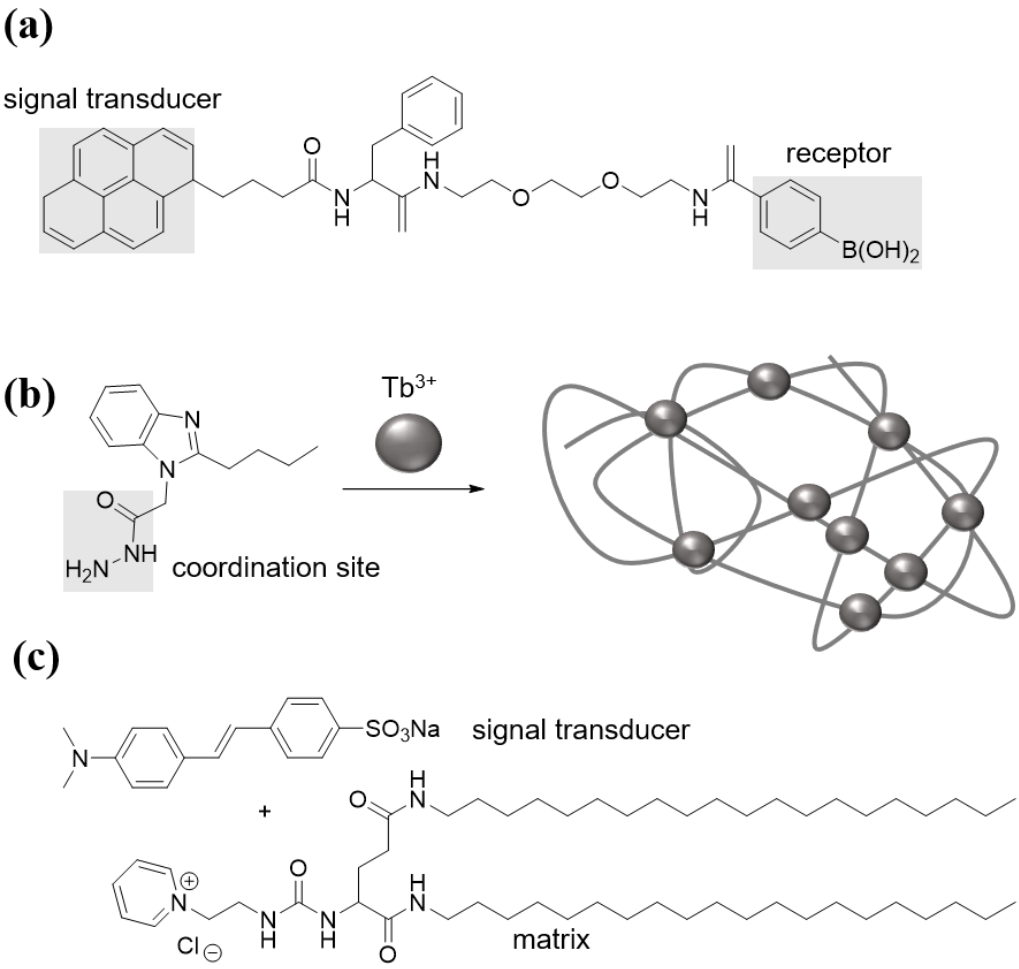

Figure I-7. Chemical structures of (a) phenylalanine-based hydrogelator that contains pyrene fluorophoreand phenylboronic acid receptor, (b) the benzimidazole-based gelatorthat contains a hydrazide group, (c) multicomponent-gelator with acationic gelator and an anionic methyl orange dye.

the structure collapsed rapidly, allowing the efficient detection of triphosphate with the unaided eye (Fig I-7c).

The crystallization of polymeric materials also induces dynamic physical cross-linking in three-dimensional networks, resulting in improved responsiveness to external stimuli by enhancing the mechanical properties of the hydrogel network. Zhang's group incorporated cellulose nanofibers (CNF) in situ into cellulose hydrogels. The polysaccharide fibers exhibited concentration-dependent gelation after loose chemical cross-linking, which further progressed to induce crystallization. Micro-fibrillated structures formed inside the gel via physical interactions. Therefore, they fabricated anisotropic, mechano-responsive hydrogels via a bottom-up approach, which switched on and off polarized light when an external force was applied.

I-3-3. Coordination bonds

Non-covalent interactions facilitate facile preparation or orthogonal synthetic methodologies, resulting in synergetic physical properties in hydrogel materials[69]. Coordination bonds or strong secondary bonds including hydrogen bonding or hydrophobic interaction are extensively used for this purpose. Among them, metal coordination is critical in the fabrication of diverse polymeric

hydrogels that typically include polysaccharides, for instance, alginate or κ-carrageenan. Such dynamic coordination bonding allows for easy synthesis and induces stimuli responsiveness, as well as reversibility to the hydrogel [70,71].

Melman's group designed light degradable hydrogels base on a natural alginate polysaccharide cross-linked with iron (III) cations [72]. The iron (III) cations undergo facile photoreduction to iron (II) cations in the presence of millimolar concentrations of sodium lactate. The formation of iron (II) causes a decrease in the ability to cross-link the alginate, which results in dissolution of the hydrogel. A long wavelength or visible light is used for photodegradation at a neutral pH. The mild condition for photodegradation and the high rate at which it occurs suggest that the hydrogel can be used as a light-controlled biocompatible scaffold (Fig I-8).

Another interesting example was reported by Liao et al. [73]. A hydrogel was fabricated using multiple non-covalent bonds (e.g., coordination bonds, hydrogen bonds, and π - π stacking,). These bonds were used as a design concept to build the entire structure and maximize the desirable properties of the hydrogel. The reversible coordination bond between the hydroxyl group and borate was responsible for the formation of a hydrogel matrix, and resulted in the self-healing properties of a fabricated sensor. Moreover, the inclusion of carbon

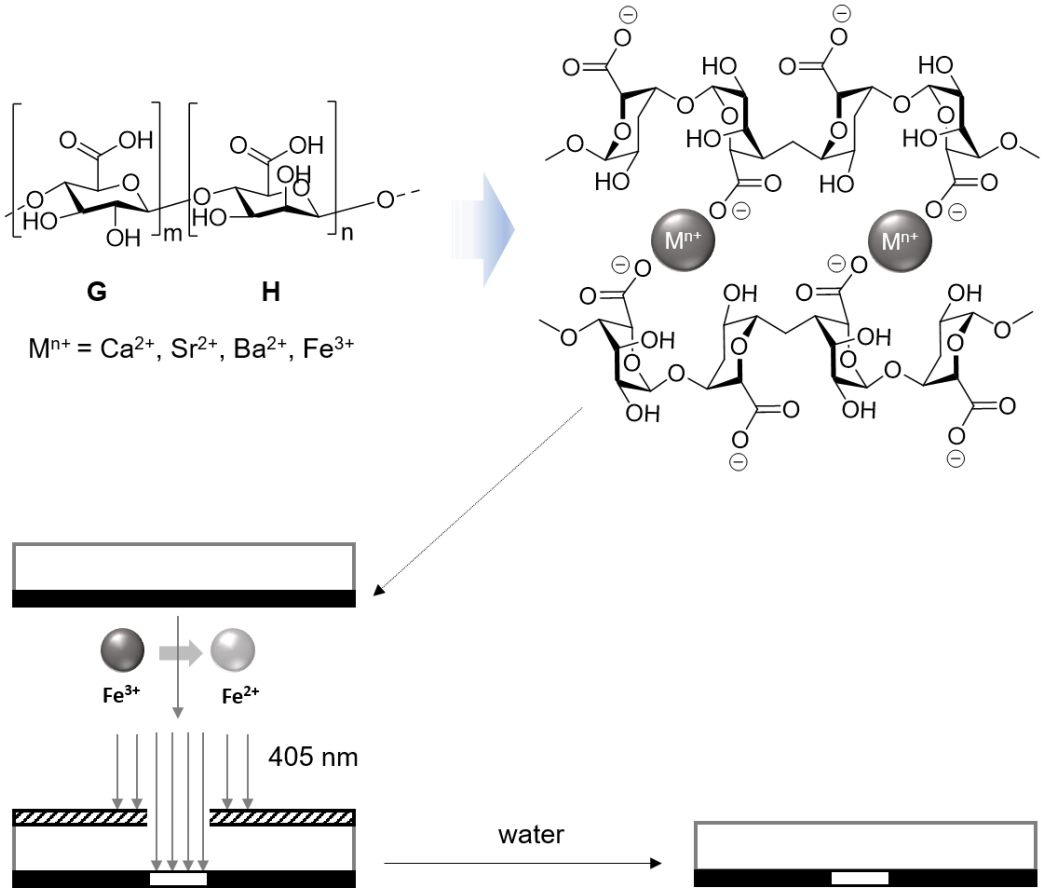

Figure I-8. Schematic representation of cross-linking of alginate using diverse metal cations and photodegradation process.

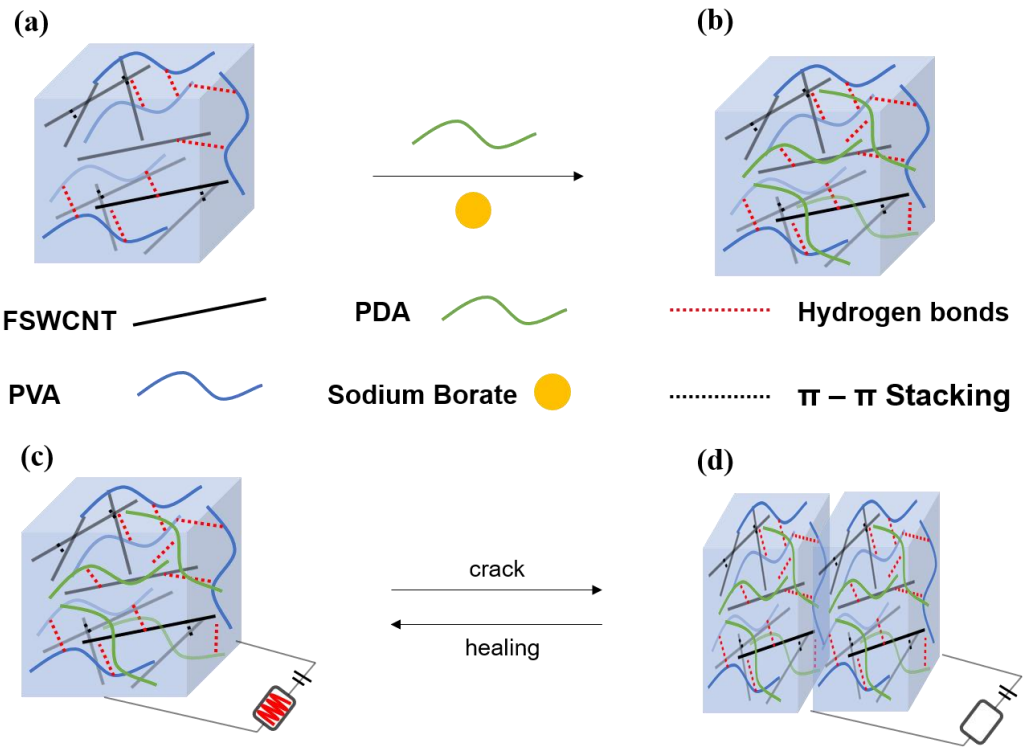

Figure I-9. Schematic representation of the fabrication of healable, adhesive, wearable, soft, human-motion sensors. (a, b) Fabrication of SWCNT-based networks obtained via dynamic supramolecular cross-linking using PDA and sodium borate. (c, d) The human-motion sensors can be assembled from the hybrid network.

adhesion facilitated the determination of the strain of the hydrogel material on nanotubes for enhanced electrical conductivity, and polydopamine for epidermal hydrogels and further be reversibly self-healed skin. Therefore, the developed multifunctional wearable sensor monitors the change in strain that arises from human motion (Fig I-9).

I-3-4. Double-network hydrogel

There is significant interest in double-network hydrogels due in part to their superior mechanical properties compared to conventional hydrogels. These hydrogels consist of two independent but reinforcing networks that form an interpenetrating structure, which is in contrast to dually cross-linked structures [74]. This material facilitates energy dissipation by network entanglement or sacrificial bonding, and thus exhibits outstanding mechanical strength, as first demonstrated by Gong et al. Furthermore, the orthogonal strategy not only provides efficient synthetic routes for the double-network structures but also facilitates tailor-made responses in these materials. As a result, these hydrogels present diverse functionalization, chemoselectivity to external stimuli, or reversible properties, due to their dynamic bonds and mechanical strength [75–79].

Li's group prepared double-network hydrogel using an ionically cross-linked κ-carrageenan network and a covalently cross-linked polyacrylamide network using a one-pot synthesis method. The resulting hydrogel exhibited good mechanical properties; for example, a high elastic modulus of 280 kPa, and a fracture energy of 6150 J/m^2. Due to thermoreversible aggregate and dissociation of κ-carrageenan, the hydrogel exhibited a recoverable property. The modulus and energy dissipation of deformed hydrogels could be recovered at almost 100% when stored at 90 °C for 20 min (Fig I-10a) [80].

Jung et al. recently demonstrated stimuli-responsive double-network hydrogels that are formed by sequential polymerization (Fig I-10b), and exhibit chemical transformation by selective de-cross-linking without structural failure, due to chemical orthogonality (Fig I-10c). Each self-immolated and thermoresponsive network was formed via a thiol-ene reaction and radical polymerization. The resulting hydrogel exhibited enhanced mechanical properties, but chemically transformed the selective de-cross-linking triggered by a molecular stimulus. The physical properties of the material, such as tunable toughness and lower critical solution temperature (LCST) behavior, are altered by the molecular stimulus. In addition, the hydrogel displayed thermo-responsive controlled-release [81].

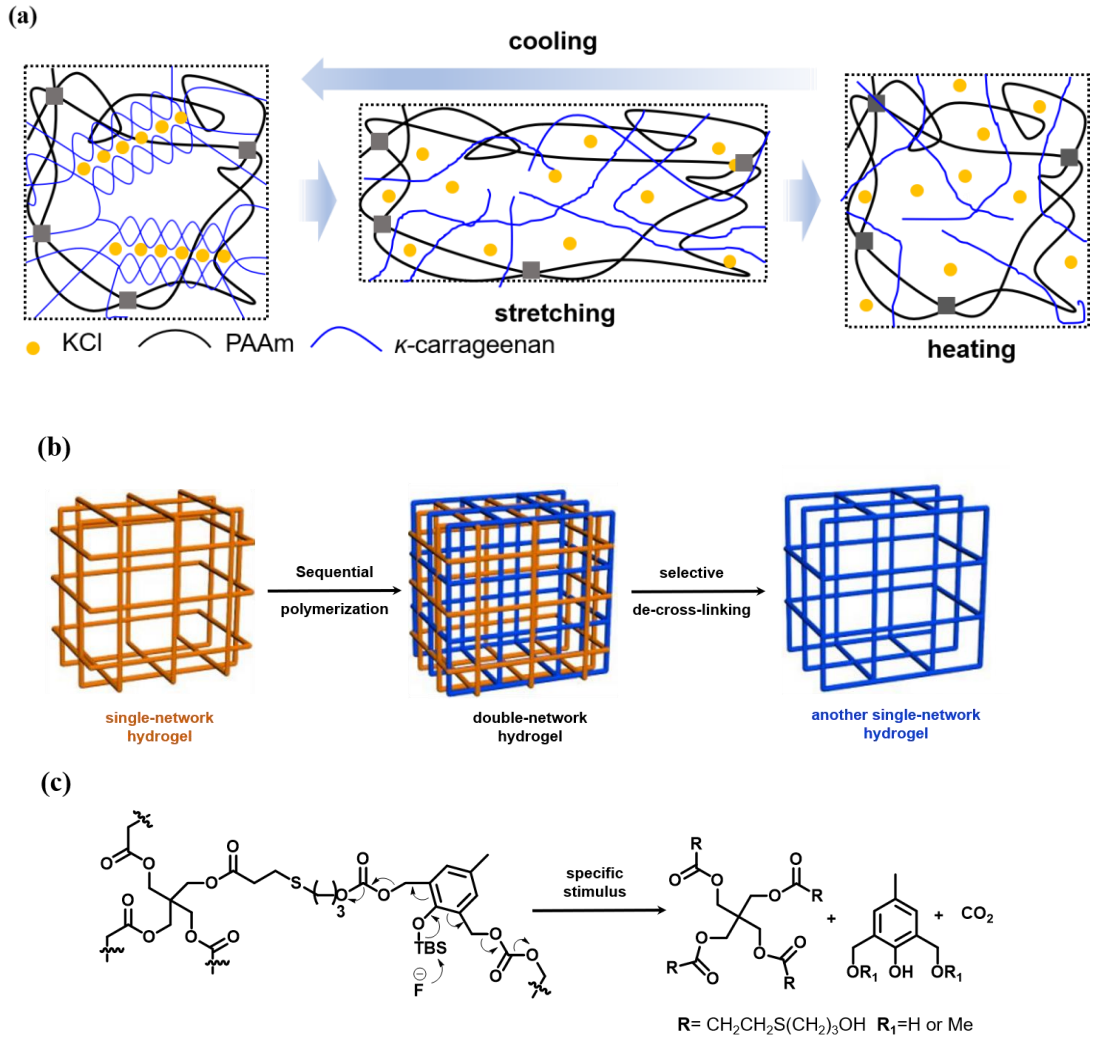

Figure I-10. (a) Schematic description of self-healable, double-network hydrogel. (b, c) Depiction of the preparation of self-immolative, double-network hydrogels via sequential polymerization (b) and their selective de-cross-linking in response to a specific stimulus via elimination reactions (c).

I-4. Aim and scope of this research

Stimuli-responsive hydrogels show the ability to change their physical and/or chemical properties upon exposure to various stimuli such as light, temperature, metal ions, humidity. These hydrogels can be prepared by various natural and synthetic materials. Free radicals polymerization is a mostly used process for the preparation of synthetic materials based on stimuli-responsive hydrogels.

I-4-1. Facile preparation of stimuli-responsive hydrogels via redox initiation system

Stimuli-responsive hydrogels were prepared by redox initiated radical polymerization in chapter II. The redox reaction between an amine and a persulfate group was used to polymerizing vinyl monomer under mild conditions. The prepared hydrogels show fluorescence in response to Al^{3+} that provides rapid detection and further advances when integrated with other properties. In chapter III, MoS_2-containing composite hydrogels were prepared. The MoS_2 promotes radical formation resulting in redox initiation for the polymerization of vinyl monomer under mild conditions and further provides a non-covalent cross-

linking point leading to the formation of a composite hydrogel. And resulting materials show self-healing ability owing to the reversible properties of the non-covalent cross-linking.

I-4-2. Facile fabrication method of bilayered hydrogels

Superabsorbent polymers contain a large amount of water within three-dimensional network. In chapter IV, a facile and green fabrication method of bilayered hydrogels base on superabsorbent polymers was demonstrated. The bilayered hydrogels show heterogeneous deformation underwater by controlling the cross-linking density. And the bilayered materials are consist of homogeneous chemical species. So The method enables low-cost, effort-saving fabrication through sequential racial polymerization in the aqueous condition .

I-5. References

[1] E. Caló and V. V. Khutoryanskiy, *Eur. Polym. J.*, 2015, **65**, 252.

[2] Q. Chai, Y. Jiao and X. Yu, *Gels*, 2017, **3**, 6.

[3] L. C. Lopérgolo, A. B. Lugão and L. H. Catalaini, *J. Appl. Polym. Sci.*, 2002, **86**, 662.

[4] S.M.F. Kabir, P.P. Sikdar, B. Haque, M.A.R. Bhuiyan, A. Ali and M.N. Islam, *Prog. Biomater.*, 2018, **7**, 153.

[5] J.-Y. Sun, X. Zhao, W.R.K. Illeperuma, O. Chaudhuri, K.H. Oh, D.J. Mooney, J.J. Vlassak and Z. Suo, *Nature*, 2012, **489**, 133.

[6] Y. Zhu, J. Zhang, J. Song, J. Yang, Z. Du, W. Zhao, H. Guo, C. Wen, Q. Li, X. Sui and L. Zhang, *Adv. Funct. Mater.*, 2019, 1905493.

[7] Z. Deng, Y. Guo, X. Zhao, P. X. Ma, and B. Guo, *Chem. Mater.*, 2018, **30**, 1729**.**

[8] C. Ma, W. Lu, X. Yang, J. He, X. Le, L. Wang, J. Zhang, M. J. Serpe, Y. Huang and T. Chen, *Adv. Funct. Mater.*, 2017, **28**, 1704568.

[9] N. Adrus and M. Ulbricht, *J. Mater. Chem.*, 2012, **22**, 3088.

[10] S. Naahidi, M. Jafari, M. Logan, Y. Wang, Y. Yuan, H. Bae, B. Dixon and P. Chen, *Biotechnol. Adv.*, 2017, **35**, 530.

[11] R. Takahashi, T. Ikai, T. Kurokawa, D. R. King and J. P. Gong, *J. Mater. Chem. B.,* 2019, **7**, 6347.

[12] X.-H. Wang, F. Song, D. Qian, Y.-D. He, W.-C. Nie, X.-L. Wang and Y.-Z. Wang, *Chem. Eng. J.*, 2018, **349**, 588.

[13] Y. Hou, C. Chen, K. Liu, Y. Tu, L. Zhang and Y. Li, *RSC. Adv.,* 2015, **5**, 24023.

[14] Y. Yang, S. Song and Z. Zhao, *Colloids and Surf A Physicochem. Eng. Asp.*, 2017, **513**, 315.

[15] L. Li, B. Yan, J. Yang, L. Chen and H. Zeng, *Adv. Mater.,* 2015, **27**, 1294.

[16] Z. Gu, L. Chen, Y. Xu, Y. Liu, Z. Zhao, C. Zhao, W. Lei, Q. Rong, R. Fang, T. Zhao and M. Liu, *ACS Appl. Mater. Interfaces.,* 2018, **10**, 4161.

[17] Y. Yang, X. Wang, F. Yang, L. Wang and D. Wu, *Adv. Mater.*, 2018, **30**, 1707071.

[18] P. Sun, H. Zhang, D. Xu, Z. Wang, L. Wang, G. Gao, G. Hossain, J. Wu, R. Wang and J. Fu, *J.Mater. Chem. B.*, 2019, **7**, 2619.

[19] Y. Liu, J. Liu, H. Yang, K. Liu, R. Miao, H. Peng and Y. Fang, *Soft Matter*, 2018, **14**, 7950.

[20] F. Yu, X. Cao, J. Du, G. Wang and X. Chen, *ACS Appl. Mater. Interfaces.*, 2015, **7**, 24023.

[21] X. Zhang, Y. Yang, J. Yao, Z. Shao and X. Chen, *ACS. Sustain. Chem. Eng.,* 2014, **2**, 1318.

[22] H. Liu, L. Rong, B. Wang, R. Xie, X. Sui, H. Xu, L. Zhang, Y. Zhong and Z. Mao, *Carbohydr. Polym.,* 2017, **176**, 299.

[23] S. Sekine, Y. Ido, T. Miyake, K. Nagamine and M. Nishizawa, *J. Am. Chem. Soc.,* 2010, **132**, 13174.

[24] M. Chen, G. Gong, L. Zhou and F. Zhang, *RSC Adv.,* 2017, **7**, 21476.

[25] J. Pang, M. Wu, X. Liu, B. Wang, J. Yang, F. Xu, M. Ma and X. Zhang, *Sci. Rep.,* 2017, **7**, 13233.

[26] P. Sautrot-Ba, N. Razza, L. Breloy, S. A. Andaloussi, A. Chiappone, M. Sangermano, C. Hélary, S. Belbekhouche, T. Coradin and D.-L. Versace, *J. Mater. Chem. B.*, 2019, **7**, 6526.

[27] D. Zhai, B. Liu, Y. Shi, L. Pan, Y. Wang, W. Li, R. Zhang and G. Yu, *ACS Nano,* 2013, **7**, 3540.

[28] H. Dai, Y. Huang, Y. Zhang, H. Zhang and H. Huang, *Cellulose*, 2019, **26**, 3825.

[29] P. Zhao, K. Wei, Q. Feng, H. Chen, D. S. H. Wong, X. Chen, C.-C. Wu and L. Bian, *Chem. Commun.,* 2017, **53**, 12000.

[30] B. C. Melo, F. A. A. Paulino, V. A. Cardoso, A. G. B. Pereira, A. R. Fajardo and F. H. A. Rodrigues, *Carbohydr. Polym.,* 2018, **181**, 358.

[31] K. Saini, *PharmaTutor*, 2017, **5(1)**, 27.

[32] K. M. Lee, H. J. Kim, D. Jung, Y. Oh, H. Lee, C. Han, J. Y. Chang and H. Kim, *ACS Omega*, 2018, **3**, 3096.

[33] D. P. Browe, C. Wood, M. T. Sze, K. A. White, T. Scott, R. M. Olabisi and J. W. Freeman, *Polymer,* 2017, **117**, 331.

[34] D. Buenger, F. Topuz and J. Groll, *Prog. Polym.Sci.,* 2012, **37**, 1678.

[35] C. Alvarez-Lorenzo, B. Blanco-Fernandez, A. M. Puga and A. Concheiro, *Adv. Drug. Deliv. Rev.*, 2013, **65**, 1148.

[36] A. Galperin, T. J. Long and B. D. Ratner, *Biomacromolecules,* 2010, **11**, 2583.

[37] K. Zhang, W. Wu, K. Guo, J. Chen and P. Zhang, *Langmuir*, 2010, **26**, 7971.

[38] Cheaburu-Yilmaz, Yilmaz, Kose and Bibire, *Polymers,* 2019, **11**, 1432.

[39] J. P. Gong, Y. Katsuyama, T. Kurokawa and Y. Osada, *Adv. Mater.,* 2003, **15**, 1155.

[40] K. M. Lee, Y. Oh, J. Y. Chang and H. Kim, *J. Mater. Chem. B.,* 2018, **6**, 1244.

[41] T. Segura, B. C. Anderson, P. H. Chung, R. E. Webber, K. R. Shull and L. D. Shea, *Biomaterials,* 2005, **26**, 359.

[42] J. Cao, J. Li, Y. Chen, L. Zhang and J. Zhou, *Adv. Funct. Mater.,* 2018, **28**, 1800739.

[43] N. Nandi, K. Gayen, S. Ghosh, D. Bhunia, S. Kirkham, S. K. Sen, S. Ghosh and I. W. Hamley, A. Banerjee, *Biomacromolecules,* 2017, **18**, 3621.

[44] A. Baral, S. Basak, K. Basu, A. Dehsorkhi, I. W. Hamley and A. Banerjee, *Soft Matter,* 2015, **11**, 4944**.**

[45] D. Ye, P. Yang, X. Lei, D. Zhang, L. Li, C. Chang, P. Sun and L. Zhang, *Chem, Mater.,* 2018, **30**, 5175.

[46] Y. Ren, Y. Zhang, W. Sun, F. Gao, W. Fu, P. Wu and W. Liu, *Polymer,* 2017, **126**, 1.

[47] E. P. Chan, Y. Hu, P. M. Johnson, Z. Suo and C. M. Stafford, *Soft Matter,* 2012, **8**, 1492.

[48] M. Abbas, R. Xing, N. Zhang, Q. Zou and X. Yan, *ACS Biomater. Sci. Eng.,* 2017, **4**, 2046.

[49] L. Zhu, J. Qiu and E. Sakai, *RSC Adv.*, 2017, **7**, 43755**.**

[50] G. Su, T. Zhou, X. Liu and Y. Ma, *Poly. Chem.,* 2017, **8**, 865.

[51] M. Zhong, Y.-T. Liu, X.-Y. Liu, F.-K. Shi, L.-Q. Zhang, M.-F. Zhu and X.-M. Xie, *Soft Matter,* 2016, **12**, 5420.

[52] M. P. Algi and O. Okay, *Eur. Polym. J.*, 2014, **59**, 113.

[53] H. He, Z. Xiao, Y. Zhou, A. Chen, X. Xuan, Y. Li, X. Guo, J. Zheng, J. Xiao and J. Wu, *J. Mater. Chem. B*, 2019, **7**, 1697.

[54] S. L. Banerjee, K. Bhattacharya, S. Samanta and N. K. Singha, *ACS Appl. Mater. Interfaces*, 2018, **10**, 27391.

[55] N. Peng, Y. Wang, Q. Ye, L. Liang, Y. An, Q. Li and C. Chang, *Carbohy. Polym.*, 2016, **137**, 59.

[56] R.Barbey and H.-A. Klok, *Langmuir.*, 2010, **26**, 18219.

[57] H. Yuk, T. Zhang, S. Lin, G. A. Parada and X. Zhao, *Nat. Mater.*, 2015, **15**, 190**.**

[58] C. Huang, Y. Li, L. Duan, L. Wang, X. Ren and G. Gao, *RSC Adv.*, 2017, **7**, 16015.

[59] W.Yang, H. Xue, W.Li, J. Zhang, J. Jiang and S. Pursuing, *Langmuir* 2009, **25**, 11911.

[60] A. Aliabadi, G.H. Rounaghi, M.H.A. Zavar, *Sens. Actuators B chem.*, 2017, **241**, 182.

[61] M. Vahedi, J. Barzin, F. Shokrolahi and P. Shokrollahi, *Macromol. Mater. Eng.*, 2018, **303**, 1800200**.**

[62] R. Dong, Y. Pang, Y. Su and X. Zhu, *Biomater. Sci.,* 2015, **3**, 937.

[63] K. Wei, X. Chen, P. Zhao, Q. Feng, B. Yang, R. Li, Z.-Y. Zhang and L. Bian, *ACS Appl. Mater. Interfaces,* 2019, **11**, 16328.

[64] D. Mandal, S.K. Mandal, M Ghosh, and P.K. Das, *Chem. Eur. J,*.2015, **21,** 12042.

[65] X. Ma, D. Yu, N. Tang and J. Wu, J. *Dalton Trans.,* 2014, **43**, 9856.

[66] D. Yang, C. Liu, L. Zhang, L. and M. Liu, *Chem. Commun.*, 2014, **50**, 12688.

[67] S. Y. Zheng, H. Ding, J. Qian, J. Yin, Z. L. Wu, Y. Song and Q. Zheng, *Macromolecules*, 2016, **49**, 9637.

[68] E.S. Dragan, *Chem. Eng. J.,* 2014, **243**, 572–590.

[69] D. E. Fullenkamp, L. He, D. G. Barrett, W. R. Burghardt and P. B. Messersmith, *Macromolecules*, 2013, **46**, 1167.

[70] Y. Si, L. Wang, X. Wang, N. Tang, J.Yu and B.Ding, *Adv. Mater.*, 2017, **29**,1700339.

[71] M. Liao, P. Wan, J. Wen, M. Gong, X. Wu, Y. Wang, R. Shi and L. Zhang, *Adv. Funct. Mater.*, 2017, **27**, 1703852.

[72] Q. Chen, H. Chen, L. Zhu, and J. Zheng, *J. Mater. Chem. B,* 2015, **3**, 3654**.**

[73] E. N. Kitiri, C. S. Patrickios, C. Voutouri, T. Stylianopoulos, I. Hoffmann, R. Schweinsd and M. Gradzielskic, *Polym. Chem.*, 2017, **8**, 245.

[74] X. Zhang, J. Wang, H. Jin, S. Wang and W. Song, *J. Am. Chem. Soc.*, 2018, **140**, 3186.

[75] W. J. Zheng, N. An, J. H. Yang, J. Zhou and Y. M. Chen, *ACS Appl. Mater. Interfaces*, 2015, **7**, 1758.

[76] J. Zhu, S. Guan, Q. Hua, G. Gao, K. Xu and P. Wang, *Chem.Eng. J.*, 2016, **306**, 953.

[77] Y. Tian, X. Wei, Z. J Wang, P. Pan, F. Li, D. Ling, Z. L. Wu and Q. Zheng, *ACS Appl. Mater. Interfaces*, 2017, **9**, 34349.

[78] Z. Wang, H. Zhou, W. Chen, Q. Li, B. Yan, X. Jin, A. Ma, H. Liu, W. Zhao, *ACS Appl. Mater. Interfaces*, 2018, **10**, 14045.

[79] Z.Wang, H. Zhou, W. Chen, Q. Li, B. Yan, X. Jin, A. Ma, H. Liu and W. Zhao, *Carbohydr. Polym.*, 2015, **132**, 490.

[80] S. Liu and L. Li, *ACS Appl. Mater. Interfaces*, 2016, **8**, 29749.

[81] D. Jung, K. M. Lee, J. Y. Chang, M. Yun, H.-J. Choi, Y. A. Kim, H. Yoon and H. Kim, *ACS Appl. Mater. Interfaces*, 2018, **10**, 42985.

Chapter II.

Facile fluorescent labeling of a polyacrylamide-based hydrogel film via radical initiation enablesselective and reversible detection

* This work presented in Chapter II was published in *J. Mater. Chem. B*, **6**, 1244(2018) entitled, "Facile fluorescent labeling of a polyacrylamidebased hydrogel film via radical initiation enables selective and reversible detection of Al^{3+}"

II-1. Introduction

Hydrogels capable of responding to external stimuli are of everincreasing interest because they offer potential in the development of new responsive systems based on their general yet crucial properties of elasticity, volumetric change, storage capability, and chemical diversification [1,2]. Stimuli-responsivehydrogels have shown distinct, programmable changes in shape, colour, mechanical strength, adhesion, refractive index, and permeability in response to pH, ions, light, temperature or chemical analytes due to physically or chemically cross-linked 3D networks that contain large amounts of water [3-7] . When fabricated as films, the smart hydrogels further exhibit remarkablecharacteristics: (i) rapid response, (ii) high loading capacities, (iii) enhanced interfacial interactions, (iv) versatility for various applications, and (v) anisotropic shape changes during their use as regulators, catalysts, sensors, or actuators[8–10].

Recently, from the perspective of synthetic chemistry, functional hydrogel materials have been achieved using sophisticated dynamic bonding including hydrogen bonds, ionic bonds, host–guest chemistry, hydrophobic interactions, and coordination bonds [11]. However, a vastmajority of hydrogelmaterials are still synthesized via free-radical polymerization, which facilitates the accessible,

economical, and large-scale synthesis of various waterborne materials. In this regard, the radical polymerization reaction can be considered that can be readily initiated by the redox reaction between amine and persulfate functional groups, which provides a facile preparation route for stimuli-responsive hydrogel films.

The amine–persulfate system is effective in polymerizing vinyl monomers under aqueous conditions. The amine group induces a redox reaction with persulfate to generate radicals on both amine and sulfate (i.e., redox initiators) via electron transfer; this initiates the polymerization reaction. To date, N,N,N',N'-tetramethylethylenediamine (TEMED), containing tertiary amines, has been extensively used for redox-initiated polymerization for preparing functional polymeric materials[12–17]. Feng et al. by amechanistic study comprehensively demonstrated that other amines, including secondary amines, also promote the polymerization of monomers such as acrylamide or acrylic acid[18-20].

The redox initiation system consisting of an amine and a persulfate group can be very useful for the synthesis of amino groupfunctionalized polymeric materials under mild conditions [21-27]. In this study, A transparent and stretchable stimuliresponsive hydrogel film that shows fluorescence in response to Al^{3+} was reported. The fluorescent film was easily synthesized via the redoxinitiated polymerization of acrylamide with a rhodamine-based probe

containing a secondary amine. Rhodamine derivatives have been widely used as chemosensors that transduce analyteinduced structural changes into photophysical responses. In thespirolactam form, rhodamine-based molecules are colourless and non-fluorescent, but the addition of metal ions alters the structure to a ring-opened form, showing colour and fluorescence [28,29]. Herein, the probe in the film detects Al^{3+} ions, which inhibit the ingestion of other essential metal ions and, with excessive intake, cause diseases such as bone softening, anemia, idiopathic Parkinson's disease, and Alzheimer's disease [30,31]. Therefore, the rhodamine-based probe performs dual roles in the hydrogel film by (i) promoting the reaction for fabricating the material and (ii) acting as a fluorogenic probe for the selective, sensitive detection of Al^{3+}. The turn-on type fluorescent system provides rapid detection, involves a binding event that increases sensitivity and selectivity, and further advances when integrated with other properties such as large Stokes shift[32,33].

Further exposure to ethylenediaminetetraacetic acid (EDTA) enables reversible on–off fluorescence switching of the probe in the film that is necessary for practical use. Therefore, fabricated and resulting material not only (i) facilitates selective, reversible sensing of Al^{3+}, but also (ii) demonstrates a facile, one-step synthesis of hydrogel, and a heterogeneous sensing system that enables (iii) recycling of material and (iv) potential removal of Al^{3+} in aqueous

environments. In addition, (v) the preparation of the film would suggest an efficient method to implant functional, less-water-soluble probes into hydrophilic matrices, allowing various investigations under aqueous conditions.

II-2. Experimental Section

Materials.

All reagents used were purchased commercially and used as received unless otherwise noted. The rhodamine probe 1 was synthesized as described before [34]. The precursors of 3-formyl-2-hydroxybenzoic acid [35] and 2-amino-3',6'-bis(ethylamino)-2',7'-dimethylspiro[isoindoline-1,9'-xanthen]-3-one were synthesized by the following previously reported procedures [36].

Preparation of the stimuli-responsive hydrogel film

Stimuli-responsive hydrogel films were prepared by redoxinitiated radical polymerization. To a solution of acrylamide 2 (1.0 g, 14 mmol, 4000 equiv.) and triethylene glycol diacrylate 3 (20 mg, 0.078 mmol, 20 equiv.) in water (4 mL), compound 1 (2.1 mg, 3.7 mmol, 1.0 equiv.) in water (5 mL) was added. Themixture was degassed by bubbling with N_2 for 1 h. Then, a solution of potassium persulfate (2.0 mg, 7.4 mmol, 2.0 equiv.) in water (1 mL) and a few drops of 1 M NaOH in water were addeddropwise to the mixture, and a solution with a pH value of approximately 6 was obtained. After this, the reaction solution was poured into a glass mold with a size of 100 mm x 75 mm x 1mm.

(width x length x thickness) and left at rt for 6 h for polymerization. A free-standing hydrogel film was obtained after polymerization and purified by gentle stirring in water for 1 h.

Selectivity test

Chloride salts of metal ions (K^+, Ca^+, Li^+, K^+, Na^+, Ni^{2+}, Zn^{2+}, Co^{2+}, Tb^{3+}, and Fe^{3+}) were dissolved in a 1 : 1 ethanol–water mixture (10 mL) at a concentration of 1.5 mM. The as-prepared hydrogel films were cut into small pieces (size, 10 mm x 10 mm x 1 mm) and washed with water. Then, the hydrogel films were exposed to the metal ion solutions for 30 min and rinsed with 1 : 1 aqueous ethanol. The emission spectra were obtained under excitation at 500 nm.

Reversible on–off fluorescence switching test

To a solution of ethylenediaminetetraacetic acid (EDTA; 0.29 g, 1.0 mmol, 1.0 equiv.) in water (23 mL), 2 M NaOH in water (2 mL) and ethanol (25 mL) were added dropwise in sequence. The film sample (size, 10 mm x 10 mm x 1mm)was pre-exposedto a 1.5 mM Al3+ solution (50 mL), rinsed with 1 : 1

aqueousethanol, and immersed in the EDTA solution for 30 min. After rinsing with aqueous ethanol, the emission spectra of the films were obtained under excitation at 500 nm. The films were then re-exposed to the Al3+ solution for 30 min and rinsed with the ethanol solution again to monitor the repeated on–off fluorescence response.

Instrumentation

Proton nuclear magnetic resonance (1H NMR) spectra were recorded using Bruker 300 MHz NMR spectrometers at 25 °C. Proton chemical shift are expressed in part per million (ppm, δ scale) and are referenced to tetramethylsilane ((CH3)4Si 0.00 ppm) or to residual protium in the solvent ($CDCl_3$, δ 7.26 ppm, DMSO, δ 2.51 ppm, and D_2O, δ 4.70 ppm). Date are represented as follows: chemical shift, multiplicity (s = singlet, d = doublet, t = triplet, q = quartet, m= multiplet and/or multiple resonances, br = broad peak), integration. For the tensile test, as-prepared hydrogel films were cut using a laser cutter. The films were glued between two PMMA clamps with a superglue following a similar manner previously reported.1 The resulting specimens have a size of 10 mm × 5 mm × 1 mm (length × width × thickness). Uniaxial tensile tests were performed using Instron 5543 universal testing machine (UTM) with a

1000-N load cell at 25 °C in air. The specimens were stretched at a rate of 5 mm/min until the samples were broken. Each hydrogel film sample was triplicated during the measurement. The stress-strain curve was recorded. The ultimate tensile strength was determined as the stress at the breaking point. The ultimate strain was determined as the strain at the breaking point. Young's modulus was obtained from the initial slope of the stress-strain curve in the strain range of 10–30%. Toughness was taken from the area under the stress-strain curve. Dynamic rheological experiments were carried out on a TA Instruments AR 2000 rheometer using 20-mm cone and plate configuration. The specimen was tested in frequency sweep mode (from 0.1 rad/s to 100 rad/s).

Tensile test of hydrogel films

The elastic modulus and toughness were calculated from the initial slope (strain range of 10–30%) and the area under stress–strain curve, respectively. Each film type was tested in triplicate; the average and standard deviations from this set were plotted.

Model Reaction for Redox-Initiated Polymerization

Acrylamide 2 (1.0 g, 14 mmol, 1.0 equiv) and N-methylaniline 4 (40 mg, 0.28 mmol, 0.02 equiv) were dissolved in water (8 mL). After the mixture solution was sonicated for 30 min and degassed by bubbling with N2, a solution of potassium persulfate (76 mg, 0.28 mmol, 0.02 equiv) in water (2 mL) was added to the mixture dropwise by syringe. Then, the solution mixture was left at rt for 6h for polymerization. The resulting product was isolated by precipitation in methanol. The polymer 5 was purified by redissolving in water and reprecipitating by addition of methanol, and obtained as a white powder. Yield, 75%.

Control Polymerization Initiated by Rhodamine 6G

Acrylamide 2 (0.5 g, 7.03 mmol) and rhodamine 6G (0.9 mg, 1.8 μmol) were dissolved in water (5 mL). After degassing with N2 bubbles for 1 h, potassium persulfate (KPS; 1 mg, 3.7 μmol) were added to the solution. After incubation for 2 h at rt, the storage and loss moduli of the polymerizing solution were measured by an oscillatory rheometer.

Effect of Cross-Linker on Mechanical Strength

The hydrogel films containing different amounts of 3 were prepared by following the procedure reported in the experimental section in the main text (for the 2 wt% film) except for using different amounts of 3. Quantities of 3 required for the fabrication of hydrogel films: For the 1 wt% film, 10 mg (0.039 mmol) of 3 was incorporated. For the 3 wt% film, 30 mg (0.117 mmol); for the 4 wt% film, 40 mg (0.156 mmol); for the 8 wt% film, 80 mg (0.312 mmol).

Fluorescence measurement

For test, hydrogel films were cut into the same size (width × length × thickness, 10 mm × 10 mm × 1 mm). After wishing with water for 30 min, the films were immersed for 30 min into solutions of Al^{3+} in an aqueous ethanol (1:1, v/v) having different concentrations.After rinsing with the ethanol solution, the emission spectra were measured under excitation at 500 nm. The limit of detection was calculated as 3 × (SD/m) where SD means standard deviation of the blank and m means the slope of the initial linear region.

II-3. Results and Discussion

II-3-1. Synthesis and Characterization of hydrogel fim

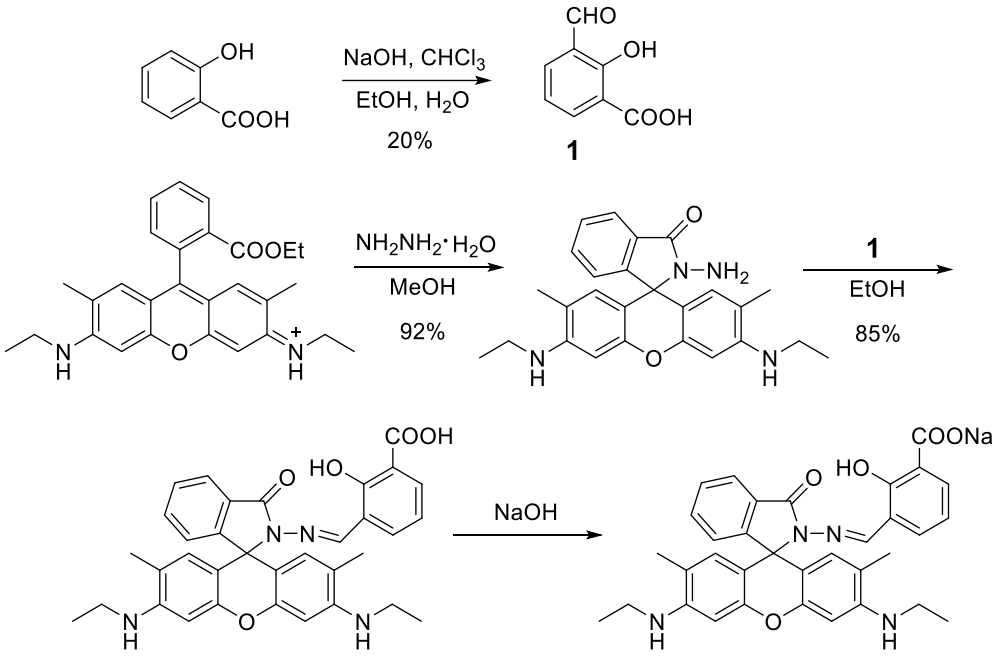

Scheme II-1. Synthetic route to the probe 1

Scheme II-3 shows the synthetic route for probe 1. And fig II-1 shows the facile preparation of the stimuli-responsive hydrogel film from acrylamide (2) and triethylene glycol diacrylate (3) in water via room-temperature, radical polymerization initiatedby the redox reaction of potassium persulfate (KPS) with therhodamine derivative 1. KPS is a common water-soluble initiator for vinyl

polymerization. In an aqueous solution, the initiator forms a dianion, which further dissociates to provide radicals at temperatures >50 ℃. However, in the presence of amine functional groups, the initiation of polymerization can be accelerated through the amine–persulfate redox reaction; the resulting amino radicals react with the monomers during polymerization. Themechanism of redox-initiated polymerization was well-studied by Feng et al [18-20]. and found to be effective for vinyl monomers including 2 under aqueous conditions. Herein, 1, containing a secondary amine that promotes the initiation with KPS, has been used and monomer 2 and cross-linker 3 in water at rt for 6 h were polymerized. This simple synthetic route yielded a clear, stretchable, and large-scale hydrogel film. Furthermore, 1 acted as a fluorogenic chemosensor for Al^{3+}. In response to the metal ions, 1 in the spirolactam structure transformed to the ring-opened form in the hydrogel matrix, translating the chemical signal (metal ions) into a fluorescence signal. Moreover, the addition of EDTA removed the coordinated Al^{3+}, and the ring-opened structure was simultaneously returned to spirolactam; this led to reversible on–off fluorescence sensing by the hydrogel matrix.

The waterborne, polyacrylamide film was fabricated in a onestep-reaction. A solution of the amine probe 1, KPS, monomer 2, and cross-linker 3 in water was confined by deposition between two planar glass substrates with 1.0 mm-thick spacers and polymerized in situ. As designed, the aniline moiety in 1

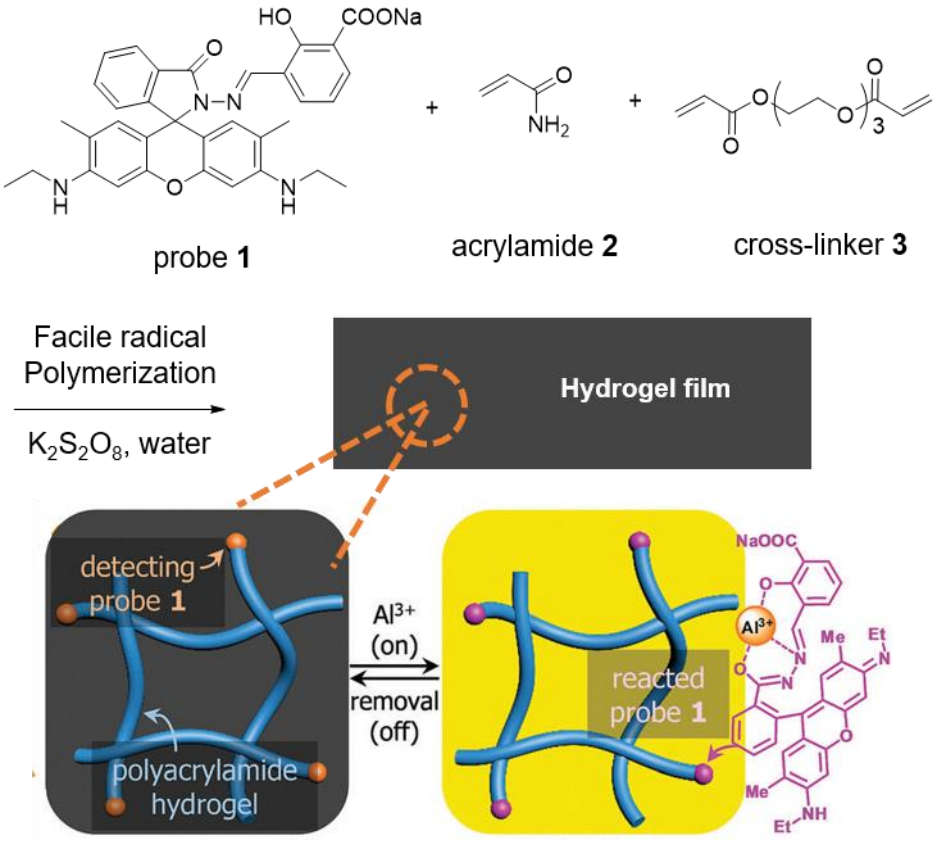

Figure II -1. Schematic of the preparation of a stimuli-responsive hydrogel film.

underwent a redox reaction with KPS, which subsequently polymerized 2 and 3 at a time, providing a transparent hydrogel film after incubation for 6 h at rt. For film fabrication, 1 and 2 at a molar ratio of 1 : 4000 (monomer concentration, 2.8 M) have been consistently incorporated. When a ratio of 1 : 8000 (1.4 M) was used, polymerization was too sluggish to handle; a ratio of 1 : 2000 (5.6 M) resulted in probe 1 not being thoroughly soluble in the monomer solution. The polymerization reaction initiated from the probe and transparency of the resulting film supports the homogeneous distribution of 1. Another monomer of acrylic acid instead of 2 was tested, but 1 showed low solubility in water in the presence of acrylic acid. Furthermore, a sodium acrylate monomer (100% degree of neutralization of acrylic acid) was used under the same conditions, but the obtained film experienced large volumetric changes in air and was thusinappropriate for further measurements [37].

a simple model polymerization reaction have conducted to support the amine–persulfate system that causes the redoxinitiated radical polymerization of 2 in water during the fabrication of the hydrogel film. Figure II-2a shows the schematic of the control polymerization reaction using N-methylaniline (4) and 2 to yield polymer 5 in the presence of KPS in water at rt. Feed molar ratio of 4/KPS/2 = 1: 1 : 50 was intentionally used a to prepare 5 with a low molecular

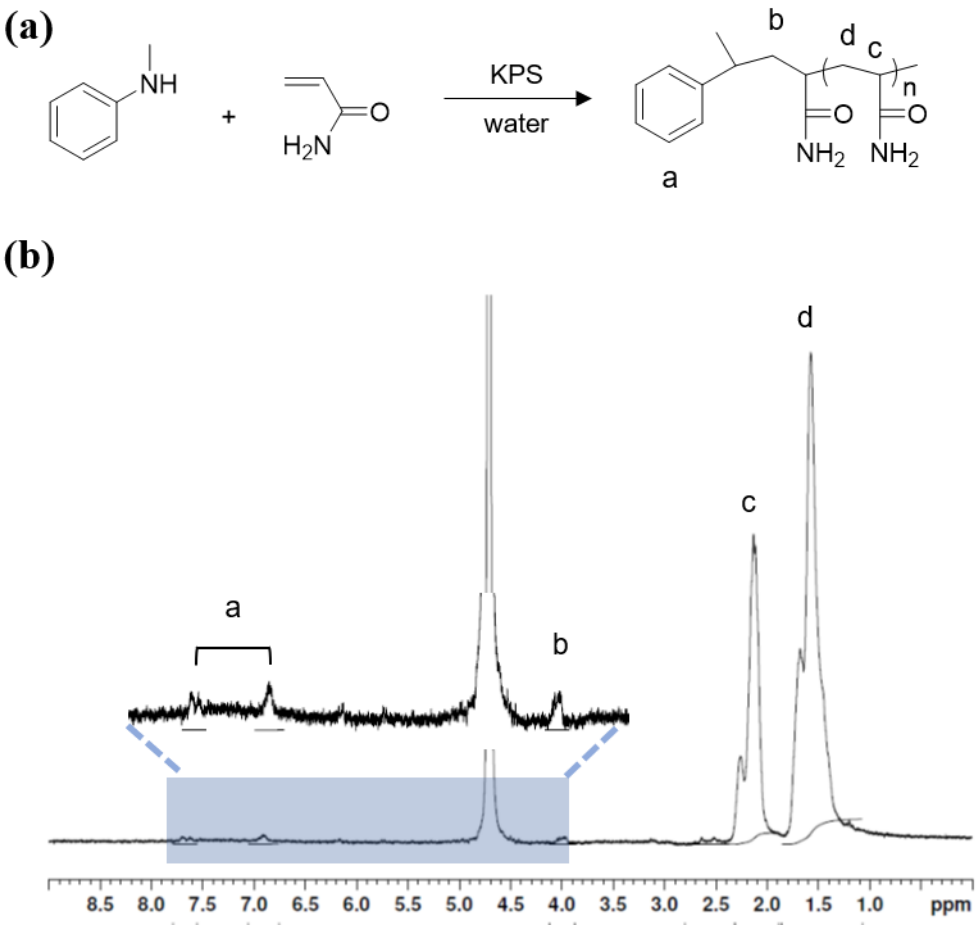

Figure II -2. (a) Schematic of model polymerization and (b) ^{1}H NMR spectrum of the resulting polymer.

weight and analysed the end group in the resulting polymer by nuclear magnetic resonance (NMR) measurement [38].

Figure II-2b displays the 1H NMR spectrum of the resulting polymer 5 in heavy water (D_2O). The peak from bridging methylene next to the methylamine group appears at 4.02 ppm, together with polyacrylamide peaks (methylene and methine of polyacrylamide at 2.64–2.11 ppm and 1.68–1.57 ppm, respectively), which corroborates the generation of the amino radical by the 4/KPS redox reaction that initiated the radical polymerization of 2 [39]. Upon comparing the integration ratio of the methylene peaks denoted as b and d in red, it was found that the number of repeating units in polymer 5 was not equivalent to the feed ratio. It presume that sulfate radicals also initiate polymerization as well as 1 after the homolytic cleavage of persulfate, or the generated radicals are transferred to other chain-transfer agents (e.g., water molecules) to form stable nitroxides.

Investigation of the change in the viscoelastic properties of a polymerizing solution of 2 further demonstrates the role of 1 as the polymerization reaction promoter. A polymerizing solution of 1.4 M 2 in water with 1 and KPS (both at 0.2 wt%) was prepared. After incubation for 2 h at rt, the solution showed an exponential increase in storage modulus over the frequency of 10 rad s^{-1} in a dynamic frequency sweep experiment using an oscillatory rheometer. However,

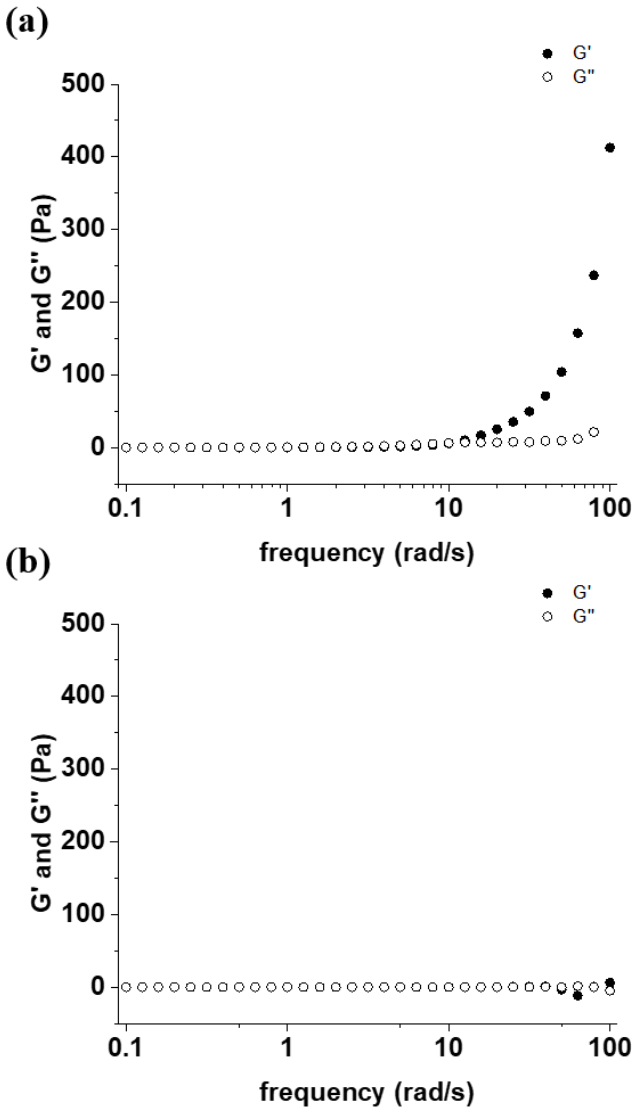

Figure II -3. (a) Dynamic frequency sweep data for solution 2 in the presence of the promoter 1 and KPS (b) the control experiment conducted the same conditions expect in the absence in 1.

the control solution without 1 only exhibited a liquid-like response as the frequency increased to 100 rad s^{-1}; this indicated that 1 promoted the radical polymerization of 2. In an inverted vial, the polymerizing solution showed gel-like properties; the absence of 1 caused no change in viscosity for the experimental time period (Figure II -3). Moreover, it found that rhodamine 6G—a starting material of 1—also polymerized 2 and showed behaviour similar to 1 during measurement.

This further supports the attribution of the polymerization initiation to the redox reaction between the aniline moiety and KPS (Figure II -4).

Overall, the abovementioned two preliminary experiments demonstrate that the secondary amine-containing 1 can be used for redox-initiated room-temperature polymerization in combination with KPS as well as a probe in polyacrylamide materials. The simple polymerization mechanism in water now allows the fabrication of a hydrogel film using 3, in which 1 gives rise to designed responses towards Al^{3+} in the film materials.

II-3-2. Mechanical propreties of hydrogel

The degree of cross-linking dramatically affects the mechanical properties

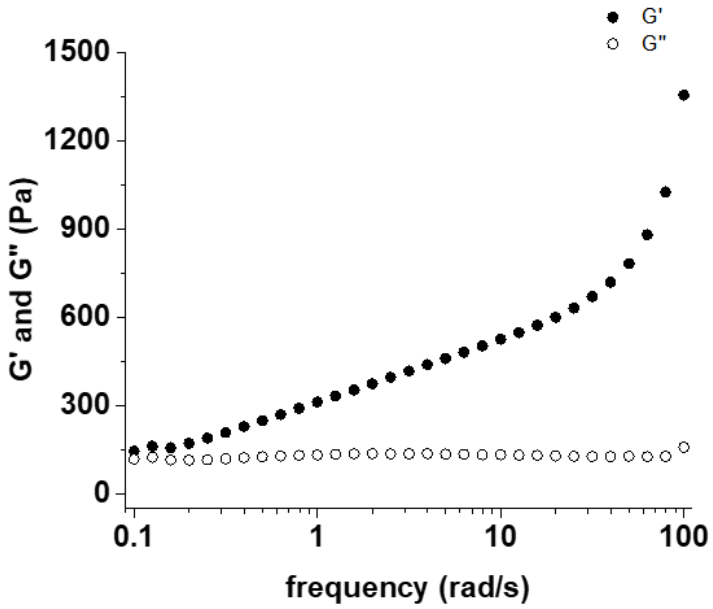

Figure II -4. Dynamic frequency sweep data for an aqueous of 2 in presence of rhodamine 6G and KPS.

of polymeric materials. Herein, Different amounts of the cross-linker 3 in the fabricated hydrogel films wincorporated. Figure II -5a shows the stress–strain curves of the films containing different amounts of 3, measured by a universal tensile machine (UTM). As seen, an increase in the incorporation of 3 brings about increased stiffness and brittleness in the obtained films. In Figure II -5b, the Young's moduli of the films are linearly proportional to the concentration of 3, but the toughness values decrease logarithmically against increased amounts of 3. When cross-linked with 1 wt% 3, the film is soft and ductile with the lowest elastic modulus, which hinders additional testing. A representative image of the tensile measurements is shown in Figure II -6a of testing the 2 wt% film. The 2 wt% hydrogel film was employed for the fluorescent sensing platform because the film was stretchable while maintaining the proper mechanical strength. After drying using a lyophilizer, the dried film revealed a porous network structure with pore diameters ranging from 4 to 27 mm in scanning electron microscopy (SEM) imaging (Figure II -6b). Furthermore, Figure II -6c shows the hydrogel film stretching under an applied external force. The sample film of 4 cm length was prepared and applied tensile force by hand. The elastic film was extended to 30 cm and returned to the original length immediately after the force was removed; this suggested the potential of the film for further application in wearable or reconfigurable materials.

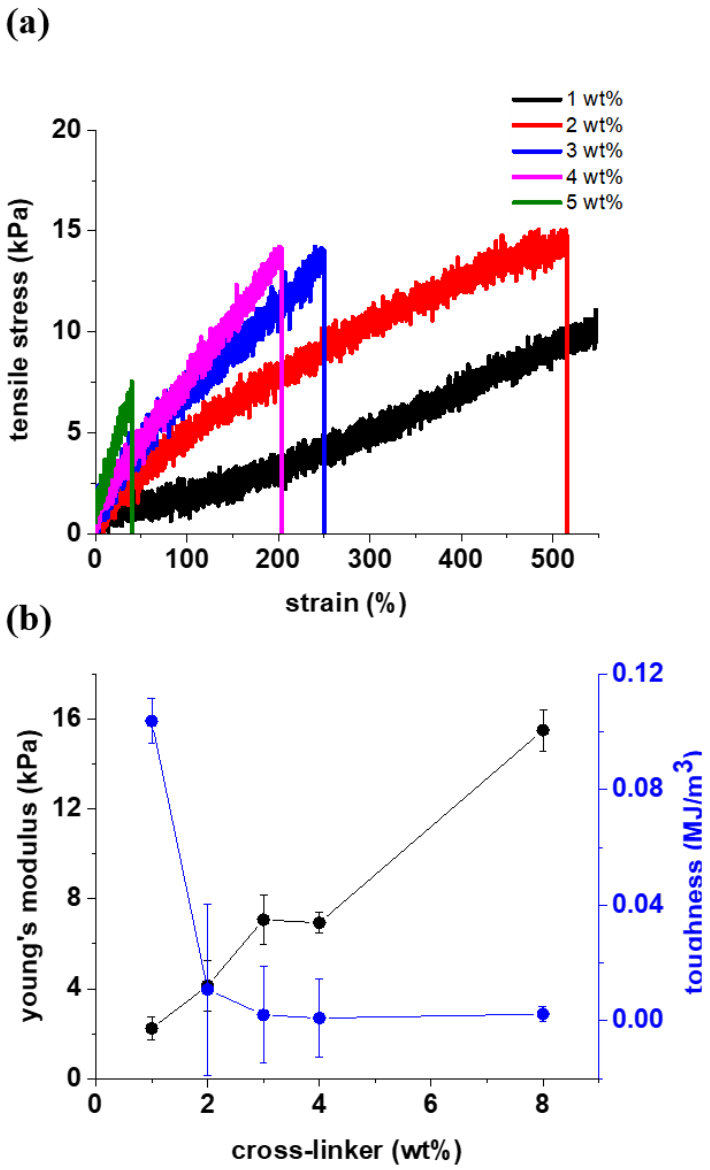

Figure II -5. (a) Representative tensile stress–strain curves for the hydrogels and (b) Change in Young's modulus and toughness of the hydrogels.

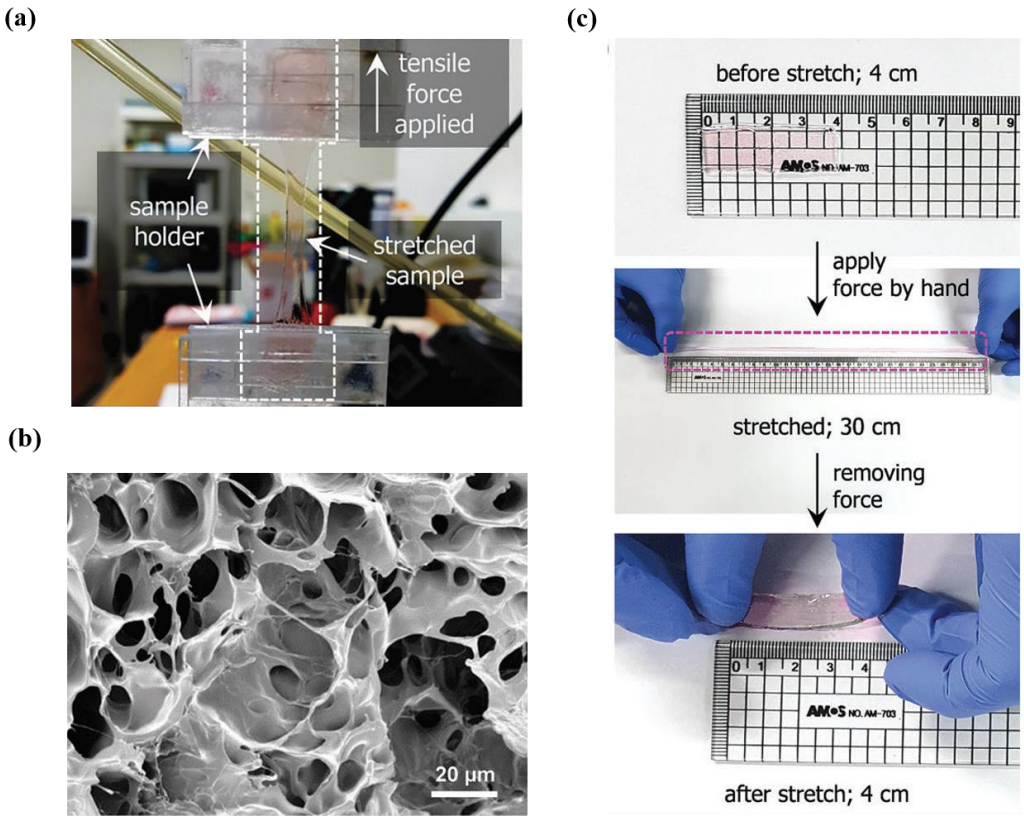

Figure II -6. (a) A representative photograph of actual tensile testing, (b) the porous network structure of the dried hydrogel, (c) Images of the stretchable film.

II-3-3. Fluorescent Responses from Hydrogel Film

Figure II -7a shows the change in yellow fluorescence from the hydrogel film after exposure to an aqueous solution of Al^{3+} for 30 min. As the concentration of Al^{3+} in 1 : 1 water–ethanol is increased gradually (0–3.00 mM), the emission of the film increases, ultimately enhanced by 3.8 times at the concentration of 3.00 mM under 500 nm excitation. Each sample was incubated in an Al^{3+} solution for 30 min to allow sufficient time for the ions to diffuse into the matrix [40]. when tested with the 1.50 mM Al^{3+} solution (Figure II -8a). The films before and after exposure to the 3.00 mM aqueous Al^{3+} solution under 365 nm irradiation are shown for comparison (Figure II -7b). In particular, any noticeable fluorescence was not observed from the remaining Al3+ solution (3.00 mM) after incubation of the film; this indicated that the leak of 1 was negligible (Figure II -8b).

These samples measure 1 cm x 1 cm x 0.1 cm and show a weak yellowish emission even before exposure to Al^{3+}. It speculated that some of 1 were converted to the ring-opened configuration during polymerization, [41–43] which would be improved through the modified polymerization conditions under investigation. Furthermore, the initial linear region was used to calculate the limit of detection (LOD). The LOD of the hydrogel film was estimated as 1.55 mM, which was below the maximum permissible concentration of Al^{3+} (0.1 mg

L^{-1}, 3.85 mM) in drinking water provided by large water treatment facilities according to the 2004 World Health Organization (WHO) regulations.

To understand the binding capability, the relationship between the fluorescence intensity and the concentration of Al^{3+} have been interpreted using a Benesi–Hildebrand plot [44] that offers information on the stoichiometry for non-covalent complexes and association constants. The linear regression between the inverse of change in fluorescence intensity $\{1/(F - F_0)\}$ and the inverse of Al^{3+} concentration $\{1/[Al^{3+}]\}$ evidenced a 1 : 1 binding stoichiometry of 1 to Al^{3+}, showing an R^2 value of 0.99, which was similar to previous results [45,46]. The binding constant was also calculated as 1 x10^9 M^{-1} from the plot.

The hydrogel film exhibited not only sensitive but also selective and reversible responses to Al^{3+}. Figure II -9a, the ions are selectively detected by 1 in the film, showing a significant enhancement in fluorescence by 234% at a concentration of 1.50 mM at rt in comparison with other metal ions. Other ions have negligible influences on the fluorescence of 1, independent of size or valence; Co^{2+} slightly decreases the initial feeble fluorescence; this verifies that the signal transducer selectively detects Al^{3+} [47]. In addition, the cross-linked hydrophilic matrix allows the investigation of the reversible on–off fluorescence switching of the film by employing EDTA, which forms a strong complex with

metal cations. When immersed in excess EDTA (20mM in 1 : 1 water–ethanol) for 30 min, the yellow emission is turned off as EDTA sequesters Al^{3+} from the hydrogel. However, re-exposure to the Al^{3+} solution (1.50 mM) triggers fluorescence in 1 again, as expected. Figure II -9b shows three repeating cycles of on–off fluorescence switching. The intensity of the regenerated fluorescence is slightly reduced as the cycle is repeated; presumably, EDTA is not fully rinsed out fromthe film before re-exposure to $Al^{3.}$ Herein, the detection of Al^{3+} was demonstrated

However, diverse hydrogel materials sensing other analytes were created since rhodamine derivatives respond to anions, reactive oxygen/nitrogen species, or biomolecules as well as metal ions—contingent on chemical structure or sensing mechanism [48]—as long as the functional probes hold the initiation capability.

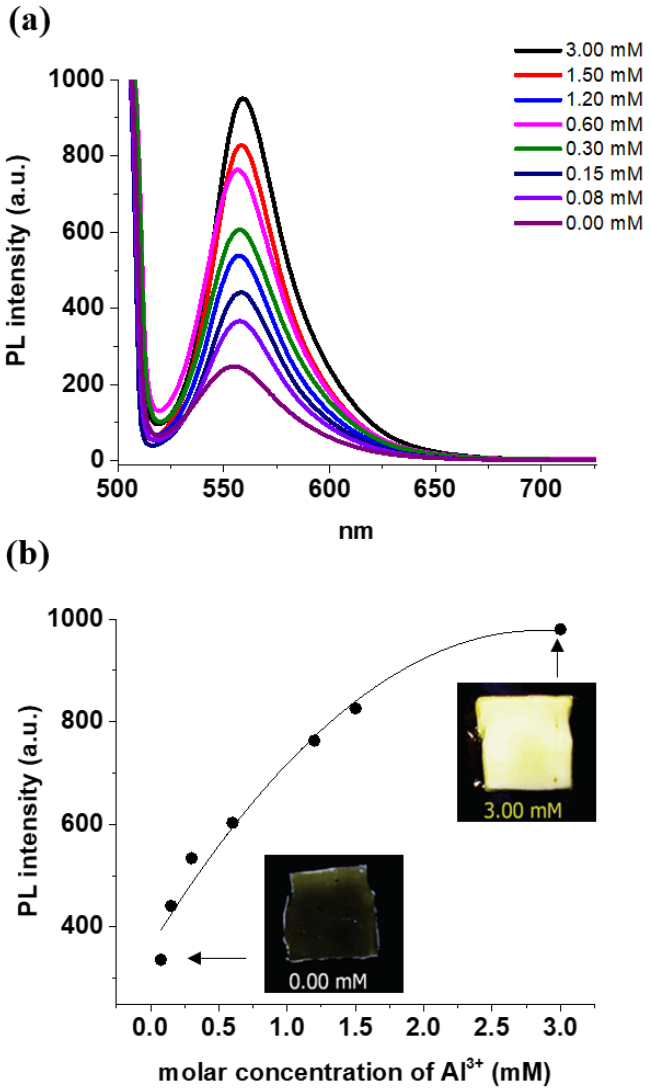

Figure II -7. (a) Fluorescence emission spectra of the film obtained upon the addition of Al^{3+} and (b) change in emission intensity of the film with different concentrations of Al^{3+}. Images of the hydrogel films before and after exposure to 3.00 mM of Al^{3+} are obtained under 365 nm irradiation.

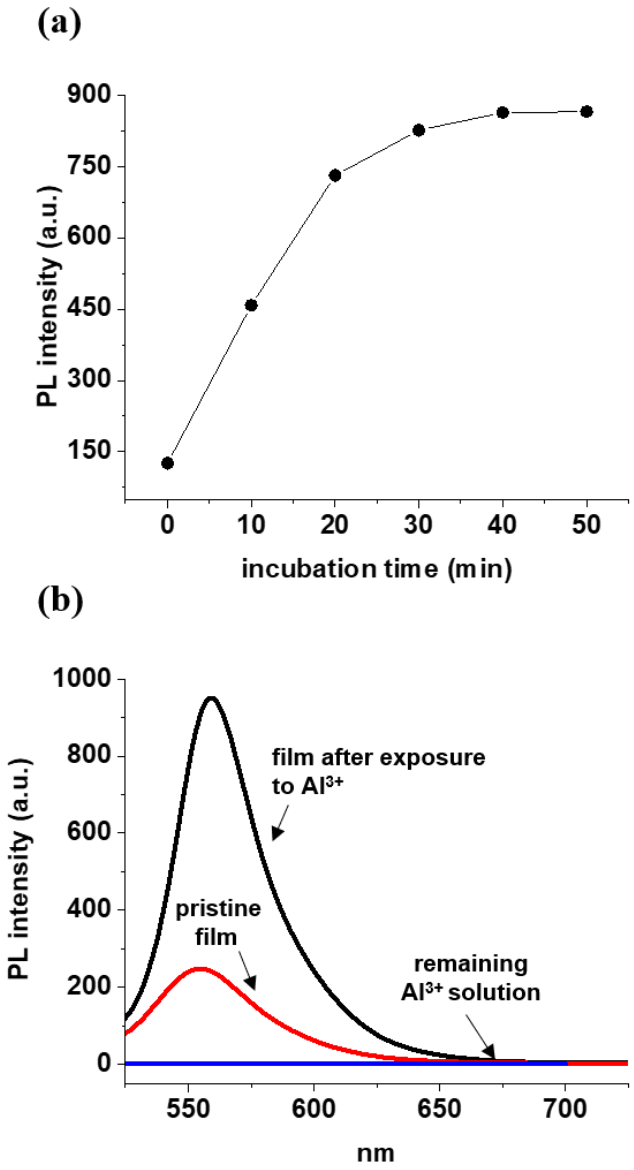

Figure II -8. (a) Change in the intensity of fluorescence monitored form film over the course of exposure time and (b) fluorescence emission spectrum form remaining Al^{3+} solution.

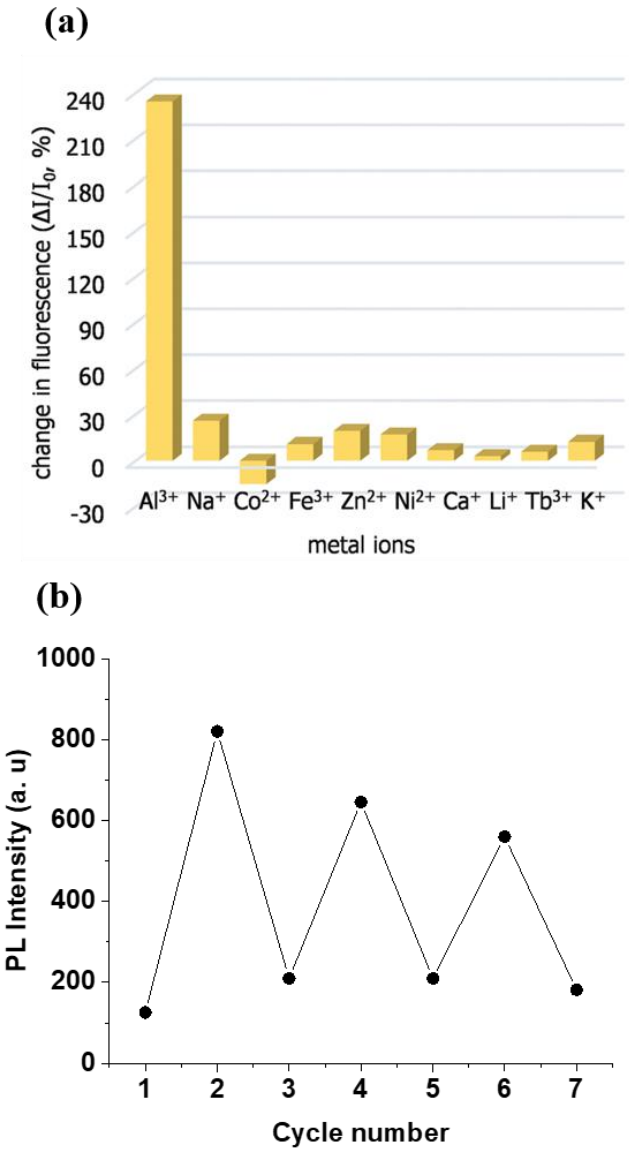

Figure II -9. (a) Selective enhancement in emission intensity of the film and (b) reversible on–off fluorescence switching of the hydrogel film.

II-4. Conclusions

In summary, the facile preparation of a functionalpolyacrylamide hydrogel film was demonstrated. The polymer film was fabricated using room-temperature radical polymerization initiated via theredox reaction between KPS and a rhodamine-based probe. The secondary amine-containing probe promoted the redox initiation reaction and imparted fluorogenic sensing abilities for Al^{3+} to the film. The hydrogel film selectively detected Al^{3+} by showing bright yellow fluorescence. Subsequent exposure to EDTA reversed the fluorescence response of the film. In this proof of concept, this study have used the rhodamine probe and investigated the Al^{3+} sensing capability; however, the functional hydrogel film can be further investigated for complex physical properties or cytotoxicity and optimized for creatively designed materials when engineered with a variety of monomers having orthogonal reactivities or specific-functionalized amine probes for programmable responsive systems. This could establish a new design strategy for autonomous interactive responses, as in nerve cells, when applied to microfluidics, wearable devices, or smart biomimetic materials.

II-5. References

[1] J. Kopecˇek, *J. Polym. Sci., Part A: Polym. Chem.*, 2009, **47**, 5929–5946.

[2] N. A. Peppas, J. Z. Hilt, A. Khademhosseini and R. Langer, *Adv. Mater.*, 2006, **18**, 1345–1360.

[3] A. Do¨ring, W. Birnbaum and D. Kuckling, *Chem. Soc. Rev.*, 2013, **42**, 7391–7420.

[4] N. Oliva, J. Conde, K. Wang and N. Artzi, *Acc. Chem. Res.*, 2017, **50**, 669–679.

[5] M. D. Konieczynska and M. W. Grinstaff, *Acc. Chem. Res.*, 2017, **50**, 151–160.

[6] H. Ko and A. Javey, *Acc. Chem. Res.*, 2017, **50**, 691–702.

[7] J. S. Kahn, Y. Hu and I. Willner, *Acc. Chem. Res.*, 2017, **50**, 680–690.

[8] I. Tokarev and S. Minko, *Soft Matter*, 2009, **5**, 511–524.

[9] E. M. White, J. Yatvin, J. B. Grubbs III, J. A. Bilbrey and J. Locklin, *J. Polym. Sci., Part B: Polym. Phys.*, 2013, **51**, 1084–1099.

[10] V. Kozlovskaya, E. Kharlampieva, I. Erel and S. A. Sukhishvili, *Soft Matter*, 2009, **5**, 4077–4087.

[11] X. Ding and Y. Wang, *J. Mater. Chem. B*, 2017, **5**, 887–906.

[12] J. Li, Z. Xu, Y. Xiao, G. Gao, J. Chen, J. Yin and J. Fu, *J. Mater. Chem. B*, 2018, **6**, 257–264.

[13] A. Baeza, E. Guisasola, A. Torres-Pardo, J. M. Gonza´lez-Calbet, G. J. Melen, M. Ramirez and M. Vallet-Regı´, *Adv.Funct. Mater.*, 2014, **24**, 4625–4633.

[14] C. Yu, C.-F. Wang and S. Chen, *Adv. Funct. Mater.*, 2014, **24**, 1235–1242.

[15] X. Peng, T. Liu, C. Jiao, Y. Wu, N. Chen and H. Wang, *J. Mater. Chem. B*, 2017, **5**, 7997–8003.

[16] C.-C. Kim, H.-H. Lee, K. H. Oh and J.-Y. Sun, *Science*, 2016, **353**, 682–687.

[17] Y. Takashima, Y. Sawa, K. Iwaso, M. Nakahata, H. Yamaguchi and A. Harada, *Macromolecules*, 2017, **50**, 3254–3261.

[18] X. D. Feng, Macromol. *Symp.*, 1992, **63**, 1–18.

[19] X.D. Feng, X. Q. Guo andK. Y. Qiu, *Polym. Bull.*, 1987, **18**, 19–26.

[20] X. D. Feng, Chin. *J. Polym. Sci.*, 1986, **4**, 109–118.

[21] J. Wang, Z. Wang, Y. Liu, J. Wang and S. Wang, *J. Membr. Sci.*, 2016, **514**, 407–417.

[22] R. Nigmatullin, M. Bencsik and F. Gao, *Soft Matter*, 2014, **10**, 2035–2046.

[23] S. Zhang, Z. Shi, H. Xu, X. Ma, J. Yin and M. Tian, *Soft Matter*, 2016, **12**, 2575–2582.

[24] H. Yang, H. Pu and F.Gong, *J. Appl. Polym. Sci.*, 2014, **131**, 41062.

[25] H. Jia, Z. Huang, Z. Fei, P. J. Dyson, Z. Zheng and X. Wang, *J. Mater. Chem. B*, 2017, **5**, 8193–8199.

[26] J. Ma, J. Lee, S. S. Han, K. H. Oh, K. T. Nam and J.-Y. Sun, *ACS Appl. Mater. Interfaces*, 2016, **8**, 29220–29226.

[27] Y. Zhu, J. Zhang, J. Song, J. Yang, T. Xu, C. Pan and L. Zhang, *J. Mater. Chem. B*, 2017, **5**, 8451–8458.

[28] Y. Yang, Q. Zhao, W. Feng and F. Li, *Chem. Rev.*, 2013, **113**, 192–270

[29] X. Li, X. Gao, W. Shi and H. Ma, *Chem. Rev*., 2014, **114**, 590–659.

[30] The World Health Organization (WHO) recommended to restrict the human intake amount of Al^{3+} to 3–10 mg per day.31

[31] Z. Krejpcio and R. W. Wojciak, *Pol. J. Environ. Stud*., 2002, **11**, 251–254.

[32] M. E. Jun, B. Roy and K. H. Ahn, *Chem. Commun.*, 2011, **47**, 7583–7601.

[33] K. Boonkitpatarakul, J. Wang, N. Niamnont, B. Liu, L. Mcdonald, Y. Pang and M. Sukwattanasinitt, *ACS Sens.*, 2016, **1**, 144–150.

[34] Y. Fu, X.-J. Jiang, Y.-Y. Zhu, B.-J. Zhou, S.-Q. Zang, M.-S. Tang, H.-Y. Zhang and T. C. W. Mak, *Dalton Trans*., 2014, **43**, 12624–12632.

[35] H. Wynberg and E. W. Meijer, *Org. React*., 1982, **28**, 1–36.

[36] Y. K. Yang, K. J. Yook and J. A. Tae, *J. Am. Chem. Soc*., 2005, **127**, 16760–16761.

[37] The acidic monomer affected carboxylate group of 1 which led to precipitation in the monomer solution before conducting polymerization, and would also prevent redox-reaction forradical initiation.

[38] The same feed molar ratio that was used for the preparation of the hydrogel film (4/KPS/2 = 1 : 1 : 2000) already were tried , but could not find the end group in the NMR spectrum dueto a high signal-to-noise ratio.

[39] The limited solubility of the resulting polymer 5 in organic solvents frustrated our endeavor to measure a molecular weight using gel permeation chromatograph (GPC).

.

[40] Z. Geng, H. Zhang, Q. Xiong, Y. Zhang, H. Zhao and G. Wang, *J. Mater. Chem. A*, 2015, **3**, 19455–19460**.**

[41] It speculate that electron transfer would be involved in the ring-opening of 1 via chain transfer reaction during radical polymerization.

[42] T. M. Geng, R. Y. Huang and D. Y. Wu, *RSC Adv.*, 2014, **4**, 46332–46339**.**

[43] E. Yoshioka, S. Kohtani, T. Jichu, T. Fukazawa, T. Nagai, A. Kawashima, Y. Takemoto and H. Miyabe, *J. Org. Chem.*, 2016, **81**, 7217–7229.

[44] C. Tablet, I. Matei and M. Hillebrand, The Determination of the Stoichiometry of Cyclodextrin Inclusion Complexes by Spectral Methods: Possibilities and Limitations, in Stoichiometry and Research – The Importance of Quantity in Biomedicine,ed. Alessio Innocenti, InTech, 2012, pp. 47–76**.**

[45] P. Ding, J. Wang, J. Cheng, Y. Zhao and Y. Ye, *New J. Chem*., 2015, **39**, 342–348.

[46] S. Das, S. Goswami, K. Aich, K. Ghoshal, C. K. Quah, M. Bhattacharyya and H.-K. Fun, *New J. Chem*., 2015, **39**, 8582–8587**.**

[48] The system was selective to Al^{3+} in this research, but some heavy metals may have potential influence to 1,34 which will be studied along with other factors such as temperature, pHand so on**.**

[49] X. Chen, T. Pradhan, F. Wang, J. S. Kim and J. Yoon, *Chem. Rev.,* 2012, **112**, 1910–1956.

Chapter III.

Multifunctional role of MoS_2 in preparation of composite hydrogels: radical initiation and cross-linking

III-1. Introduction

Polymer nanocomposites that include nanomaterials in viscoelastic polymer matrices have so far attracted great attention owing to their capability to overcome the intrinsic limitations of classical polymers. While a variety of nanomaterials such as metals, clays, or carbon allotropes have been incorporated, the resulting composites show enhanced mechanical strength and also provide designed functionalities beyond the capability of each component; for example, biomimetic behavior, electrical or thermal conductivity, and optoelectronic properties [1,2].

In particular, soft, nanocomposite hydrogels have benefited from the elastic, cross-linked networks that confine a considerable amount of water and additive nanomaterials that induce tailored, complex properties, and now hold privileged positions in the development of smart, elastic materials [3-11]. Typically, colloidal nanoparticles including nanowires or carbon dots have been widely used [12-15], and more recently, two-dimensional layered materials such as ceramic nanosheets, carbides, graphene oxides, and covalent organic framework (COF) have been extensively researched [16-20]. They have relatively weak intermolecular interactions between the layers, and thus, show large surface areas and accessible active sites that are exposed on the surface, which imparts

sophisticated yet essential properties to the polymeric networks [21,22] Among many layered materials, molybdenum disulfide (MoS_2) has been incorporated in hydrogel networks due to its mechanical or electronic properties; recently, the embedded hydrogels have been used as a functional platform for energy-related or environmental applications such as separation or catalysis under aqueous conditions [23-27].

When designing the materials via a bottom-up approach, MoS_2 and other monomeric components are dispersed on a molecular level; thereafter, the composite networks are set, usually, by radical polymerization while leaving the inorganic material as an exogenous additive in most cases. Conversely, from the perspective of polymer chemistry, the chemical function of MoS_2 that can play a significant role as a reactive component in the formation of hydrogels through radical polymerization has been rarely investigated. Thus, the role of MoS_2 in the polymerization reaction and the formation of functional composite hydrogels that are capable of exhibiting a designed behavior have been explored.

In this study, the facile preparation of MoS_2-containing composite hydrogels has newly been demonstrated. The MoS_2 nanoplatelets promote radical formation resulting in redox initiation for the polymerization of acrylamide under mild conditions and further provide non-covalent cross-linking points leading to the formation of a uniform, composite material. Therefore, the

nanocomposite hydrogels could be readily obtained via a single-step, radical polymerization without requiring external stimulus (e.g., pH, heat, or light) or additional chemical cross-linkers. Simultaneously, metal chalcogenide flakes were incorporated in the polymer matrix without severe aggregation, accompanying the polymerization-induced phase transformation. The resultant materials had the typical properties of hydrogels but were more malleable and sturdy than a chemically cross-linked hydrogel at the same level. For example, a trace amount of MoS_2 (<0.02 wt%) was able to form a better elastic and tough hydrogel than a conventional chemical cross-linker; large amounts of MoS_2 (>0.2 wt%) still formed the hydrogel composites, although the control cross-linker no longer produced elastic materials. Interestingly, the hydrogel materials exhibit self-healing properties owing to the reversible nature of the non-covalent cross-links. Therefore, hydrogels were able to re-join two cut hydrogel strips by heating to 70 °C due to the bond exchange at the cross-linking points, while restoring the mechanical strength as before cut.

III-2. Experimental Section

General Experimental

All reactions were performed in flame-dried glassware. *N*-Isopropylacrylamide (NIPAM) was purified by recrystallization in *n*-hexane before use, and *N*,*N*-dimethylacrylamide (DMA) was also purified by distillation. Other reagents or solvents were purchased commercially and used as received unless otherwise noted.

Instrumentation

Uniaxial compressive and tensile tests were performed using a universal tensile machine (UTM) (MCT-2150, A&D, Japan) with a 500-N load cell at 25 °C in air. Cylindrical or film hydrogels were prepared for the compressive or tensile measurements, respectively (for compressive test: diameter × height, 15 mm × 10 mm; for tensile test: width × length × thickness, 10 mm × 40 mm × 1 mm). The film samples were glued between two acrylic clamps using a superglue for the testing. The hydrogel samples were elongated at a rate of 10 mm min^{-1} until broken, and then, the stress–strain curves were recorded in triplicate. Young's modulus was obtained from the initial slope of the stress–strain curves

(strain, 0-10%) from three independent samples, and toughness was also estimated from the area under the curves. Those values were presented with average and standard deviation.

Morphology of dried hydrogels was observed using a JSM-7500F scanning electron microscope (SEM) at an accelerating voltage of 1 kV. Before the measurement, the sample was dried using a lyophilizer and coated with a thin platinum layer at an accelerating current of 10 mA for 60 sec.

The images of individual MoS_2 coated with polymers were observed using a JEM-3010 transmission electron microscope (TEM) at an accelerating voltage of 300 kV.

Dynamic rheological experiments were carried out using a rheometer (HR-2, TA instrument, USA) with 20 mm cone and plate configuration. The specimens were tested in a time sweep mode at 1 rad/s. UV–Vis absorption spectra of aqueous bromophenol blue solutions were measured using a spectrophotometer (Optizen 2120uv, K LAB, Korea).

Phase transition of MoS_2 was observed using high-performance X-ray photoelectron spectroscopy (XPS) (K-ALPHA+, Thermo Fisher Scientific, USA). Before measurement, the samples were fully dried at reduced pressure to remove solvent molecules in polymer networks.

MoS2-containing composite hydrogels synthesis

MoS_2-containing composite hydrogels were prepared by radical polymerization initiated by the reaction from MoS_2 and KPS. To a solution of acrylamide (0.5 g, 7.03 mmol, 1.0 equiv) in water (2 mL) was added predesigned amounts of MoS_2 flakes (0.5–25 mg; 0.02−0.83 wt%). The mixture was and sonicated for 30 min to disperse and exfoliate the nanosheets, and further degassed by bubbling with nitrogen. Then, a solution of potassium persulfate (5.7 mg, 0.02 mmol, 0.003 equiv) in water (0.5 mL) was added to the mixture. After which, the reaction mixture was stored at rt for 48 h to afford a free-standing, three-dimensional, composite hydrogels.

Control hydrogels synthesis

Control samples were prepared by radical polymerization in the presence of a chemical cross-linker instead of MoS_2. To a solution of acrylamide (0.2 g, 2.81 mmol, 1.0 equiv) was added an aqueous solution of N,N'-methylenebis(acrylamide) (0.8–4 mg; 0.03–0.16 wt%) and a consistent amount of potassium persulfate (2.28 mg, 0.01 mmol, 0.003 equiv) in water (2 mL). Then, the reaction mixture was heated at 60 °C for 12 h to afford the control

hydrogels.

Composite hydrogels with other monomers synthesis

Other acrylic monomers, N,N-dimethylacrylamide (DMA) and N-isopropylacrylamide (NIPAM), were tested for the formation of composite hydrogels. These composite hydrogels were prepared following the same manner as described for the acrylamide-based composite hydrogel except for using different monomers.

Quantities of reagents: acrylic monomers (0.5 g), MoS2 (2.5 mg, 0.08 wt%), potassium persulfate (5.7 mg), water (2.5 mL).

III-3. Results and Discussion

III-3-1. Synthesis and Characterization of hydrogel

Figure III -1 depicts the preparation of an acrylamide-based hydrogel initiated by the redox reaction of MoS_2 flake (2H phase; diameter, <2 μm) and potassium persulfate (KPS). The combination of the two components produces radical species that are mainly sulfate radicals or hydroxyl radicals following their mixing in water at 25 ℃, which can initiate the radical polymerization of acrylamide. In particular, the inorganic material induces cross-linking without requiring additional cross-linkers, resulting in monolithic composite hydrogels. For example, a cylindrical hydrogel from an aqueous solution of acrylamide (2.8 M, 2.5 mL) at 25 ℃ in the presence of exfoliated MoS_2 (2.5 mg; 0.08 wt%) and KPS (0.02 mmol; 0.2 wt%) has prepared , as shown in the inset of Figure 1.

A change in the amount of MoS_2 can considerably alter the mechanical properties of the composite hydrogels. Thus, the capability of the MoS_2 for the formation of hydrogels from 2.8 M acrylamide in water (2.5 mL; 200 mg/mL) in the presence of KPS (0.02 mmol; 0.3 mol% to the monomer) was tested. It found that the resultant composite hydrogels were formed after storing for 48 h at 25 ℃ using 0.02–0.83 wt% MoS_2 (0.5–25 mg) incorporated, as confirmed by the vial inversion method (Figure III-2). Incomplete gelation was observed when

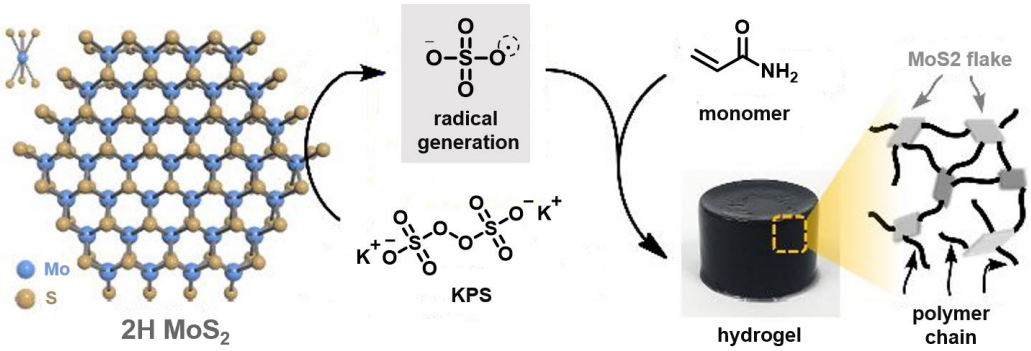

Figure III -1. Schematic description for the preparation of a composite hydrogel containing 2H MoS_2 flakes. The MoS_2 Photograph of acylindrical hydrogel is shown in the inset.

using less than 0.02 wt% MoS_2, while the hydrogel with 0.83 wt% MoS_2 lost its elasticity and was entirely no longer compressible. Furthermore, the compressive stress–strain curves of the hydrogels were examined (Figure III-3a). The cylindrical samples had an average diameter of 16 mm and a height of 13 mm, and the compressive Young's modulus was obtained from an initial linear region of each curve. The higher the MoS_2 incorporated from 0.02 to 0.08 wt%, the higher the Young's modulus obtained; the material exhibited the highest modulus of 0.05 ± 0.01 MPa at 0.08 wt% similar to those of the gelatins or agarose gels [28]. After exceeding the point, the modulus decreased gradually and reached 0.03 ± 0.01 MPa at 0.67 wt%, similar to the value from the 0.02 wt% (Figure III-3b). Thus, it found that the increase in the cross-linking points that are caused by the added MoS_2 enhanced the mechanical strength resulting in tough hydrogels; however, the excessive addition of the inorganic flakes hampered the elasticity of the hydrogel networks and resulted in rather weak materials instead. Notwithstanding, all the composite hydrogels were still entirely compressible during the loading–unloading cycles up to 85% strain, regardless of the amount of MoS_2 incorporated. When comparing the compressive stresses of the hydrogels at a strain of 60%, a comparable behavior as shown in the case of the Young's modulus was found. The large deformation would be attributed to the non-covalent cross-linking points that allow the re-

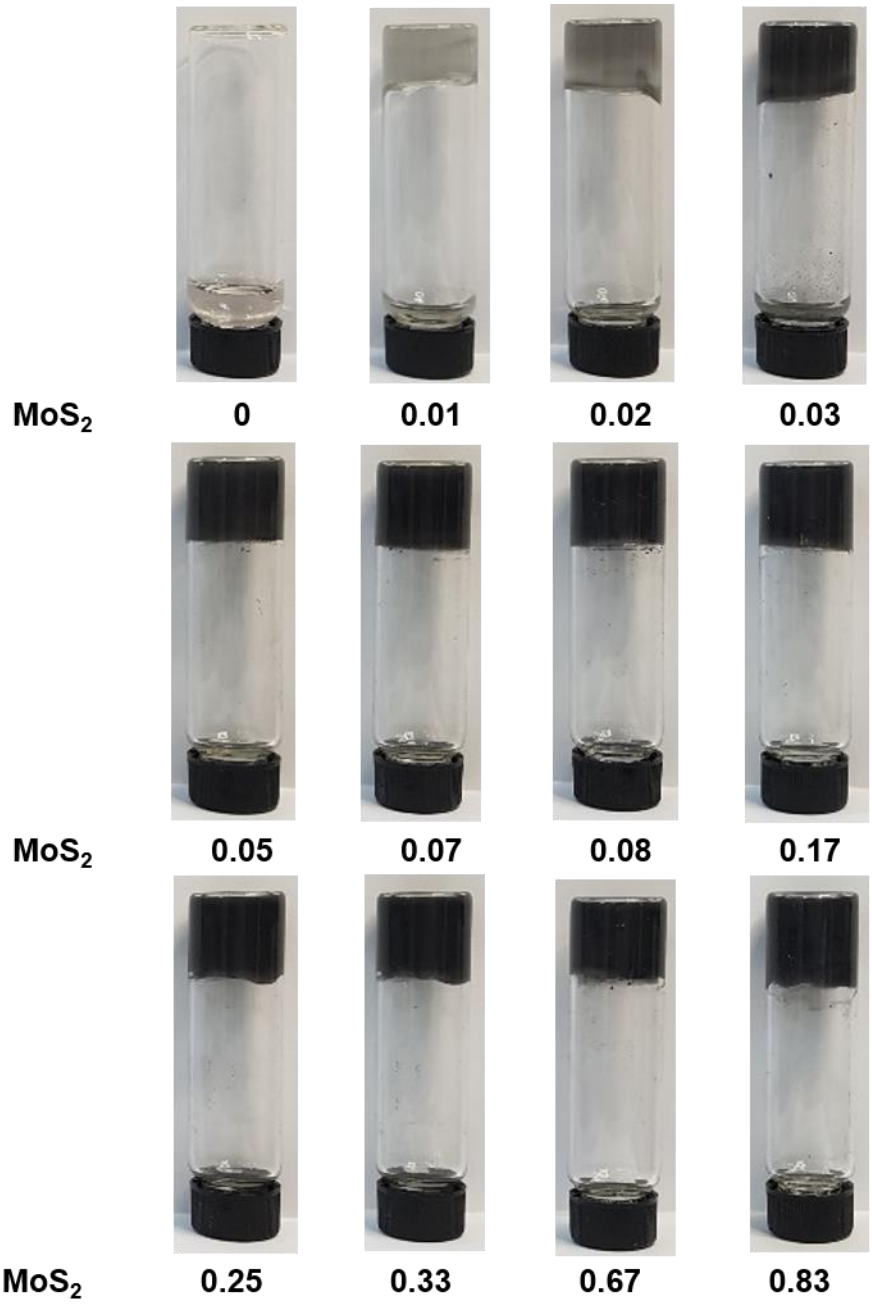

Figure III-2. Gelation test for the formation of MoS_2-containing composite hydrogels via redox initiation, while the exfoliated MoS_2.

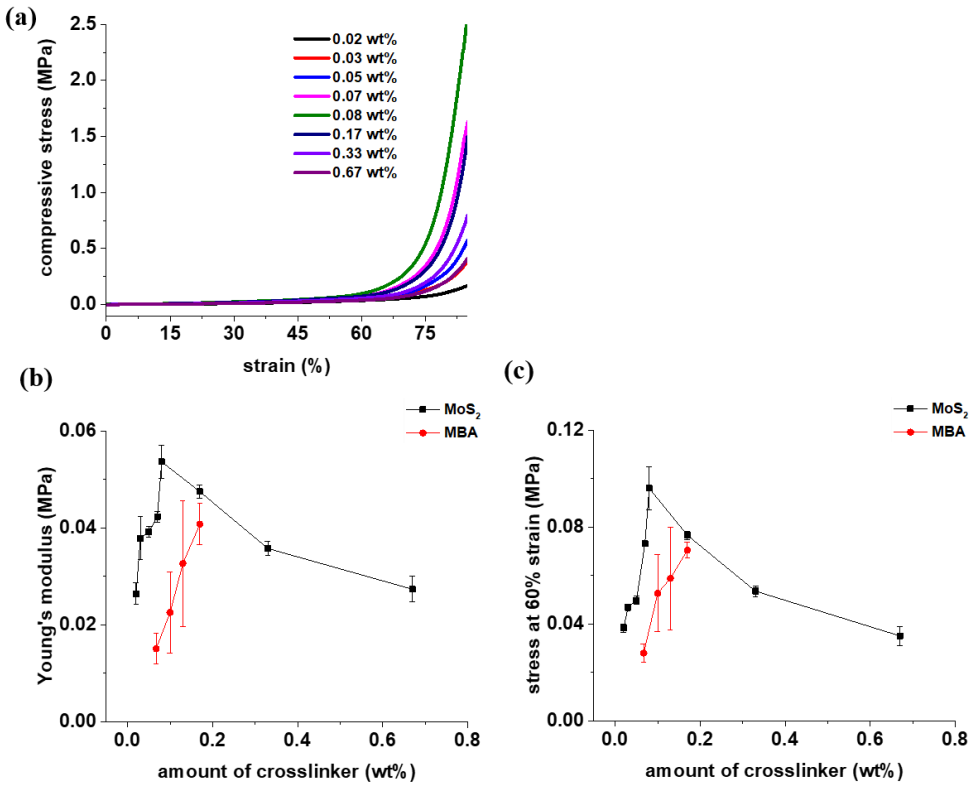

Figure III-3. (a) Change in Young's modulus of the composite hydrogels, (b) representative tensile stress–strain curves for the hydrogels.sive Young's modulus, (c) compressive stress at 60% strain of the hydrogels.

organization of the viscoelastic, poly(acrylamide)-based matrix surrounding the inorganic platelets [29]. In addition, control hydrogels using N,N′-methylenebis(acrylamide) (MBA) at 60 °C without MoS_2 (Figure III-3b, Figure III-3c) were prepared . The hydrogels increased in toughness linearly as the amount of MBA increased from 0.03 to 0.16 wt%, and, above this point, only a very stiff monolith instead of elastic hydrogels were obtained, which were merely broken into pieces under a strain of 30% due to irreversible, covalent crosslinking points.

Moldable composite hydrogels could be prepared as a film, which allowed additional tensile testing (Figure III-4). The hydrogel films (size: 40 mm × 10 mm × 1.3 mm) were prepared and found that the materials exhibited similar performance as achieved in the case of the compressive test. The higher the amount of MoS_2, the higher the tensile Young's modulus obtained until 0.08 wt%, at which point the modulus then decreased (Figure III-4a). The maximum Young's modulus was found to be 0.06 ± 0.01 MPa while showing a high extension (strain to fracture, 1110%; toughness, 0.6 MJ m^{-3}) as expected. The representative tensile stress–strain curves obtained are shown in Figure III-4b .

The MoS_2 flake promotes the generation of radicals and causes the simultaneous cross-linking while existing as an additive in the hydrogel networks in contrast to the general chemical cross-linkers, which provide the

one-step, room-temperature preparation of the composite hydrogels. The hydrogels could not be obtained when a commercial, linear poly(acrylamide) (Mn, 150 kDa; 200 mg/mL) was incorporated instead of an acrylamide monomer under the same conditions in the presence of KPS and MoS_2; [30] moreover, the gelation did not occur apparently only in the presence of KPS without MoS_2, which corroborates the significance of the radical generation for the formation of the hydrogel network.

The formation of the composite hydrogel, triggered by the redox reaction of MoS_2 (0.08 wt%) and KPS (0.3 mol% to the monomer) was investigated while monitoring the change in the compressive curves, as shown in Figure III-5.

A tangible, cylindrical hydrogel that exhibited a low compressive Young's modulus of 0.01 MPa only after 3 min of mixing at 25 °C was obtained. Afterward, the modulus swiftly increased and eventually reached 0.05 MPa within 6 h (Figure III-5b). On the contrary, the toughness, which represents the energy absorbed in the network, gradually increased from 2.4 to 17.4 KJ m^{-3} over 48 h when measured under a strain of 60% (Figure III-5a), which reveals the rapid formation of the primary covalent structure via radical polymerization and the steady occurrence of secondary, non-covalent structures on the MoS_2 plates [31,32].

Figure III-5c shows the initial change in the viscoelastic properties of

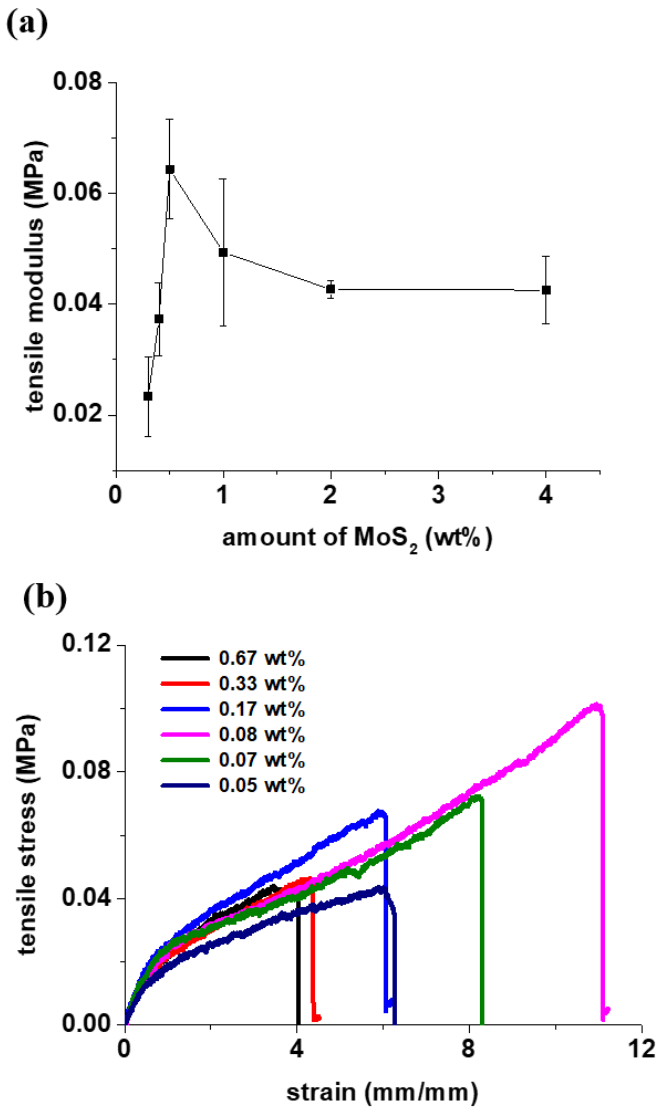

Figure III-4. (a) Change in Young's modulus of the composite hydrogels and (b) Representative tensile stress–strain curves for the hydrogels.

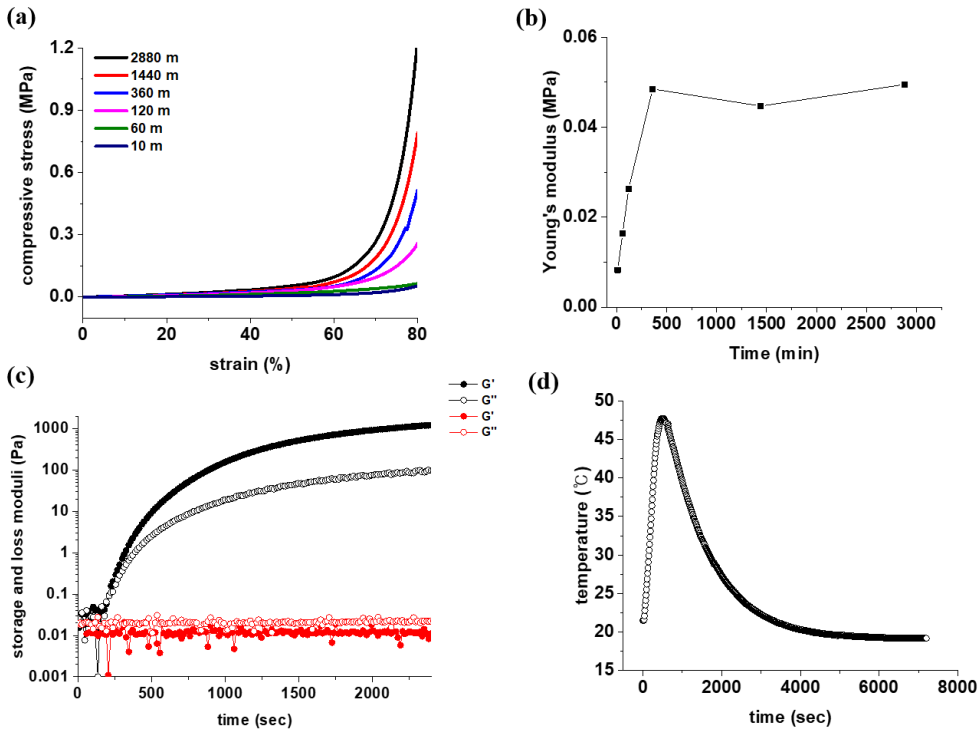

Figure III-5. (a) Compressive stress–strain curves measured at different time intervals during the gelation, (b) changes in the Young's modulus as time elapsed, (c) Dynamic time sweep data for an aqueous solution, (d) change in temperature during the gelation.

the polymerizing solution for the composite hydrogel, measured by an oscillatory rheometer at 1 rad s^{-1} at rt. The storage modulus of the solution became greater than the loss modulus after the crossover point at 220 s, indicating that the solution started becoming viscoelastic; afterward, the value increased exponentially as time elapsed (black, Figure III-5c). In addition, the temperature change of the solution was measured. At the initial stage within 10 min, the temperature sharply increased to 48 °C and cooled in a short time, probably due to the Trommsdorff effect, as shown in Figure III-5d, indicating the rapid formation of the covalent structure corresponding to the rheological data [33]. Contrarily, the control solution without MoS_2 only exhibited a liquid-like response given that the loss modulus was found to be 1.6 times larger than the storage modulus under the same conditions at 25 °C during measurement (red, Figure III-5c). This further supports the dual role of MoS_2 in the redox radical initiation and concomitant cross-linking, leading to the hydrogel network.

The generation of radicals are confirmed from the mixture of MoS2 and KPS in water (Figure III-6). For this, a chromophoric radical indicator, bromophenol blue (BPB) that scavenges free radicals as indicated by the stark contrast in color was used. An aqueous solution of the dye (7.8 μM, 2.5 mL) was violet, and it exhibited the absorption maximum at 590 nm when measured by UV–Vis spectrometry. After the incorporation of MoS_2(0.08 wt%) and KPS

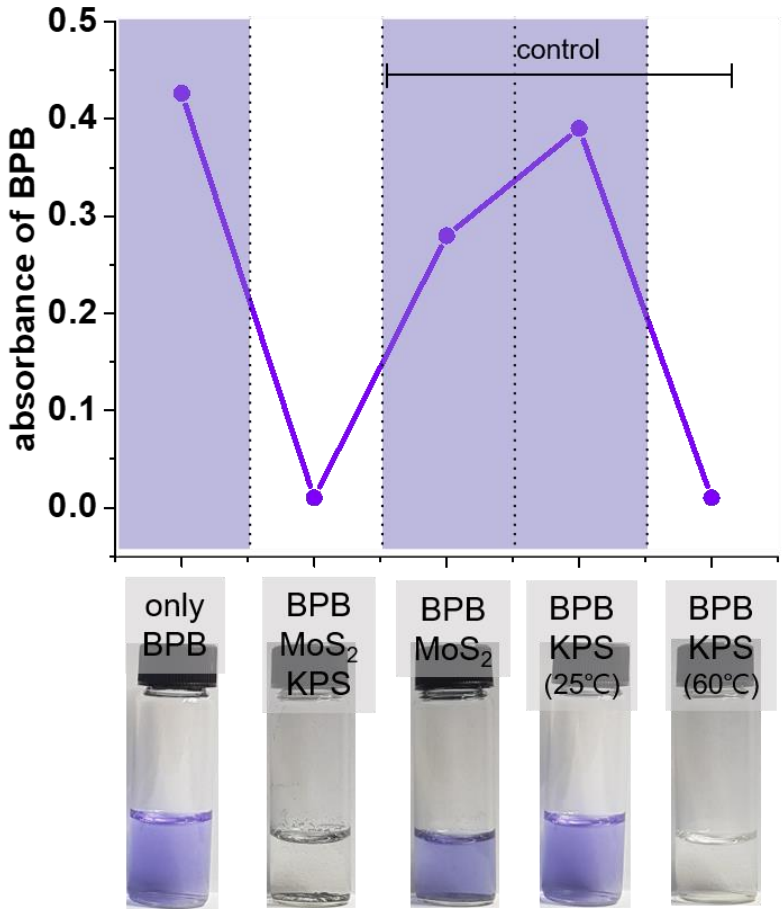

Figure III-6. Investigation of radical formation by MoS_2 and KPS using bromophenol blue (BPB) Photographs in the inset visualize the radical formation

(0.02 mmol) at 25 °C for 6 h, the solution became completely colorless, which visualized the radical formation via redox reaction; correspondingly, the absorption peak of BPB at 590 nm also disappeared. It assume that the electron transfer from defects such as the sulfur vacancies in MoS_2 (unsaturated Mo) on basal planes or edges to KPS would occur under aqueous conditions, which primarily generates sulfate radicals along with hydroxyl radicals when transferred into water [34,35]. In contrast, the single addition of each component did not change the color of the BPB solution as expected, indicating the absence of radicals. The only slight decrease in the absorption intensity was found after adding MoS_2, which would be attributed to the physical adsorption of the chromophores on the surface of the inorganic flakes. The KPS-containing sample did not show color change at 25 °C either. However, once heated to 60 °C, the sample readily became transparent owing to the thermal homolysis of KPS that forms resultant radicals.

Figure III-7 displays that redox polymerization induces the phase transition of the MoS_2 incorporated when observed by X-ray photoelectron spectroscopy (XPS). The pristine bulk MoS_2 showed Mo 3d peaks at 233.2 and 230.1 eV and S 2p peaks at 164.2 and 162.9 eV after deconvolution, which indicates the semiconducting 2H phase (black). A trace amount of metallic 1T phase was also found considering that the corresponding XPS peaks for Mo 3d (232.2 and 229.3

eV) and S 2p (163.7 and 162.3 eV) appeared (red), and were estimated to be 5% based on the comparison of the Mo 3d peaks (top, Figure III-7). Interestingly, the addition of KPS slightly increased the degree of the 1T phase after the radical initiation. The generated radical species can be tightly bound to the surface of MoS_2 and induce atomic plane gliding, [36–38] inducing phase transition and the evolution of a 10% 1T phase, as shown in the middle of Figure III-7. The redox polymerization of acrylamide remarkably caused the phase transition, and thus, the metallic phase increased to 45% showing the red-shift of binding energies of MoS_2 (bottom, Figure III-7). The surface-bound radicals are considered to provide physical cross-linking points and to form the hydrogel network in which intramolecular interactions or steric hindrance between the polymer chains on the platelets would give rise to internal strains and promote the phase transition of MoS2 [39,40]. The broad, certain XPS peak for C 1s was also developed at 288 eV after the reaction, indicating the formation of the poly(acrylamide) network. Contrarily, the phase of MoS_2 in the control sample with the linear poly(acrylamide), in which the composite hydrogel was not formed as mentioned above, did not change, which further suggests the importance of the adsorption of radicals and sequential polymerization.

Figure III-8 shows the morphology of the composite hydrogel (MoS_2, 0.08 wt%) after the redox initiation. When lyophilized for 48 h at 0 °C, the dried

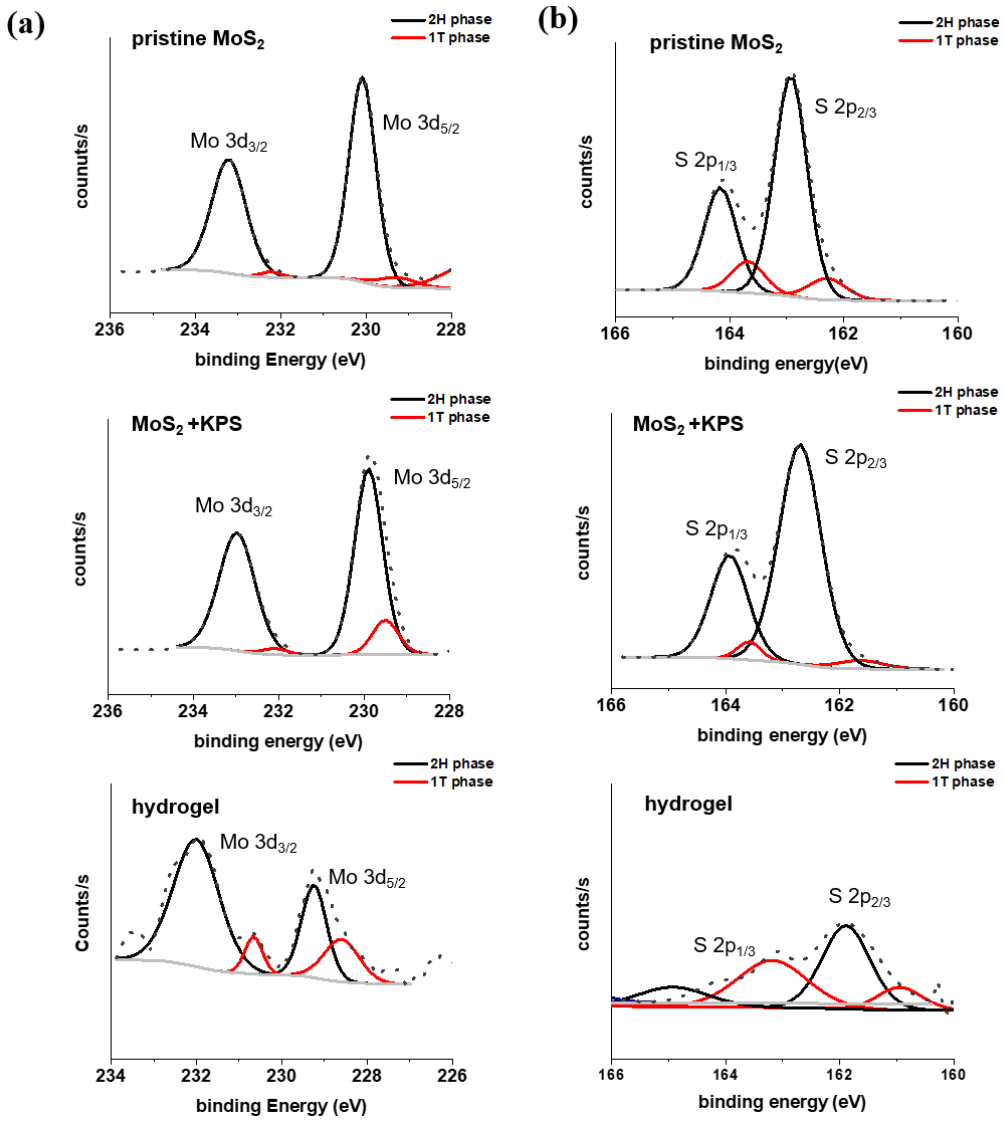

Figure III-7. Evolution of the 1T phase of MoS_2 after gelation when observed by XPS. The spectra for (a) Mo 3d core level peaks and (b) S 2p core level peaks.

measured by SEM (Figure III-8a). The MoS_2 flakes after polymerization was network was found to have a global porous structure, as similarly found in normal hydrogel networks. The pore diameter ranged from 0.6 to 2 μm,con firmed through TEM (Figure III-8b). When preparing the sample, the aqueous solution of acrylamide (0.3 M, 2.5 mL) was deliberately diluted to impede the overall gelation for the measurement; thereafter, the same amounts of MoS_2 (0.08 wt%) and KPS (0.02 mmol) were added as previously used. After stirring for 48 h at 25 °C and vigorous washing by filtration, the individual flake that was covered with poly(acrylamide), which gives the notion that the cross- linking mainly resulted from the MoS_2 nanoplates for the formation of the hydrogel networks was observed.

The swelling behavior of the composite hydrogel was also investigated The hydrogel kept absorbing water for over 250 h and the swelling degree reached near 1500% at saturation, although it did not swell at all in N,N-dimethylformamide (DMF). The continuous and considerable absorption of water would be ascribed to the reversible nature of the physical cross-linking in the hydrophilic network [41,42]

Taken together, conjecture that the electron transfer between MoS_2 and KPS causes the redox reaction under aqueous conditions and produces the radical species, which initiate the radical polymerization of acrylamide. The

incorporated MoS_2 flakes simultaneously provide physical cross-linking points, taking advantage of surface-bound radicals or potential non-covalent interaction with the polymer chains, such as electrostatic force or hydrophobic effect, which brings about the formation of composite hydrogels involving the phase transition of MoS_2 [43,44].

In addition, I investigated the redox-initiated radical polymerization under various conditions, which would provide a versatile synthetic route for acrylic, composite hydrogels. In Figure III-9a, the polymerization was performed as wrapping the reaction vessel in aluminum foil. After degassing and storing for 48 h at 25 °C, the hydrogels was obtained under dark conditions showing the same mechanical properties, which would exclude the spurious chance of radical formation by light. Furthermore, other monomers were tested to form diverse composite hydrogels. For example, a very soft hydrogel using N,N-dimethylacrylamide (DMA) at a concentration of 200 mg/mL, of which the Young's modulus was measured as an average of 8.1 ± 1.1 kPa, which is far lower than the value of the acrylamide-based hydrogels (~0.05 MPa) was prepared. It presume that acrylamide, which causes highly efficient hydrogen bonds, resulted in a studier composite hydrogel when polymerized compared to that from DMA [45,46]. The copolymerization of 1:1 acrylamide–DMA (w/w) in water at the same concentration also produced the hydrogel without showing

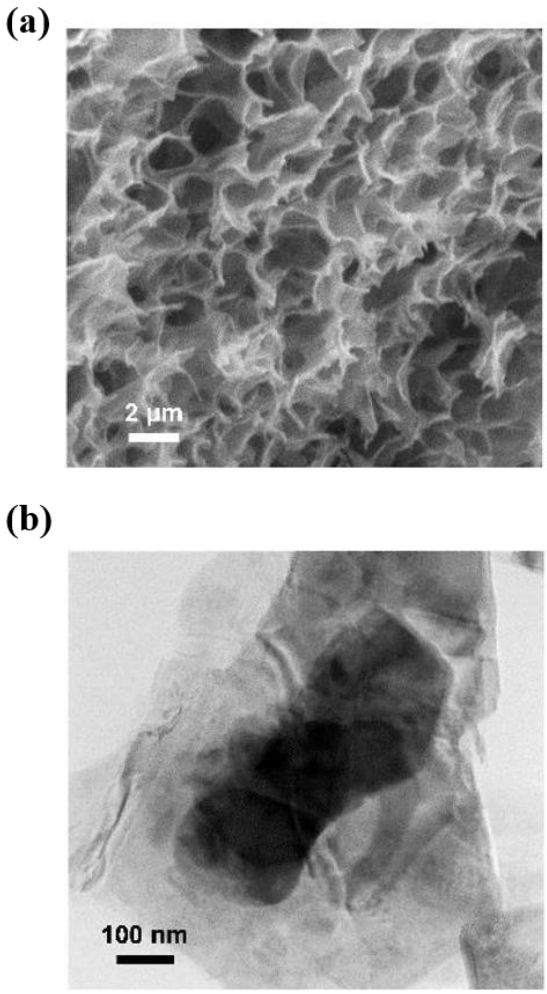

Figure III-8. (a) Scanning electron microscopy (SEM) after lyophilization and (b) transmission electron microscopic (TEM) image of MoS_2 after polymerization.

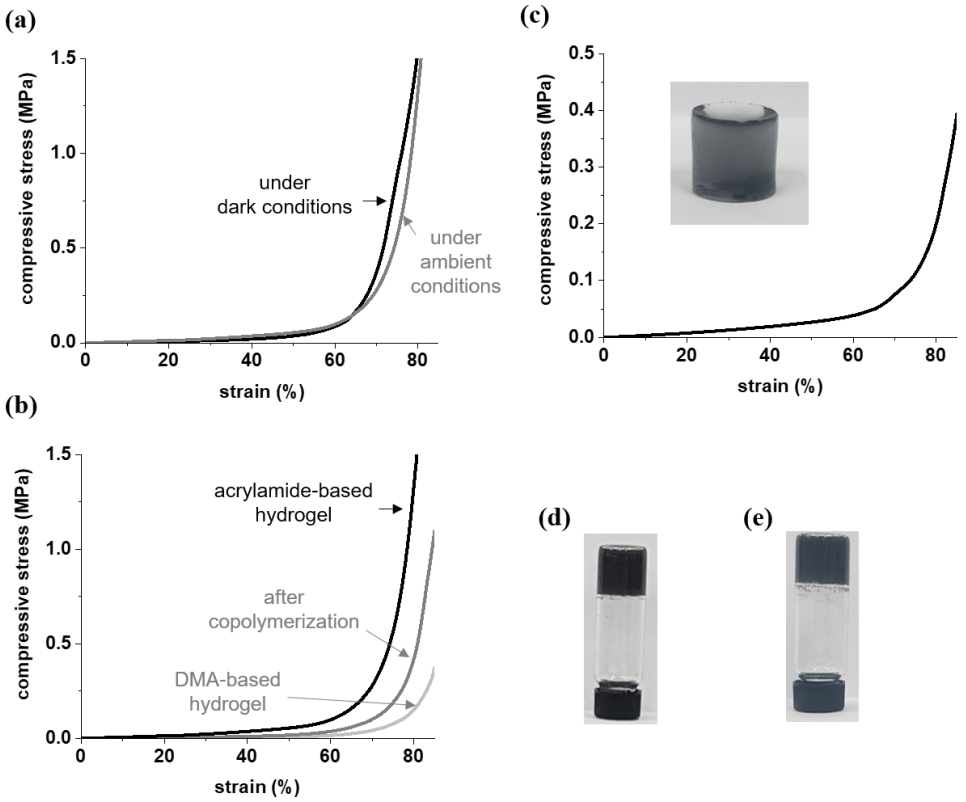

Figure III-9. (a) Compressive stress–strain curve from the composite hydrogel prepared under dark conditions (black), (b) the curves of the hydrogels obtained from DMA (light gray) or after copolymerization of DMA and acrylamide (gray), (c) compressive stress–strain curve of the hydrogel using $MoSe_2$.The inset shows the photograph of the resulting cylindrical hydrogel. Photographs of (d) DMA and (e) 1:1 acrylamide–DMA (w/w).

self- which is in-between the values of the individual hydrogels sorting. The elastic modulus was found to be an average of 0.02 ± 0.01 MPa, indicating the inclusion of both components. The obtained curves are shown in Figure III-9b. I attempted to prepare a composite hydrogel using N-isopropylacrylamide (NIPAM); however, the material due to the lower critical solution temperature (LCST) behavior of poly(NIPAM), which hindered the uniform gelation of the material could not been obtained[47]. Moreover, other metal chalcogenides were tesed . For example, $MoSe_2$ (0.08 wt%) created an acrylamide-based composite showing a very low compressive modulus of 0.03 ± 0.01 MPa (Figure III-9c), whereas the same amount of WS_2 could not polymerize the monomer under the same conditions and agglomerated on the surface . It was deemed that the surface and electronic properties of the inorganic components would also affect the formation of the composite hydrogels [48].

III-3-2. Self-healing of hydrogel

The self-healing properties of the composite hydrogels were further demonstrated, taking advantage of the nature of the physical cross-linking points on the MoS_2 flakes. The composite hydrogel film was similarly prepared using 0.08 wt% MoS_2 and 0.02 mmol KPS, after which it was cut in half. The two

half-strips measured 2.75 cm × 0.8 cm × 0.1 cm each, and one strip was dyed in red by brief immersion in a solution of Rhodamine 6G (0.2 mM, 10 mL) for visual clarity. After thermal treatment at 70 °C for 3 h, it found that both separate ends of the two strips were held together due to the intrinsic elasticity and reversibility of the physical cross-links in the network [49]. Thus, a whole single strip that exhibited negligible expansion in length (less than 8%) was obtained and was comparable to the pristine sample. The half portion of the healed strip was fluorescent under yellow light due to the dye molecules under 365-nm irradiation using a UV hand lamp, as shown in Figure III-10b. Some of the dye molecules diffused to the other side of the cut, supporting that the two cut strips were rejoined via the internal exchange of physical cross-linking points at the interface during the heating process. Moreover, the tensile properties of the healed sample were investigated (Figure III-10c). Almost 70% recovery in the elastic modulus and the ultimate strength and 83% recovery in the toughness as compared to those of the pristine sample before it was cut were achieved. Meanwhile, the maximum strain at the fracture was measured to be similar, which implies that some defects or pinholes would be formed during the healing process, which slightly reduced the mechanical strength of the sample 5. However, the healed sample was still malleable as before; it could be repeatedly stretched more than 800% by hand without exhibiting structural failure (Figure

III-10d). I further prepared two cut-control hydrogel strips (cross-linked by MBA, 0.16 wt%) that exhibited similar mechanical performance, and found that they did not cling together when heated. Furthermore, the interface between the MoS_2-containing composite and the control sample did not adhere either, presumably due to the lackof the exchange of the cross-linking points.

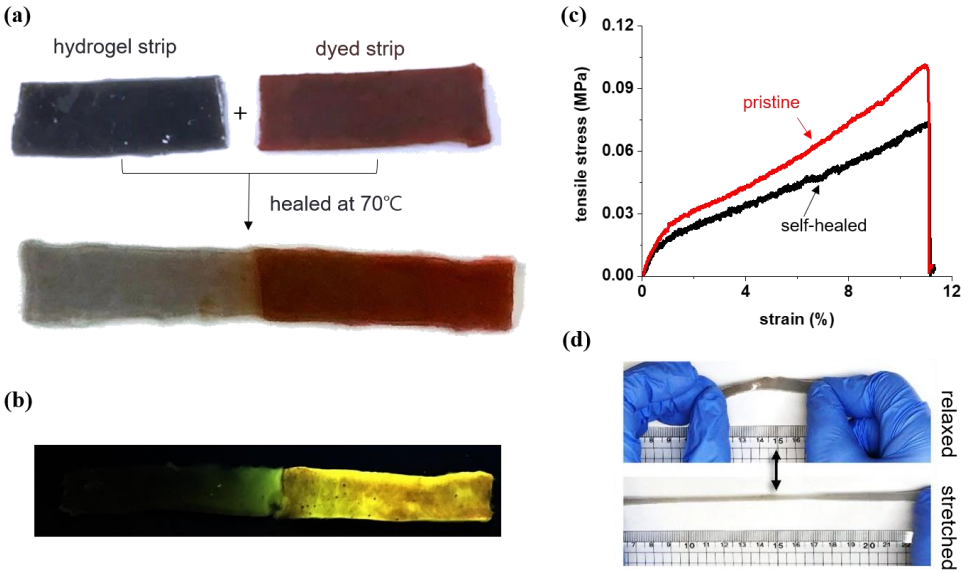

Figure III-10. (a) Self-healing of the hydrogel materials, (b) Photograph of the healed hydrogel taken under 365-nm irradiation, (c) Representative tensile stress–staincurves of a pristine hydrogel strip (red) and the healed one(black). (d) Photographs of the healed strip when stretched by hand and relaxed.

III-4. Conclusion

This study has newly demonstrated the multifunctional role of MoS_2 in the preparation of composite hydrogels through radical polymerization. The addition of a trace amount of 2H-phase MoS_2 remarkably promoted the generation of radical species when reacted with KPS, which initiated radical polymerization under aqueous conditions. The inorganic flakes simultaneously provided cross-linking points and formed the network structure, accompanying the 45% structural transformation from 2H to 1T phase. The resulting composite materials exhibited enhanced mechanical strength than the control hydrogels that included the same amounts of chemical cross-linkers. Moreover, they exhibited self-healing properties owing to their reversible, non-covalent network. Thus, the healed materials recovered their mechanical strength as was found prior to the cutting process. This design approach would not only streamline the synthetic procedures for general composite hydrogels when expanded to other radical-mediated polymerization reactions, but also offer a modular design of complex, functional hydrogelscapable of showing autonomous responses, catalytic activity, and enhanced mechanical strength.

III-5. References

[1] J. R. Capadona, K. Shanmuganathan, D. J. Tyler, S. J.Rowan, C.Weder, *Science*, 2008, **319**, 1370–1374.

[2] M. S.de Luna, Y. Wang, T. Zhai, L.Verdolotti, G. G.Buonocore, M. Lavorgna, H. Xia, *Prog. Polym. Sci.*, 2019, **89**, 213–249.

[3] K. Sano, Y. Ishida, T. Aida, *Angew. Chem. Int. Ed.,* 2018, **57**, 2532–2543

[4] S. Naficy, H. R. Brown, J. M. Razal, G. M.Spinks, P. G. Whitten, *Aust. J. Chem.,* 2011, **64**, 1007–1025.

[5] H. Qin, T. Zhang, N. Li, H.-P. Cong, S.-H.Yu, *Nat. Commun.* 2019, **10**, 2202.

[6] K. Sano, Y. O.Arazoe, Y. Ishida, Y. Ebina, M. Osada, T. Sasaki, T. Hikima, T. Aida, *Angew. Chem. Int. Ed.,* 2018, **57**, 12508–12513.

[7] B. W. Walker, R. P. Lara, E. Mogadam, C. H. Yu, W. Kimball, N. Annabi, *Prog. Polym. Sci.,* 2019, **92**, 135–157.

[8] Z. Li, G. Davidson-Rozenfeld, M. Vázquez-González, M. Fadeev, J. Zhang, H. Tian, I. Willner, *J. Am. Chem. Soc*., 2018, **140**, 17691–17701.

[9] W. Tanaka, H. Shigemitsu, T. Fujisaku, R. Kubota, S. Minami, K. Urayama, I. Hamachi, *J. Am. Chem. Soc.*, 2019, **141**, 4997–5004.

[10] M. Karimi, P. S. Zangabad, S. Baghaee-Ravari, M. Ghazadeh, H.

Mirshekari, M. R. Hamblin, *J. Am. Chem. Soc.*, 2017, **139**, 4584−4610.

[11] M. F.-C. omera, R. Göstl, H. Shaikh, G. ter Huurne, J. Schill, I. K.Voets, C. Storm, R. P. Sijbesma, *J. Am. Chem. Soc.*, 2019, **141**, 1989-1997.

[12] B. Mandal, A. P. Rameshbabu, S. R. Soni, A. Ghosh, S. Dhara, S. Pal, *ACS Appl. Mater. Interfaces.*, 2017, **9**, 36583–36595

[13] K. Liu, X. Pan, L. Chen, L. Huang, Y. Ni, J. Liu, S. Cao, H. Wang, *ACS Sustainable Chem. Eng.*, 2018, **6**, 6395−6403.

[14] S. Singh, N. Shauloff, R. Jelinek, *ACS Sustainable Chem. Eng.*, 2019, **7**, 13186–13194.

[15] R. Takahashi, T. Ikai, T. Kurokawa, D. R. King, J. P. Gong, *J. Mater. Chem. B*

[16] M. Boota, B. Anasori, C. Voigt, M.-Q. Zhao, M. W. Barsoum, Y. Gogotsi, *Adv. Mater.*, 2016, **28**, 1517–1522.

[17] J. Zhou, S. Zhang, X. Song, R. Wei, X. Zhang, W. Zhao, C. Zhao, *ACS Biomater. Sci. Eng.*, 2019, **5**, 3987−4001.

[18] Y. Chen, X. Xie, X. Xin, Z.-R. Tang, Y.-J. Xu, *ACS Nano*, 2019, **13**, 295–304.

[19] D. Ji, S. Choi, J. Kim, *Small*, 2018, **14**, 1801042.

[20] Q. Hao, C. Zhao, B. Sun, C. Lu, J. Liu, M. Liu, L.-J Wan, D. Wang, *J. Am.Chem. Soc.*, 2018, **140**, 12152−12158.

[21] Y. Wang, N. Xu, D. Li, J. Zhu, *Adv. Funct. Mater.*, 2017, **27**, 1604134.

[22] R. A. Vaia, J. F. Maguire, *Chem. Mater.*, 2007, **19**, 2736–2751.

[23] J. Zhang, P. Du, D. Xu, Y. Li, W. Peng, G. Zhang, F. Zhang, X. Fan, *Ind. Eng. Chem. Res.*, 2016, **55**, 4526−4531.

[24] X. Wang, P. Wu, *ACS Appl.Mater. Interfaces.*, 2018, **10**, 2504−2514.

[25] Y. Zhang, T. He, G. Liu, L. Zu, J. Yang, *Nanoscale*, 2017, **9**, 10059

[26] J. Zhang, W. Lei, J. Schutz, D. Liu, B. Tang, C. H. Wang, X. Wang, X. *J. Polym. Sci. Part B: Polym. Phys.*, 2019, **57**,406–414

[27] H. S. Kim, J. An, B. Y. Lee, *Adv. Mater.Technol.*, 2019, **4**, 1900021.

[28] K. S. Kolahi, A. Donjacour, X. Liu, W. Lin, R. K. Simbulan, E. Bloise, E. Maltepe, *PLoS ONE*, 2012, **7**, e41717.

[29] T. Nishida, H. Endo, N. Osaka, H.-J. Li, K. Haraguchi, M. Shibayam, *Phys. Rev. E Stat. Nonlin. Soft Matter Phys.*, 2009, **80**, 030801(R).

[30] The linear poly(acrylamide) could not show the gelationby itself at the concentration of 200 mg/mL .

[31] B. A. Grzybowski, K. Fitzner, J. Paczesny, S. Granick, S., *Chem. Soc. Rev*., 2017, **46**, 5647–5678.

[32] R. Freeman, M. Han, Z. Álvarez, J. A. Lewis, J. R. Wester, N. Stephanopoulos, M. T. McClendon, C. Lynsky, J.M. Godbe, H. Sangji, E. Luijten, S. I. Stupp, *Science*, 2018, **362**, 808–813

[33] K. M. Lee, H. J. Kim, D. Jung, Y. Oh, H. Lee, C. Han, J. Y. Chang, H. Kim, *ACS Omega*, 2018, 3, 3096–3103.

[34] X. Xu, J. Qin, Y. Wei, S. Ye, J. Shen, Y. Yao, B. Ding, Y. Shu, G. He, H. Chen, *Chem. Eng. J.*, 2019, **365**, 259–269.

[35] X. Duan, Z. Ao, H. Sun, S. Indrawirawan, Y. Wang, J. Kang, F. Liang Z. H. Zhu, S. Wang, *ACS Appl. Mater. Interfaces*., 2015, **7**, 4169−4178.

[36] H. H. Huang, X. Fan, D. J. Singh, W. T. Zheng, *Phys. Chem. Chem. Phys.*, 2018, **20**, 26986–26994.

[37] Y.-C. Lin, D. O. Dumcenco, Y.-S. Huang, K. Suenaga, *Nat. Nanotechnol.*, 2014, **9**, 391–396.

[38] D. Dahanayake, S. Gunasekara, V. Jayaweera, C. Sandaruwan, V. arunarathne, G. A. J. Amaratunga, *CrystEngComm*, 2018, **20**, 6482–6489.

[39] R. Bissessur, M. G. Kanatzidis, J. L. Schindler, C. R. Kannewurf, *J. Chem. Soc., Chem. Commun.*, 1993, **20**, 1582–1585

[40] D. Voiry, A. Mohite, M. Chhowalla, *Chem. Soc. Rev.* 2015, **44**, 2702

[41] M. Suzuki, K. Hanabusa, *Chem. Soc. Rev.*, 2010, **39**, 455–463.

[42] D. Jung, K. M. Lee, T. Tojo, Y. Oh, H. Yoon, H. Kim, *Chem. Mater.*, 2019, **31**, 6249–6256.

[43] K. Haraguchi, *Curr. Opin. Solid State Mater. Sci.*, 2007, **11**, 47–54

[44] K. Haraguchi, H. J. Li, K. Matsuda, T. Takehisa, E. Elliott, *Macromolecules*, 2005, **38**, 3482–3490.

[45] Z. W. Low, P. L. Chee, D. Kai, X. J. Loh, *RSC Adv.*,2015, **5**, 5767-57685.

[46] S. H. Cho, M. S. Jhon, S. H. Yuk, H. B. Lee, *J. Polym. Sci. B Polym.*,Phys., 1997, **35**, 595–598.

[47] The elevating temperature of the solution during the initial stage of polymerization induced the volumetric collapse of poly(NIPAM), leading to the phase separation of the entire hydrogel.

[48] J. Gusakova, X. Wang, L. L. Shiau, A. Krivosheeva, V. Shaposhnikov, V. Borisenko, V. Gusakov, B. K. Tay, B. K., *Phys. StatusSolidi A*, 2017, **214**, 1700218.

[49] It found that the size expansion is insignificant and less than 9%.

[50] It also observed that the fracture occurred at the healedcut unde tensile stress.

Chapter IV.

Rapid accessible fabrication and engineering of bilayered hydrogels

* This work presented in Chapter IV was published in *ACS. Omega*., **3**, 3096 (2018) entitled, "Rapid Accessible Fabrication and Engineering of Bilayered Hydrogels: Revisiting the Cross-Linking Effect on Superabsorbent Poly(acrylic acid)"

IV-1. Introduction

Since poly(2-hydroxyethyl methacrylate) was reported to form a hydrogel in the presence of a cross-linker [1], a myriad of hydrogels have been widely researched for biomedical and environmental purposes. Among them, superabsorbent hydrogels (SHs) confine considerable amount of water into a threedimensional, cross-linked network, which is typically greater than hundreds to thousands times their dry weight, and swell while maintaining the original shape [2−4]. Acrylic acid (or acrylate) and acrylamide are extensively used as monomers, along with other monomers such as N-isopropylacrylamide, N,N-diethylacrylamide, and more interestingly, bioextractable sodium 4-hydroxy-2-methylenebutanoate [5] or polymers including poly(vinyl alcohol), which are further cross-linked covalently or noncovalently in situ or ex situ. [2,6] When exposed to aqueous conditions, hydrophilic groups in the polymer network are primarily hydrated by water molecules, and then, the additional water can be absorbed via capillary force and osmotic pressure for filling the space inside the network. Such wet materials essentially possess small yet functionally crucial cross-linking density, which not only leads to water absorbency but also modulates the physical properties of the entire material on demand, for example, elasticity or swelling ratio.

The versatility of SHs has offered privileged, sustainable applications. For instance, from the perspective of polymeric materials, swellable materials have been used as elastomers, watery matrices, containers, supports, and films, which can be further applied in many fields such as soil conditioning, tissue engineering, desalination, catalysis, and health care [6]. In particular, stimuli-responsive SHs have gained notable interest because of the following characteristics [7-21]: (i) bio- and environmental compatibility, (ii) wide range of functionalmonomers/building blocks including cost-effective natural roducts (e.g., cellulose, alginate, starch, chitosan, polysaccharides, and proteins), (iii) possible use of water as an eco-friendly ubiquitous stimulus, (iv) use of a broad library of wellestablished chemistry for synthesis, for example, radical polymerizations, (v) distinguishable volumetric change, and (vi) processability into smart composites integrated with inorganic components that render synergy effects via hybridization. Besides, responsive SHs have been remarkably used as a hydrogel actuator under aqueous conditions. The materials show reconfigurable shape changes in response to Ph [22], temperature [23-25] salinity [26] metal ions [27,28], light [29], or electric potential [30,31], taking one step forward to biomimetic responses.

In this study, a green fabrication method of bilayered hydrogels that show heterogeneous deformation under aqueous conditions by controlling the cross-

linking density was demonstrated. The bilayer structure consists of homogeneous chemical species (i.e., cross-linked poly(acrylic acid)) and enables low-cost effort-saving fabrication through sequential radical polymerization in water without the need of ancillary Adhesives-eliminating possible interfacial complexity that raises the outbreak of debonding. Instead, only the gap in cross-linking density significantly alters the physical properties of hydrogels, building up programmed responses of the bilayer. Therefore, the effect of cross-linking density on superabsorbency, mechanical strength, and thermal stability of hydrogels, which allows a controlled deformation triggered by water was evaluated . As designed, the bilayered hydrogel curls into a circle when wet; the behavior is dependent on pH. Each layer can be colored with disperse dyes for visual clarity, and the bilayer exhibits material properties emanating from both layers. Furthermore, a circuit switch using a patterned hydrogel was prepared. A small firmly cross-linked hydrogel patch induces enough hydraulic force to bend the loosely cross-linkedhydrogel strip, which closes the circuit and switches on a light-emitting diode (LED).

IV-2. Experimental Section

Materials.

Acrylic acid, di(ethylene glycol)diacrylate, and KPS were obtained from Sigma-Aldrich. Disperse dyes such as Synolon N/Blue S-GLS (navy blue color) and Synolon Rubine S-GEL (red color) were purchased from Kimco. Acrylic acid was distilled under reduced pressure at 50 °C before use. Deionized water was prepared using a water purification system (Pure Power I+, DAIHAN Scientific). All other reagents and solvents used were purchased commercially and were used as received unless otherwise noted.

Characterization.

For nuclear magnetic resonance (NMR) measurement, hydrogel sample 2 was prepared in an NMR tube using D_2O instead of water. ^1H NMR spectrum was recorded using a Bruker 300 MHz NMR spectrometer at 25 °C. Proton chemical shifts are expressed in parts per million (ppm, δ scale) and are referenced to tetramethylsilane ($(CH_3)_4Si$, δ 0.00 ppm) or to residual protium in the solvent (D_2O, δ 4.70 ppm). Data are represented as follows: chemical shift, multiplicity (s = singlet, d = doublet, t = triplet, q = quartet, m = multiplet and/or multiple resonances, and br =broad peak), integration. Carbon nuclear magnetic

resonance (^{13}C NMR) was recorded using a Bruker 500 MHz NMR spectrometer at 25 °C. Carbon chemical shifts are expressed in parts per million (ppm, δ scale) and are referenced to tetramethylsilane ($(CH_3)_4Si$, δ 0.00 ppm).

For the tensile test, the as-prepared hydrogel films were cut using a laser cutter. The films were glued between two PMMA clamps with a superglue. The resulting specimens have a size of 10 mm × 10 mm × 1 mm (length × width × thickness). Uniaxial tensile tests were performed using an Instron 5543 universal testing machine with a 1000 N load cell at 25 °C in air. The specimens were stretched at a rate of 5 mm/min until the samples were broken.

The elastic modulus and toughness were calculated from the initial slope (strain range of 10−30%) and the area under the stress−strain curve, respectively. Each film type was tested in quintuplicate; the average and standard deviations from this set were plotted. Micromorphology of the dried hydrogel film was observed using a Carl Zeiss SUPRA 55VP scanning electron microscope at an accelerating voltage of 2 kV. Before the measurement, the sample was dried using a lyophilizer for 3 d and coated with a thin platinum layer. Attenuated total reflection Fourier transform infrared spectroscopy measurements were performed using a Nicolet-6700 instrument (Thermo Scientific) at room temperature. The spectrum was obtained by averaging 32 scans over the range of 4000 to 400 cm^{-1}.

Synthesis of a Poly(acrylic acid)-Based Hydrogel

Hydrogel films were prepared via typical free-radical polymerization. A representative example of hydrogel 2 was prepared as follows: To a solution of acrylic acid (14.7 g, 0.204 mol, 1490 equiv) in water (8 mL), sodium hydroxide (6.6 g, 0.165 mol, 1190 equiv) was added dropwise in water (16 mL), resulting in 80% neutralization of acrylic acid. The monomer solution was degassed by vigorous N_2 bubbling for 1 h. After adding KPS (37 mg, 0.14 mmol, 1.0 equiv, 0.25 wt %) and di(ethylene glycol) diacrylate (50 mg, 0.23 mmol, 1.7 equiv, 0.34 wt %), the reaction mixture was transferred to a glass template having a size of 11.5 cm × 15 cm × 0.1 cm (width × length × thickness) and placed on a heating plate having a set temperature of 55 °C for 2 h. A freestanding hydrogel film was obtained after unloading from the mold in a quantitative yield. IR (cm^{-1}): 3361, 2932, 2852, 1685.8, 1552, 1405, 1294; 1H NMR (300 MHz, D_2O): δ 1.82 (br s, methine protons), 1.23 (br s, methylene protons); 13C NMR (125 MHz, D_2O): δ 183.6, 44.8, 37.3, 36.1. The amounts of initiator and cross-linker were varied from 0.05 to 0.75 and from 0.20 to 0.80 wt %, respectively, with reference to the amount of acrylic acid monomer. For investigating the cross-linker effect (Figure 4), the amount of initiator was set at 0.25 wt %; for the initiator effect (Figure S1), 0.34 wt % cross-linker was used, as shown in Table IV-1.

Table IV-1.. Compositions of Cross-Linker and Initiator

for crosslinker effect		for initiator effect		
cross-linker (wt %)	**Initiator (wt %)**	**cross-linker (wt %)**	**Initiator (wt %)**	**control variables**
0.20			**0.05**	
0.34			**0.17**	
0.42	**0.25**	**0.34**	**0.25**	**acrylic acid**
0.50			**0.43**	**NaOH**
0.63			**0.56**	
0.80			**0.75**	

Preparation of Bilayered Hydrogels.

Bilayered hydrogels were prepared by sequential radical polymerization. Di(ethylene glycol)diacrylate (50 mg, 0.233 mmol, 1.7 equiv, 0.34 wt %), KPS (37 mg, 0.14 mmol, 1.0 equiv, 0.25 wt %), and a navy blue dye (10 mg) were added to 80%-neutralized acrylic acid (14.7 g, 0.204 mol, 1490 equiv) solution. The first polymerizing solution was poured into a glass template (11.5 cm × 15 cm × 0.1 cm), which was covered with a glass lid, and heated at 55 °C for 2 h to afford the first layer. The second layer was synthesized onto the first layer in a similar manner. After the fabrication of the first layer inside the glass template, additional glass slides (thickness, 0.1 cm) were placed as a spacer. In this step, the first layer was masked with glass pieces when preparing the patterned bilayer. The second polymerizing solution was prepared by adding di(ethylene glycol)diacrylate (119 mg, 0.556 mmol, 4.1 equiv, 0.80 wt %), KPS (37 mg, 0.14 mmol, 1.0 equiv, 0.25 wt %), and a red dye (10 mg) to the 80%-neutralized

acrylic acid solution. The second solution was carefully injected into the gap between the first layer and glass lid and then heated at 55 °C for 2 h. The freestanding bilayer hydrogel was obtained in a quantitative yield after unloading from the mold and cut into pieces of desired sizes by using a laser cutter or razor.

IV-3. Results and Discussion

IV-3-1. Synthesis and Characterization of hydrogel film

Figure IV-1 shows the synthetic procedure of a poly(acrylic acid)-based hydrogel film under aqueous conditions by radical polymerization. First, acrylic acid (14 mL) was added to water (8 mL). Two phases were separated initially, but 80% neutralization with NaOH gave a homogeneous solution with a molar concentration of 8 mM. Then, di(ethylene glycol) acrylate (cross-linker) and potassium persulfate (KPS) (initiator) were added to provide a ready-topolymerize solution, which was transferred by a syringe to a glass template having a rectangular space inside (11.5 cm × 15 cm × 0.1 cm) for polymerization. The template had a high ratio of surface area to volume and could facilitate efficient heat transfer, which is similar to controlling autoacceleration process in the sheet-type mold. After the displacement, the monomer solution was polymerized on a heating plate at a set temperature of 55 °C for 2 h; the cross-linked hydrogel film was obtained and unloaded from the mold. The soft film was even and transparent without the inclusion of severe cavitation and had a size similar to that of the template. The chemical structure of the hydrogel is shown in the inset of figure IV-1**.**

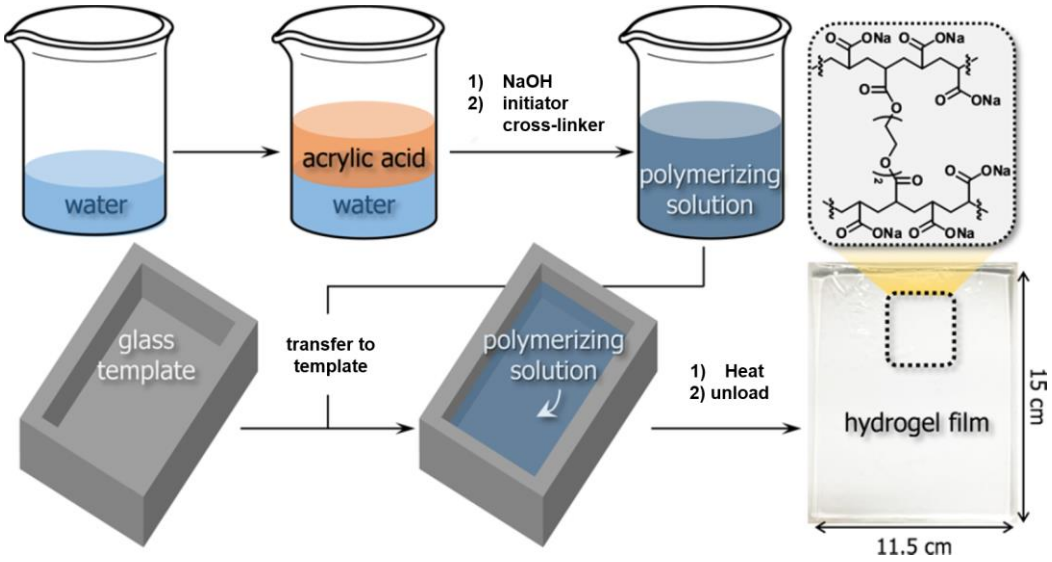

Figure IV-1. Schematic description for the preparation of a poly(acrylic acid)-based hydrogel film**.**

A poly(acrylic acid) film dramatically absorbs water and shows a distinct size expansion while maintaining its initial shape. During swelling, the diacrylate cross-linker in the hydrogel films fundamentally affected the superabsorbency. As shown in Figure IV-2a, hydrogel films 1−6 containing different amounts of cross-linker under the same conditions were prepared, the films with deionized water were wetted, and the effect of crosslinker on the absorbency by calculating the degree of swelling and cross-linking density (ρ) was expressed [32].

The initial as-prepared samples had similar values for degree of swelling (44−47%), irrespective of the amount of crosslinker, because the films were consistently prepared from 0.8 M monomer solutions in water. However, after drying and reswelling in water for 48 h, the hydrogel films showed different swelling ratios, which hinged on the cross-linking density. Film 2 (0.34 wt % of cross-linker) swelled for a maximum of 200 times, and then, the value decreased as more cross-linkers were involved. Figure IV-2b shows an isotropic dimensional change in 2. The initial film had a side of 1.15 cm, which decreased by 26% when lyophilized, but exposure to water increased the side 4.1×. The black square behind the hydrogel film indicates the transparency of the film and supports the size estimation. As expected, the cross-linking density revealed the inverse proportion against the swelling ratio of the films, except for the case of 1, which has the least amount of crosslinker. it reason that the partially soluble

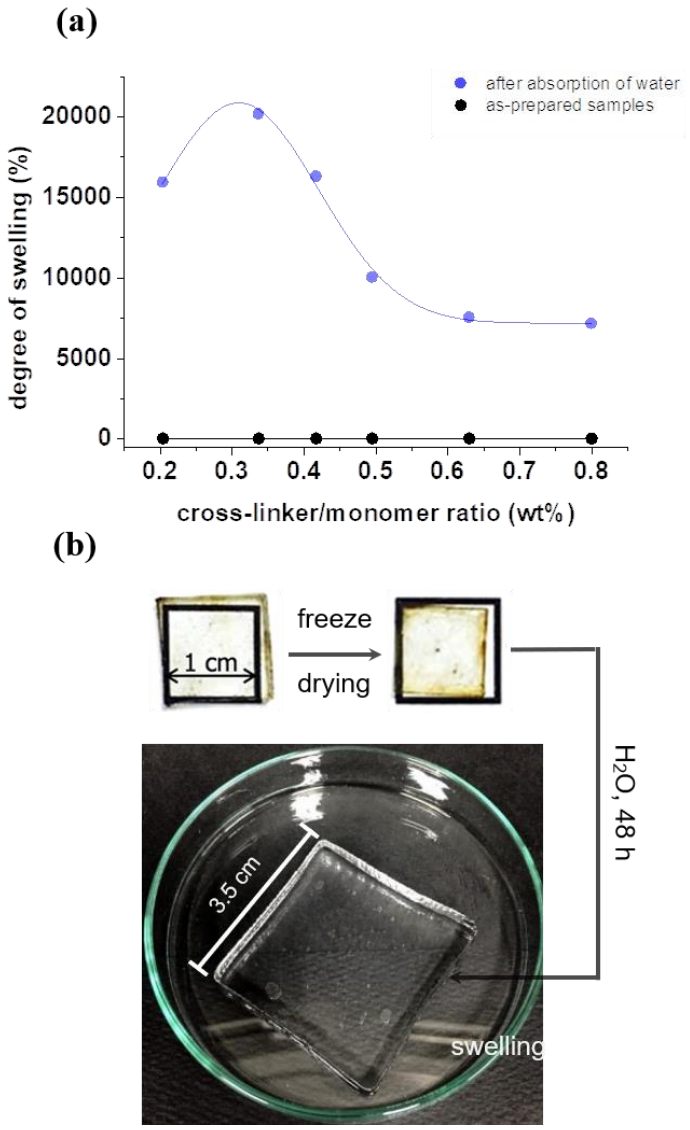

Figure IV-2. (a) Change in degree of swelling of hydrogel films and (b) representative volumetric change in film 2.

loose network of 1 hindered the capillary force for water that the partially soluble loose network of 1 hindered the capillary force for water absorption [34]. In Figure IV-3, the example porous network of 2 was observed using scanning electron microscopy (SEM), which was developed after swelling in water. The pore size ranges from 3 to 20 μm. All experimental values of the obtained hydrogels are summarized in Table IV-2.

Table IV-2. Degree of Swelling and Cross-Linking Density of Hydrogel Films 1−6.

hydrogel film	cross-linker (wt %)	degree of swelling (%)	cross-linking density (mmol/L)
1	**0.20**	**15912**	**0.71**
2	**0.34**	**20164**	**0.47**
3	**0.42**	**16287**	**0.68**
4	**0.50**	**10011**	**1.55**
5	**0.63**	**7509**	**2.54**
6	**0.80**	**7140**	**2.77**

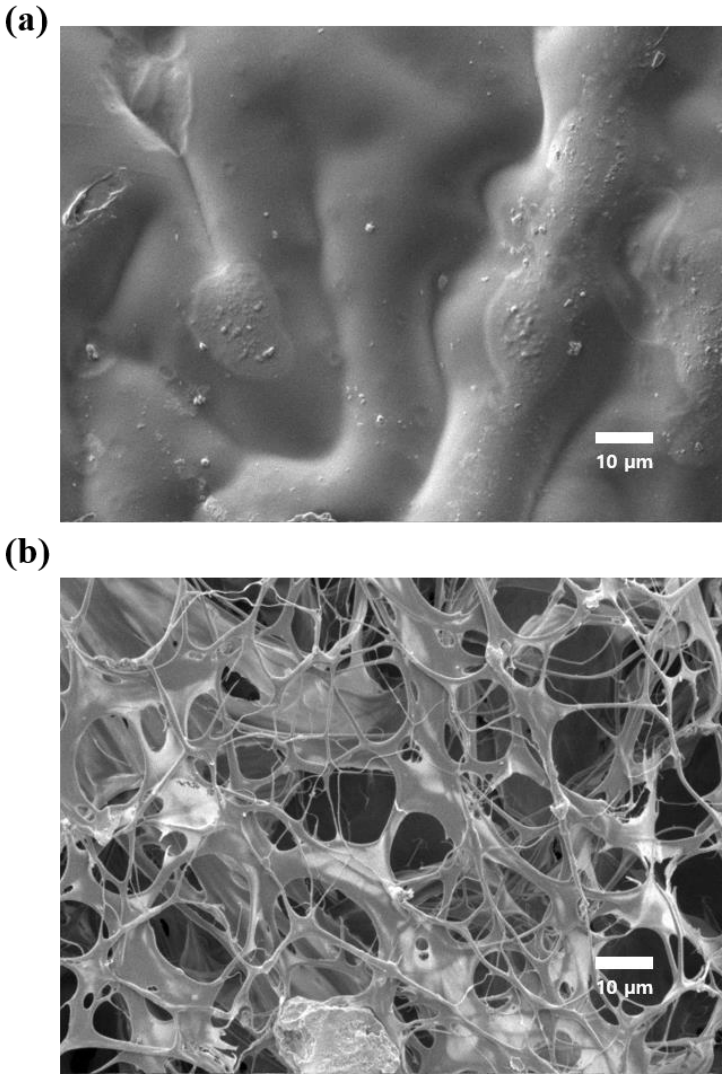

Figure IV-3. (a) SEM images of as-prepared sample and (b) after swelling in water for 48 h.

In addition, the actual change in the temperature of the polymerizing solution during radical polymerization was measured. Therefore, a flexible thermocouple probe was inserted into the polymerizing solution of 2, which was cast inside the template on a heating plate (set temperature, 55 °C), and the temperature was tracked by a digital thermometer, as shown in Figure IV-4a. The temperature exponentially increased for the initial 20 min and then slightly elevated more for 15 min, indicating an accelerated polymerization (Figure IV-4b). In general, Trommsdorff effect aggravates undesirable properties in polymeric materials, such as cavitation or unevenness, during polymerization [35,36]. However, the cast solution of 2 exhibited only a weak exothermic process, from which the regular hydrogel film 2 was produced. The maximum temperature was found to be 50.4 °C; thereafter, the temperature of the film was stabilized at 48 °C until the end of the reaction.

Chemical cross-linking provides an effective approach to control the mechanical strength of polymeric materials. Herein, the stress−strain curves of the resulting films was measured. As described in Figure IV-5 , toughness values increased until the amount of cross-linker increased from 0.20 (film 1) to 0.34 wt % (film 2) and then decreased in inverse proportion to the amount of cross-linker. A similar tendency was observed for elongation at fracture. As an example, at 0.34 wt %, the toughness of film 2 was found to be

(a)

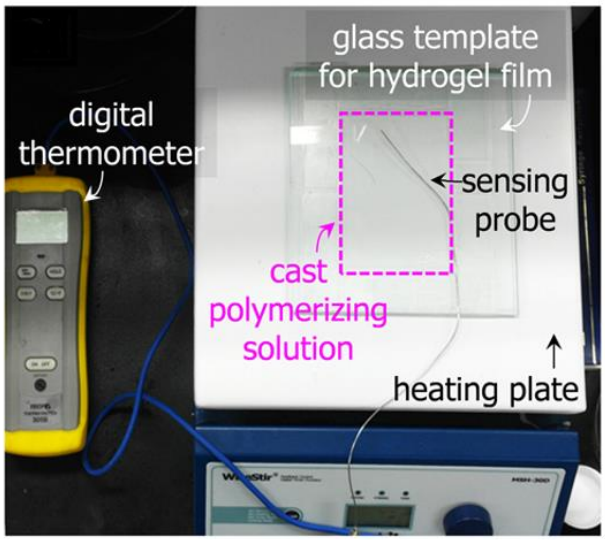

(b)

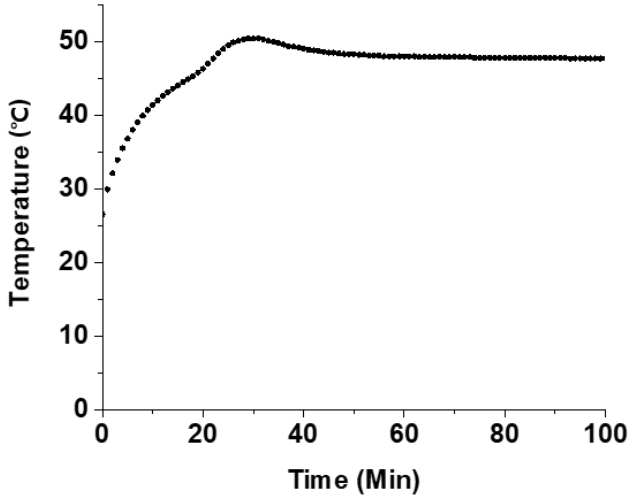

Figure IV-4. (a) Photograph of measuring temperature of the polymerizing solution of 2 and (b) Change in the temperature of the solution during radical polymerization.

0.28 MJ m^{-3} with 300% elongation at fracture. On the other hand, Young's modulus only fluctuated within a narrow range of 0.12−0.15 MPa. Presumably, small change in cross-linker concentration would manipulate microstructures or induce microdeformation in hydrogels, leading to a change in ductility of materials rather than stiffness. The initiator concentration was changed, which can control the molecular weight between the cross-links (Mc), another factor affecting the crosslinking density, during polymerization [37,38]. Thus, film 2 using different initiator concentrations was polymerized. Toughness increased in proportion to the amount of initiator until 0.56 wt % of KPS was incorporated (a maximum toughness, 0.40 MJ m^{-3}) and then decreased; in contrast, elongation at fracture decreased above 0.43 wt %. Although the total changes were much smaller than the results from the cross-linker concentration, a detailed future investigation would elaborate complementary effects of both factors on the mechanical properties of the hydrogel materials.

Furthermore, 1, 3, and 6 were Taken and their tensile strengths at 80 °C to investigate a thermal effect were measured. At 80 °C, the films stiffened more-toughness and elastic modulus increased and elongation reduced-as compared to the measurement at 25 °C (Figure IV-6a−c). The total exposure time to heat during testing was less than 2 min. The fractured specimen from 3 (0.42 wt %) was hard and brittle. To examine the effect of thermal treatment on hydrogels,

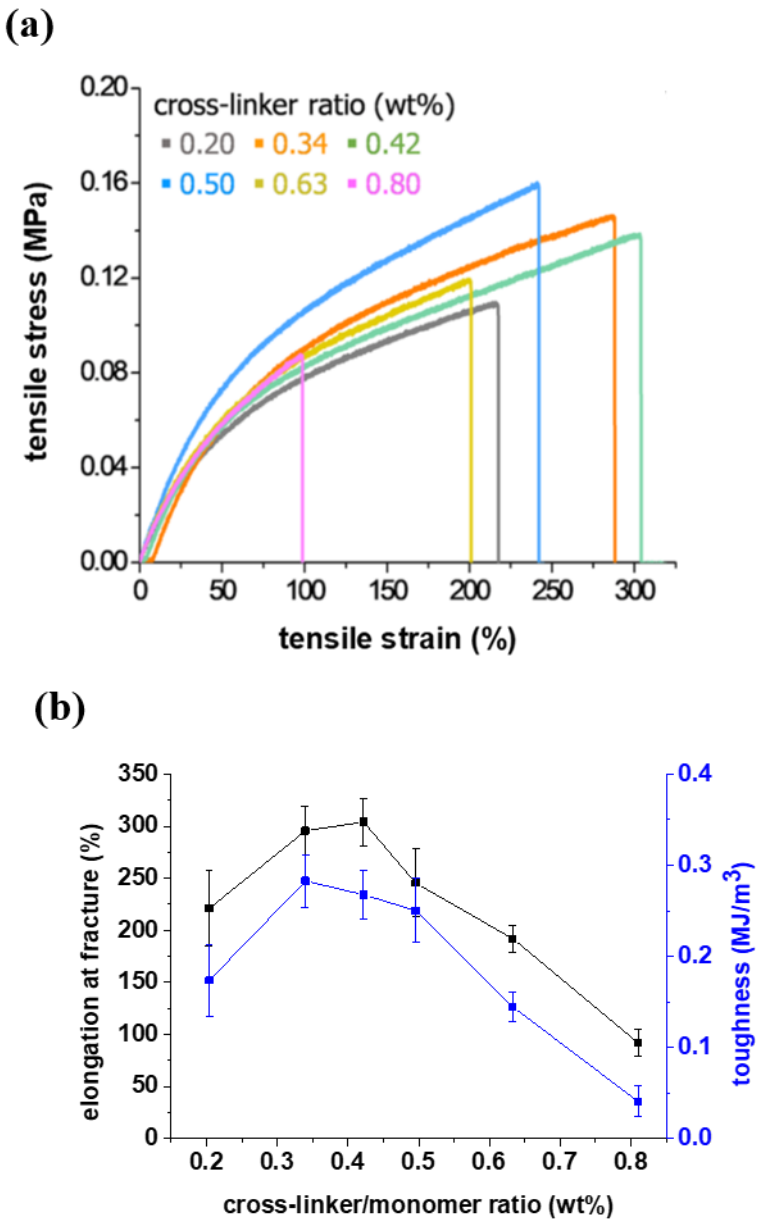

Figure IV-5. (a) Representative tensile stress−strain curves from the hydrogel and (b) change in toughness (blue), elongation at fracture (black).

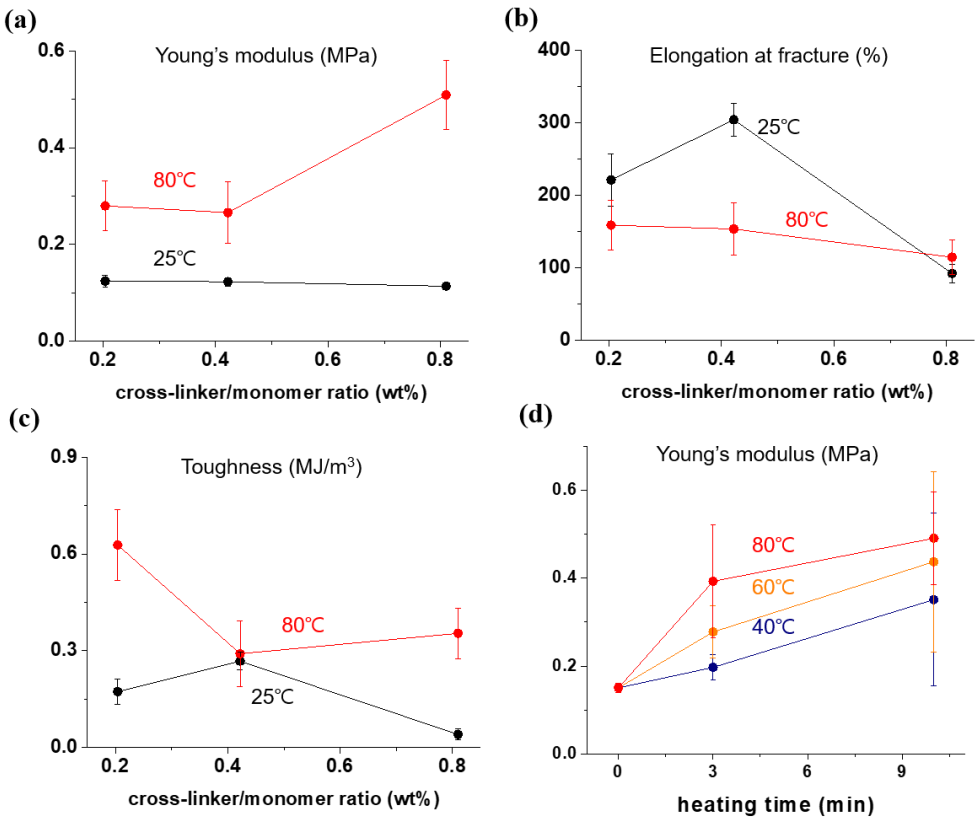

Figure IV-6. Young's modulus (a), elongation at fracture (b), and toughness (c) of hydrogel films 1, 3, and 6, measured at 80 °C (red). The results from 25 °C (black) and (d) Change in Young's modulus of 3 after exposure to different temperatures.

film 3 at 40, 60, and 80 ℃ for 3 and 10 min were incubated and their mechanical strengths at the same temperatures were tested (Figure IV-6d). The longer the exposure time at a higher temperature, the more rapidly did the Young's modulus increase, which indicates that the film hardened by thermal drying. On the other hand, potential thermal annealing would occur together inasmuch as the modulus gradually increased even at 40 ℃ less than the polymerizing temperature.

IV-3-2. Synthesis and Characterization of hydrogel bilayers

A minor modification in the chemical structure (i.e., cross-linking density) alters the macroscopic physical properties of polymeric materials, highly encouraging us to develop responsive hydrogels capable of showing designed behaviors in water. In particular, when two adjacent parts with different cross-linking densities are joined together, the interface in between gives rise to heterogeneous deformation of the entire material, taking advantage of the different swelling ratios in an aqueous medium. Hence, this study have designed and fabricated bilayered hydrogels by sequential radical polymerization (Figure IV-7a). In a glass template, the first layer containing 0.34 wt % dyed with of 0.25 wt % KPS was prepared . Each polymerizing solution was dyed with navy blue and red disperse dyes for differentiation before conducting polymerization. Therefore, in situ polymerization provided a bilayered structure of hydrogel in

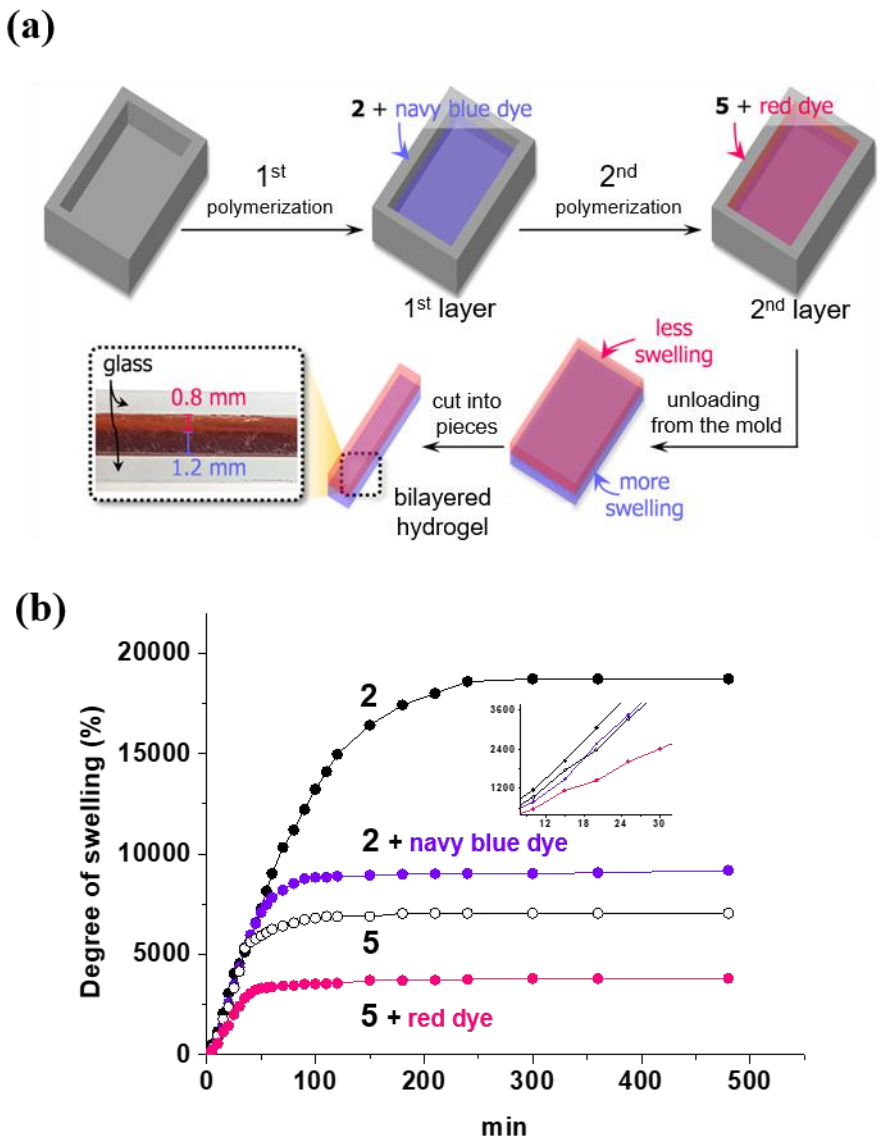

Figure IV-7. (a) Fabrication of the bilayered hydrogel via sequential polymerization and (b) Change in the degree of swelling of each colored layer.

which the thickness of the first (navy blue) and second (red) layers measured 1.2 and 0.8 mm, respectively. The hydrogel layers adhered tightly to one another because of the probable interpenetration that would occur at the interface during the second polymerization reaction. After unloading from the glass mold, the bilayer was obtained, which had a volume of 2.8 cm × 0.2 cm × 0.3 cm and displayed an anisotropic shape change.

Figure IV-7b shows the change in the degree of swelling of each layer in deionized water the navy blue 2 and red 5 hydrogels exhibited a total degree of swelling that decreased in half when fully swelled, compared to 2 and 5 before dying. The insoluble dyes also affected the swelling rates of both hydrogel layers, which reduced from 193 to 177% min^{-1} for 2 and from 161 to 96% min^{-1} for 5 after dying, calculated from the linear slopes of the initial region (inset in Figure IV-7b). The dyes in the layers were swapped , which yielded red 2 and navy blue 5 films. However, both samples showed less difference in the swelling ratios, meaning that the bilayer from navy blue 2 and red 5 can better induce the reconfiguration. Inclusion of the dyes also altered the mechanical strength of the hydrogel bilayer (Figure IV-8b). The hydrophobic dyes enhanced the elongation at fracture of 2 and 5, which could sustain cross-linked structures during the elongation under tensile stress [40]. However, the bilayer displayed an average elongation at fracture of both hydrogels as expected, whereas the Young's

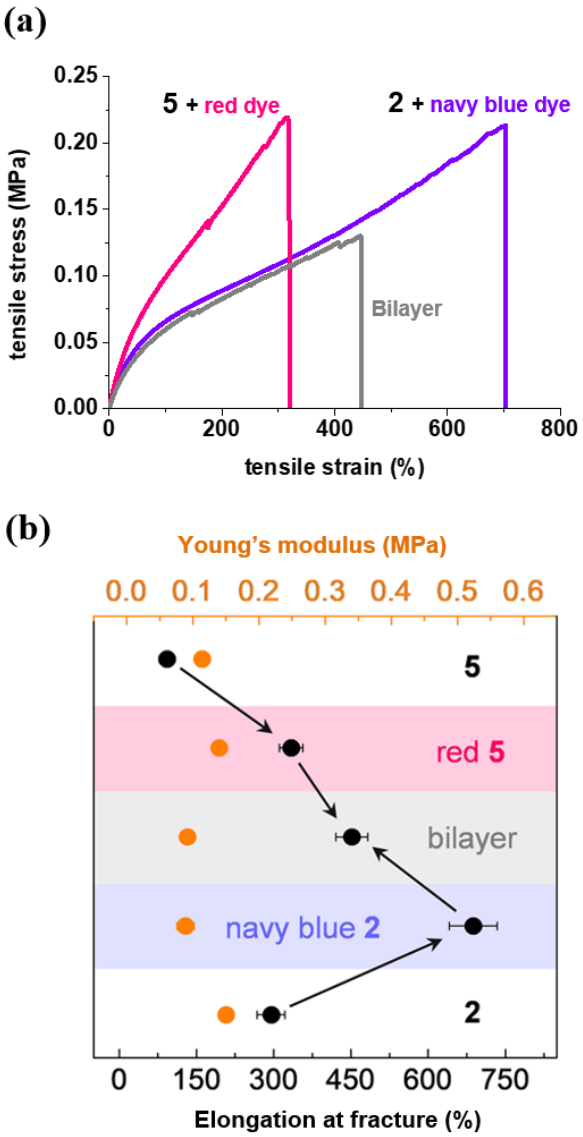

Figure IV-8. (a) Representative tensile stress–strain curves measured from navy blue 2, red 5, and the resultingbilayer and (b) Change inelongation at fracture (black) and Young's modulus (orange) of hydrogels when dyed and integrated.

modulus did not change much. Representative stress−strain curves are shown in Figure IV-8a.

A designed behavior of bilayer is presented in Figure IV-9 . Here, the bending of the bilayer in various pHs, which can affect the actuation of polyelectrolyte materials was investigated . Figure IV-9 shows the bilayer bending in a neutral pH 7 buffer. As soon as immersed in the buffer, the linear material bent in a round shape in 15 min, as the navy blue layer (2, 0.34 wt % crosslinker) that positioned outside swelled more than the red layer (5, 0.80 wt % cross-linker) inside. A longer exposure to the medium only increased the whole size of the bilayer to a small extent but did not unfold the shape . In addition, the effect of pH on the behavior of the hydrogel in aqueous media was investigated. Figure IV-10a reveals the change in the curvature of the deformed hydrogels when exposed to various pHs of 3, 7, and 10. The curvature of hydrogels autonomously increased as time elapsed. The curvature increased slightly faster (the rate of folding was found to be 28.1 m^{-1} s^{-1}, calculated from the initial linear region) at pH 3 than that at pH 7 (26.7 m^{-1} s^{-1}), but the final curvature was slightly lower than the value resulted from pH 7, accompanying less folding. Interestingly, the curvature increased most rapidly at pH 10 (rate, 33.6 m^{-1} s^{-1}; 1.3 times faster than that at pH 7), and the final curvature reached 224 m^{-1}-thet heoretical curvature of a circle that has 2.8 cm circumference-in 9 min, as

Figure IV-9. Time-lapsed photographs of the bending of the hydrogel bilayer in a pH 7 buffer solution at 25 ℃.

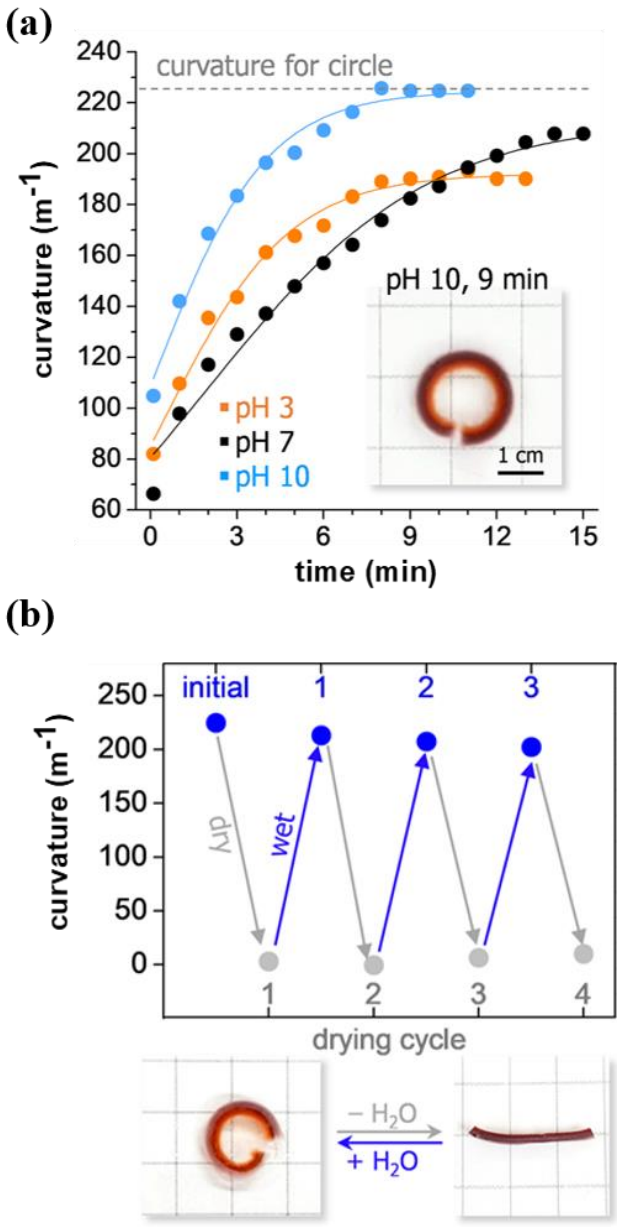

Figure IV-10. (a) Change in the curvature of the bilayer over time while exposed to buffer solutions of various pHs and (b) Change in the curvature of the bilayer during drying−rewetting cycles.

shown in the inset of Figure IV-10a. It assume that protonation of carboxylates at pH 3 could hinder a complete folding of the bilayer as decreasing hydrophilicity and water absorbency as well. However, the remaining acid groups would be deprotonated at pH 10, which could promote water absorbency and the following folding behavior while hydrophilicity increased. Furthermore, tested the reversible shape change of the bilayer that was pre-exposed to pH 10 for 10 min was tested. As expected, the curled bilayer recovered its original shape after taking away from water and drying under air for 1 h at 70 °C but bent again when rewet for 10 min at pH 10. During five drying−rewetting cycles, the bilayer iterated the programmed response without structural degeneration (Figure IV-10b). In addition, the hydrogel bilayer through patterning with glass masks (Figure IV-11a) has been engineered . The small glasses masked the first layer (navy blue 2; size, 3 cm × 0.5 cm × 1.3 mm) during the second polymerization, leaving a small red patch (red 5; size, 0.5 cm × 0.5 cm × 0.7 mm) on the bottom layer. The small patch caused the bending of the entire hydrogel in deionized water. The patterned hydrogel between two parallel copper plates was positioned, and the hydrogel was held onto the bottom plate with a crocodile clip. The copper plates were connected to an LED bulb and a dry cell battery, resulting in an open electronic circuit (Figure IV-11b). Asdesigned, the hydrogel bending in deionized water touched the other copper plate 1 cm distant, closing the circuit.

A dim red light before deformation because the hydrogel contains charged ions, which would diffuse into deionized water was seen. However, the underwater actuation lit the LED bulb in bright red in 2 min (Figure IV-11c).

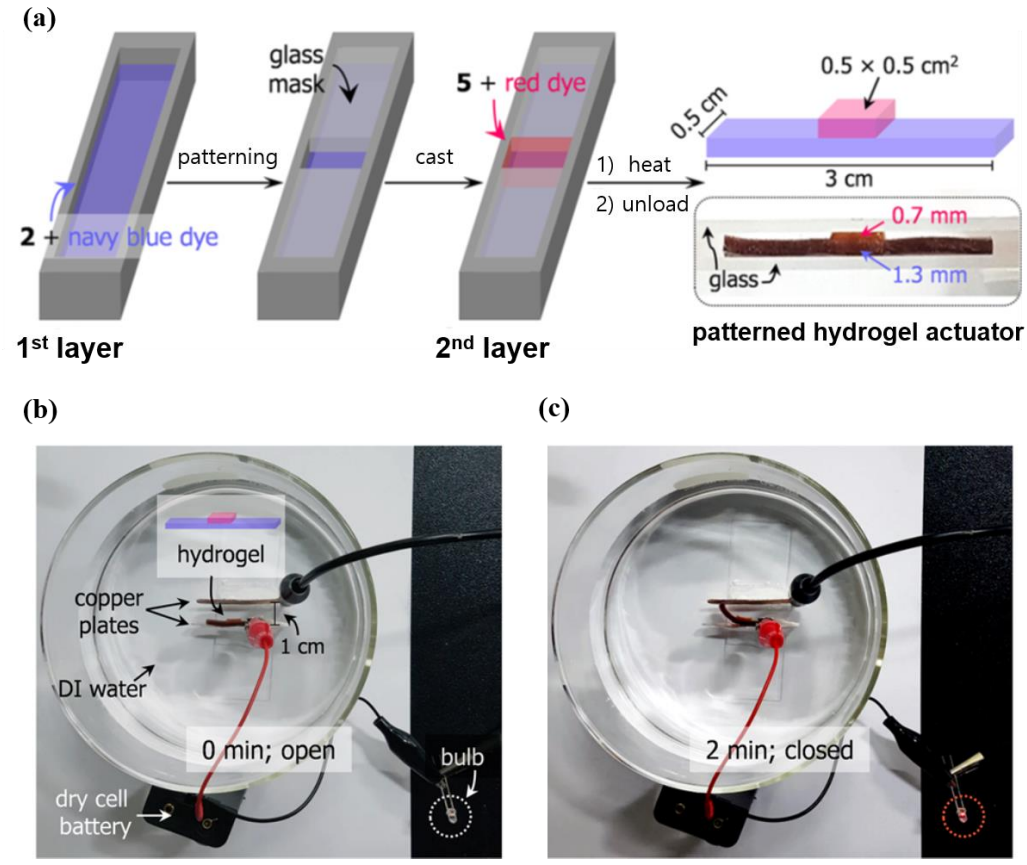

Figure IV-11. (a) Depiction for fabrication of the patterned hydrogel. (b,c) Circuit switch based on the patched hydrogel (b, open circuit). In deionized water, the bending hydrogel connects two plates, switching on the LED in red (c, closed circuit).

IV-4. Conclusion

Bilayered hydrogels capable of showing programmed responses have been demonstrated. The hydrogels are made by crosslinking superabsorbent poly(acrylic acid), where cross-linking density plays a crucial role in manipulating the swelling behavior as well as mechanical strength. In particular, engineering cross-linking density provides heterogeneous deformation when two SHs containing different cross-linking densities are consolidated via sequential in situ polymerization. Through the rapid accessible fabrication, bilayered hydrogels were prepare and each layer with disperse dyes was colored . The concomitant physical changes were investigated. The linear hydrogel bilayer revealed a pH dependent folding behavior and showed remarkably fast complete deformation at pH 10. Furthermore, patterning on the hydrogel brought about a polyelectrolyte switch that closed the circuit and lit an LED bulb in red. This fabrication method can be expanded to other superabsorbent systems using biocompatible monomers, and a merger with diverse functionalities would expedite the development of cross-linked polymeric systems that feature smart responses for many biomedical or eco-friendly applications, for example, microlenses that show a controlled release or functional membranes that remove specific pollutants (e.g., microplastics) in the ocean.

IV-5. References

[1] O. Wichterle, D. Lím, *Nature*, 1960, **185**, 117−118.

[2] F. H. A.Rodrigues, C. Spagnol, A. G. B.Pereira, A. F.Martins, A. R. Fajardo, A. F.Rubira, E. C.Muniz, *J. Appl. Polym. Sci.*, 2014, **131**,39725.

[3] M. R. Guilherme, F. A. Aouada, A. R. Fajardo, A. F. Martins, A. T. Paulino, M. F. T. Davi, A. F. Rubira, E. C. Muniz, *Eur. Polym. J.*, 2015, **72**, 365−385.

[4] F. Ullah, M. B. H.Othman, F. Javed, Z. Ahmad, H. M. Akil, *Mater. Sci. Eng. C.*, 2015, **57**, 414−433.

[5] J. Kollár, M. Mrlík, D. Moravčíková, Z. Kroneková, T. Liptaj, I. Lacík, J. Mosnáček, *Macromolecules*, 2016, **49**, 4047−4056.

[6] K. Kabiri, H. Omidian, M. J. Zohuriaan-Mehr, S. Doroudiani, *Polym. Compos.*, 2011, **32**, 277−289.

[7] J. A. Kelly, A. M. Shukaliak, C. C. Y.Cheung, K. E. Shopsowitz, W. Y. Hamad, M. J. MacLachlan, Angew. Chem., Int. Ed., 2013, 52, 8912−8916

[8] M. Kettunen, R. J. Silvennoinen, N. Houbenov, A. Nykänen, J. Ruokolainen, J. Sainio, V. Pore, M. Kemell, M. Ankerfors, T. Lindström, M. Ritala, R. H. A. Ras, O. Ikkala, *Adv. Funct. Mater.*, 2011, **21**, 510−517

[9] T. Lu, T. Xiang, X.-L. Huang, C. Li, W.-F. Zhao, Q. Zhang, C.-S. Zhao, *Carbohydr. Polym.*, 2015, **133**, 587−595.

[10] M. T. Haseeb, M. A. Hussain, S. H. Yuk, S. Bashir, M. Nauman, *Carbohydr. Polym.*, 2016, **136**, 750−756

[11] K. Deligkaris, T. S. Tadele, W. Olthuis, A. van den Berg, *Sens. Actuators, B*, 2010, **147**, 765−774.

[12] A. W. Chan, R. A. Whitney, R. J. Neufeld, *Biomacromolecules*, 2009, **10**, 609−616.

[13] X. Shi, W. Wang, Y. Zheng, A. Wang, *RSC Adv*. 2014, **4**, 50478−50485.

[14] Y. Gao, X. Li, M. J. Serpe, *RSC Adv*. 2015, **5**, 44074−44087.

[15] F. Chen, A. Greiner, S. Agarwal, *Macromol. Mater. Eng*., 2011, **296**, 517−523.

[16] W. Wang, A. Wang, *Polym. Adv.*, Technol. 2011, **22**, 1602−1611..

[17] C. Chang, L. Zhang, *Carbohydr. Polym.*, 2011, **84**, 40−53

[18] S. Tang, M. Floy, R. Bhandari, M. Sunkara, A. J. Morris, T. D. Dziubla,; J. Z. Hilt, *ACS Omega*, 2017, **2**, 8723−8729.

[19] H. Matsumoto, H. Seto, T. Akiyoshi, M. Shibuya, Y. Hoshino, Y. Miura, *ACS Omega*, 2017, **2**, 8796−8802.

[20] A. Ahiabu, M. J. Serpe, *ACS Omega*, 2017, **2**, 1769−1777.

[21] T. Jiao, H. Zhao, J. Zhou, Q. Zhang, X. Luo, J. Hu, Q. Peng, X. Yan, *ACS*

Sustainable Chem. Eng., 2015, **3**, 3130−3139.

[22] F. Chen, J. Guo, D. Xu, F.Yan, *Polym. Chem.*, 2016, **7**, 1330−1336.

[23] L. Gao, G.Guo, M. Liu, Z. Tang, L. Xie, Y. Huo, *RSC Adv*., 2017, **7**, 40005−40014.

[24] H. Jia, Z. Huang, Z. Fei, P. J. Dyson, Z. Zheng, X.Wang, *J. Mater. Chem. B.*, 2017, **5**, 8193−8199.

[25] Y.-N. Chen, L. Peng, T. Liu, Y.Wang, S. Shi, H. Wang, *ACS Appl. Mater. Interfaces*, 2016, **8**, 27199−27206.

[26] F. Yang, S. Sukhishvili, H. Du, F. Tian, *Sens. Actuators, B*, 2017, **253**, 745−751

[27] B. P. Lee, A. Narkar, Sens. Actuators. B, 2016, **227**, 248−254.

[28] S. Wu, F. Yu, H. Dong, X. Cao, *Carbohydr. Polym.*, 2017, **173**, 526−534.

[29] K. Peng, K. Yang, Y. Fan, A.Yasin, X. Hao, H. Yang, *Macromol. Chem. Phys.*, 2017, **218**, 1700170.

[30] C.Yang, Z. Liu, C. Chen, K. Shi, L. Zhang, X.-J. Ju, W. Wang, R.Xie, L.-Y. Chu, *ACS Appl. Mater. Interfaces.*, 2017, **9**, 15758−15767.

[31] K. Takada, T. Iida, Y. Kawanishi, T. Yasui, A.Yuchi, *Sens. Actuators, B*, 2011, **160**, 1586−1592

[32] D. P. Browe, C. Wood, M. T. Sze, K. A.White, T. Scott, R. M. Olabisi, J. W. Freeman, *Polymer*, 2017, **117**, 331−341.

[33] S. J. Bryant, T. T. Chowdhury, D. A. Lee, D. L. Bader, K. S. Anseth, *Ann. Biomed. Eng.,* 2004, **32**, 407−417

[34] T. K. Mudiyanselage, D. C. Neckers, *J. Polym. Sci., Part A: Polym. Chem.,* 2008, **46**, 1357−1364.

[35] G. A.O'Neil, M. B.Wisnudel, J. M. Torkelson, *Macromolecules*, 1996, **29**, 7477−7490.

[36] J. Chen, Y. Zhao, *J. Appl. Polym. Sci.,* 2000, **75**, 808−814.

[37] R. Singhal, R. S. Tomar, A. K. Nagpal, *Int. J. Plast. Technol.,* 2009, **13**, 22−37.

[38] G. Odian, Principles of Polymerization, 4th ed.; John Wiley & Sons, Inc.: New York, 2004**.**

[39] K. K. H. Wong, M. Zinke-Allmang, *J. Mater. Sci.,* 2010, **45**, 2456−2465

[40] B. Xing, C.-W. Yu, K.-H.Chow, P.-L. Ho, D. Fu, B. Xu, *J. Am. Chem. Soc.,* 2002, **124**, 14846−14847

국문 초록

하이드로젤은 물리적 또는 화학적으로 가교된 3 차원의 친수성 고분자 재료이다. 이러한 하이드로젤은 다양한 소재로부터 만들어질 수 있으며, 기본적으로 다량의 물을 내부에 포함할 수 있고 탄성력을 보인다. 특히, 외부 자극에 반응하여 성질이 변화하는 자극 응답성 하이드로젤은 탄성, 부피 변화, 저장 능력 및 화학적 다양성을 이용하는 새로운 반응 시스템의 개발에 적용할 수 있기 때문에 최근 상당한 관심을 받고 있다. 본 연구에서는 다양한 형태 및 기능을 갖는 자극 응답성 하이드로젤을 설계하고 합성하며, 재료로서의 특성을 분석하였다.

첫 번째로 필름 형태의 자극 응답성 하이드로젤의 구조를 설계하고 제조하였다. 일반적으로 필름으로 가공된 하이드로젤은 넓은 면적에서 기인하는 빠른 반응 속도와 높은 로딩 용량, 그리고 향상된 계면 상호 작용을 보인다. 본 연구에서는 기능성 로다민계 프로브를 설계하여 폴리아크릴아마드 하이드로젤 필름을 제조에 이용하였다. 해당 기능성 프로브는 라디칼 개시제와의 산화 환원 반응을 통해 라디칼 생성을 촉진하여 상온에서 쉽게 하이드로젤이 형성되게 하며, 알루미늄 이온에 대한 형광 반응을 보인다. 이러한 프로브를 포함하는 하이드로젤 필름은 투명하며 인장 시 5 배 이상 연장되는 신축성을 보였다. 또한 필름 내부에 도입된 프로브로 해당 필름은 알루미늄 이온에 대해 민감하고 선택적인 검출 능력을 보였으며 약 1.5 mM 검출한계를 보였다. 또한, 에틸렌 디아민테트라아세트산을 이용한 후처리를 이용하여 필름을 알루미늄 검출에 재사용할 수 있었다.

두 번째 연구에서는 이황화물리브덴(MoS_2)의 다기능 효과를 연구하고 이를 통하여 하이드로젤 나노 복합체를 제조하였다. 판상형의 MoS_2 가 증류수에 분산되면 과황산칼륨과 산화 환원 반응을 통해 라디칼을 형성하며 아크릴 단량체의 중합을 개시할 수 있는 것을 확인하였으며, 또한 외부 자극이나 추가적인 가교제 없이 비공유 가교점을 제공하여 하이드로젤이 형성될 수 있는 것을 확인하였다. 나아가 판상형의 MoS_2 는 동일한 수준에서 범용 화학 가교제(*N.N'*−metylenebisacrylamide)를 사용하는 하이드로젤보다 더 높은 탄성 계수를 보였다. 예를 들어, 0.08 wt%의 MoS_2 가 포함된 하이드로젤은 *N.N'*−metylenebisacrylamide 를 사용한 하이드로젤보다 2.5 배 더 큰 탄성 계수를 보였다. 또한, 해당 하이드로젤은 가역적인 물리적 가교로 이루어져 있어서 자가 치유가 가능한 것을 확인하였다. 절단된 하이드로젤 필름을 70 도에서 가열하면 재결합할 수 있으며, 새롭게 생성된 하이드로젤은 절단되기 전의 최초의 시료와 비슷한 기계적 물성을 나타내었다.

마지막으로, 아크릴산 기반의 고흡수성 하이드로젤을 제조하고 가교 밀도에 따른 재료의 물리적 거동을 분석하였다. 가교 밀도가 재료의 흡수 거동에 영향을 미치는 것을 분석하였으며, 특히 서로 다른 가교 밀도를 갖는 하이드로젤 필름을 기반으로, 순차적인 중합 반응을 거쳐, 거시적인 물성 변화를 보이는 하이드로젤 이중 층을 제조할 수 있었다. 해당 이중 층의 하이드로젤은, 기본 화학 조성이 같더라도 다른 흡습성으로 인해 흡수 시 원형으로 구부러지는, 비선형적인 물성 변화를 보이는 것을 확인하였다. 이러한 설계 원리를 바탕으로 거시적인 응답을 보이는 패턴화된 하이드로젤을 제조할 수 있었고, 이를 이용한 전기 회로 스위치를 만들었다.

패턴화된 하이드로젤의 비선형적인 변형은 회로의 단선을 닫고 발광 다이오드를 적색으로 점등시켰다.

주요어: 하이드로젤, 자극 응답성 물질, 산화-환원 중합,로다민 6G, 하이드로젤 필름, 알루미늄 센서, 이중 층 하이드로젤, 고흡성 고분자, 이황화몰리브덴, 자가치유

학번: **2014-21457**

Appendix:

List of Publications and Presentations

A.1. Publications

[1] "Highly luminescent tetra(biphenyl-4-yl)ethene-grafted molecularly imprinted mesoporous silica nanoparticles for fluorescent sensing of diethylstilbestrol"
Youngdo Kim, Kyoung Min Lee and Ji Young Chang, *Sens Actuators B Chem* , **242**, 1296 (2017).

[2] "Facile fluorescent labeling of a polyacrylamide-based hydrogel film via radical initiation enables selective and reversible detection of Al^{3+}"
Kyoung Min Lee, Yuree Oh, Ji Young Chang and Hyungwoo Kim, *J. Mater. Chem. B,* **6**, 1244 (2018).

[3] "Rapid acessible fabrication and engineering of bilayered hydrogels: revisiting the cross-linking effect on superabsorbent poly(acrylic acid)"
Kyoung Min Lee, Hea Ji Kim, Doyoung Jung, Yuree Oh, Hyemin Lee, Changsun Han, Ji Young Chang and Hyungwoo Kim, *ACS omega*, **3,** 3096 (2018).

[4] "Chemical Design of Functional Polymer Structures for Biosensors: From Nanoscale to Macroscale"
Kyoung Min Lee, Kyung Ho Kim, Hyeonseok Yoon and Hyungwoo Kim, *Polymers,* **10,** 551 (2018).

[5] "Selective De-Cross-Linking of Transformable, Double-Network Hydrogels: Preparation, Structural Conversion, and Controlled Release"

Doyoung Jung, Kyoung Min Lee, Ji Young Chang, Misun Yun, Hak-Jong Choi, Yoong Ahm Kim, Hyeonseok Yoon and Hyungwoo Kim, *ACS Appl. Mater. Interfaces*, 10, 42985 (2018).

[6] "Preparation ofcarbon-containing, compressible, microporous, polymeric monoliths that regulate macroscopic conductivity"
Kyoung Min Lee, Hea Ji Kim, Cheon-Soo Kang, Tomohiro Tojo, Ji Ae Chae, Yuree Oh, Min Chul Cha, Kap Seung Yang, Yoong Ahm Kim and Hyungwoo Kim, *Polym. Chem.,* **10**, 852 (2019).

[7] "One-step preparation of hydrogel particles that show rapid detection of hydrogen peroxide: The dual role of new methylene blue"
Kyoung Min Lee and Hyungwoo Kim, *Dyes. Pigm.,***170**, 107546 (2019).

A.2. Presentations (International and Domestic)

[1] 2015년 4월, 춘계 한국고분자학회, "Preparation of fluorescent microporous organic polymers via Knoevenagel condensation and their optical properties"

[2] 2017년 4월, 춘계 한국고분자학회, "Preparation of luminescent hydrogels cross-linked by hyperbranched polymers"

[3] 2018년 4월, 춘계 한국고분자학회, "Facile fluorescent labeling of a polyacrylamide-based hydrogel film via radical initiation enables selective and reversible detection of Al^{3+}"

[4] 2018년 10월, 추계 한국고분자학회, "Rapid Accessible Fabrication and Engineering of Bilayered Hydrogels: Revisiting the Cross-Linking Effect on Superabsorbent Poly(acrylic acid)